

**CHARACTERISATION OF IRON ORE — A CASE STUDY OF MOUNT
TOKADEH, WESTERN NIMBA AREA, LIBERIA**

by

CHARLES AYINGAYURE AMIKIYA, BSc. Chemistry (Hons)

KNUST

A Thesis Submitted to the School of Graduate Studies

Kwame Nkrumah University of Science and Technology, Kumasi

in Fulfillment of the Requirements for the Degree of

MASTER OF PHILOSOPHY IN CHEMICAL ENGINEERING

Department of Chemical Engineering

College of Engineering

© April 2014

DECLARATION

I hereby declare that except for reference to other people work, which I have dully cited, this thesis submitted to the School of Graduate Studies, Kwame Nkrumah University of Science and Technology, Kumasi is the result of my own investigation, and has not been presented for any other degree elsewhere.

Charles Ayingayure Amikiya (PG3654109)
(Student)

.....
Signature

.....
Date

Certified by:

Mrs. Zsuzsanna Momade
(Supervisor)

.....
Signature

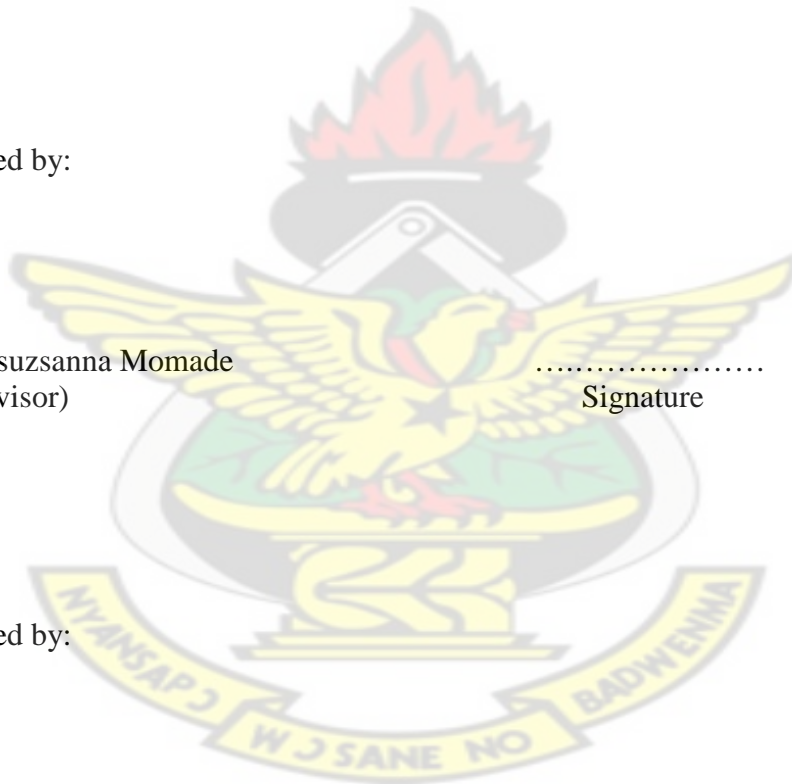
.....
Date

Certified by:

Dr. M.Y. Woode
(Head of Department)

.....
Signature

.....
Date



ABSTRACT

ArcelorMittal Liberia is currently evaluating opportunities to develop the Mount Tokadeh iron ore deposit in Liberia. This deposit is defined in three zones: the top layer that is largely soft and limonitic (weathered oxide ore), the middle layer that consists of transitional oxidised ore including magnetite and hematite and the bottom layer that is magnetite in a hard rock matrix similar to taconite.

The main objective of this research was to explore the feasibility of recovering the iron oxides and iron oxyhydroxides/hydroxides using physical separation techniques such as magnetic separation proposed by ArcelorMittal Liberia. Composite samples were prepared from each ore zone for ten different drill holes for Davis tube, SATMAGAN and chemical analysis. Due to weathering, the magnetite content is much lower in the oxidised ore than in the transitional and bottom primary layer.

Iron recovery for both the oxide and transition material is only 34-35% and 71-74% for the primary ore, indicating that magnetic separation technique can be used to recover valuable iron bearing minerals in the primary ore zone. The quality of concentrate produced from the magnetic separation in the Davis tube is observed to be 66-68% Fe for all ore zones. Results from the Davis tube analysis indicated that a maximum of 42-44% of valuable iron would be lost to tailings in the oxide zone and a minimum 16-17% in the primary zone.

There is strong positive correlation between the Davis tube and SATMAGAN results with an average correlation coefficient of 0.94 for all particle size groups studied.

TABLE OF CONTENTS

TABLE OF CONTENTS	ii
LIST OF TABLES	v
LIST OF FIGURES	vii
LIST OF ABBREVIATIONS	viii
ACKNOWLEDGEMENT	ix
CHAPTER ONE	1
INTRODUCTION	1
1.1 Overview	1
1.2 Problem statement.....	2
1.3 General objective	2
1.4 Specific objectives	2
CHAPTER TWO	4
LITERATURE REVIEW	4
2.1 Formation of iron ore deposits	4
2.1.1 Processes of iron ore formation	4
2.1.2 Classification of iron ore deposits.....	5
2.2 Types of minerals in iron ore	8
2.2.1 Types of iron minerals	9
2.2.2 Gangue minerals.....	11
2.2.3 Metal oxides	12
2.2.4 Deleterious elements	12
2.3 Global iron ore production and consumption.....	13
2.4 Iron ore requirement for steel industry.....	15
2.5 Location of the study area	18
2.5.1 History of exploration and mining of iron ore in Liberia.....	19

2.5.2 Geology of the study area	23
2.5.3 Geology of Mt. Tokadeh	24
2.5.4 Mineralogy of Mt. Tokadeh iron ore deposit	25
2.6 Iron ore mining	29
2.7 Iron ore processing	29
2.7.1 Crushing and grinding	31
2.7.2 Concentration methods	31
2.7.3 Fine iron ore processing	34
2.8 Iron ore characterisation	35
2.8.1 Chemical characterisation	36
2.8.2 Physical and mineralogical characterisation	36
2.9 Magnetic material content determination by Davis tube method	38
2.10 Magnetite content measurement by SATMAGAN	39
2.11 X-ray diffractometric analysis	42
2.12 ArcelorMittal proposed iron ore beneficiation plant	42
2.12.1 Process description	43
CHAPTER THREE	47
MATERIALS AND METHODS	47
3.1 Sampling	47
3.2 Drilling for sample collection	47
3.3 Core sample splitting	51
3.4 Sample grinding	52
3.5 Composite sample preparation	53
3.6 Loss on ignition determination	53
3.7 Fused bead preparation	54
3.8 Chemical analysis	55

3.9 Magnetic material content determination by Davis tube tester.....	55
3.10 Magnetite content measurement by SATMAGAN.....	57
CHAPTER FOUR.....	58
RESULTS AND DISCUSSION	58
4.1 Composite sample concentration	58
4.2 Particle size distribution.....	64
4.3 Results from Davis tube measurements	68
4.3.1 Mass recovery	74
4.3.2 Davis tube concentrate	74
4.3.3 Iron recovery	78
4.3.4 Tailings (Non-magnetic material from the Davis tube separation).....	79
4.4 Magnetite content of composite samples by Satmagan method	81
4.5 Magnetite and magnetic material content correlation.....	81
CHAPTER FIVE.....	86
CONCLUSIONS AND RECOMMENDATIONS.....	86
5.1 CONCLUSIONS.....	86
5.2 RECOMMENDATIONS	89
REFERENCES.....	90
APPENDIX.....	99

LIST OF TABLES

Table 2.1: Geological processes of iron formation	5
Table 2.2: Properties of major iron minerals	9
Table 2.3: Iron ore production	14
Table 2.4: Apparent steel consumption.....	15
Table 2.5: Typical properties of pellets suitable for use in blast furnaces.....	17
Table 2.6: Summary history of exploration and mining in the Yekepa area	22
Table 2.7: Mt. Tokadeh general stratigraphy	27
Table 2.8: Final product specification for the proposed magnetic separation plant	43
Table 3.1: Drill hole data	50
Table 3.2: Core lengths and number of samples	52
Table 3.3: Composite samples for a particular grinding time.....	54
Table 3.4: Conditions for Davis Tube separation	56
Table 4.1: Chemical composition of composite samples.....	59
Table 4.2: Chemical composition of composite samples (continued)	60
Table 4.3: Particle size analysis of composited samples.....	65
Table 4.4: Davis tube results – 95% of particles under 150 μm	69
Table 4.5: Davis tube results – 95% of particles under 106 μm	70
Table 4.6: Davis tube results – 95% of particles under 90 μm	71
Table 4.7: Davis tube results – 95% of particles under 75 μm	72
Table 4.8: Davis tube and Satmagan results – 95% of particles under 63 μm	73
Table 4.9: Average concentration in the Davis tube magnetic concentrates for the different fineness	75
Table 4.10: Calculated Fe recovery by Davis tube method	78
Table 4.11: Average concentration in non-magnetic tailings	80
Table 4.12: Summary Satmagan and Davis tube measurement results	82
Table A1: Drill hole T501 and T512 physical data.....	99
Table A2: Drill hole T520 physical data.....	100
Table A3: Drill T536 T556 physical data	101
Table A4: Drill hole T594, T627 and T643 physical data	102
Table A5: Drill hole T662 and T673 physical data.....	103
Table A6: ArcelorMittal Liberia Lithology codes	104
Table A7: ArcelorMittal Liberia Minerals code	105
Table A8: ArcelorMittal Liber Grain size codes.....	105

Table A9: ArcelorMittal Liberia Structure code.....	106
Table A10: ArcelorMittal Liberia Texture codes.....	106
Table A11: ArcelorMittal Liberia Weathering codes	107
Table A12: ArcelorMittal Liberia Colour codes.....	107
Table A13: ArcelorMittal Liberia Strength/Cohesion codes	107

KNUST



LIST OF FIGURES

Figure 2.1: Map of Liberia showing location of ArcelorMittal concession area	18
Figure 2.2: Iron ore mineralisation at the Nimba Range and “Western Area”	19
Figure 2.3: Map of Liberia showing locations of past four major iron ore mining companies.....	20
Figure 2.4: Types of iron formation in Mt. Tokadeh	25
Figure 2.5: Davis Tube Tester.....	39
Figure 2.6: Saturation Magnetization Analyser	40
Figure 2.7: Proposed process block diagram	45
Figure 3.1: Map of Mt. Tokadeh showing sample collection points	49
Figure 3.2: Drill hole chart.....	51
Figure 4.1: Concentration of composite samples	61
Figure 4.2: Average concentration of composite samples	62
Figure 4.3: Particle size distribution for 2 min grinding time.....	66
Figure 4.4: Particle size distribution for 4 min grinding time.....	66
Figure 4.5: Particle size distribution for 6 min grinding time.....	67
Figure 4.6: Particle size distribution for 8 min grinding time.....	67
Figure 4.7: Particle size distribution for 10 min grinding time.....	68
Figure 4.8: Mass recovery	74
Figure 4.9: Average iron concentration in the Davis tube magnetic concentrates.....	76
Figure 4.10: Average silica concentration in the Davis tube magnetic concentrate	77
Figure 4.11: Average alumina concentration in the Davis tube magnetic concentrates .	77
Figure 4.12: Iron recovery.....	79
Figure 4.13: Average magnetite concentration	81
Figure 4.14: Average mass recovery and magnetite content	83
Figure 4.15: Magnetite and magnetic material correlation for all ore zones	84
Figure 4.16: Magnetite and magnetic material correlation for the oxide ore.....	84
Figure 4.17: Magnetite and magnetic material correlation for the transition ore	85
Figure 4.18: Magnetite and magnetic material correlation for the primary ore.....	85
Figure A1: Atlas Copco ROC L8 drill rig.....	108
Figure A2: Panalytical Axios ^{mAX} X-ray fluorescence spectrometer.....	108

LIST OF ABBREVIATIONS

ASTM	American Society for Testing and Materials
ASC	Apparent Steel Consumption
BIF	Banded Iron Formation
BMC	Bong Mine Company
CIS	Commonwealth of Independent States
DRI	Direct Reduction Iron
EU	European Union
GIBC	Global Investment and Business Center, USA
GOI	Gain on Ignition
IOCG	Iron Oxide Copper Gold
ISO	International Organization for Standardization
LAMCO JV	Liberian America-Swedish Minerals Company Joint Venture
LIMS	Low Intensity Magnetic Separator
LMC	Liberia Mining Company
LOI	Loss on Ignition
MR	Mass Recovery
MSL	Mean Sea Level
NAFTA	North American Free Trade Agreement
NIOC	National Iron Ore Company
PMA	Particle Mineralogical Analysis
ppm	parts per million
QEMSCAN	Quantitative Evaluation of Minerals by Scanning Electron Microscopy
RC	Reverse Circulation
rpm	revolutions per minute
SAG	Semi-Autogenous Grinding
SATMAGAN	Saturation Magnetization Analyzer
SGS	Société Générale de Surveillance (General Society of Monitoring)
USA	United States of America
UTM	Universal Transverse Mercator
XRD	X-Ray Diffraction
XRF	X-Ray Fluorescence

ACKNOWLEDGEMENT

I wish to acknowledge the following persons for their contributions towards the successful completion of this research work.

1. Mrs. Zsuzsanna Momade, Senior Lecturer at the Department of Chemical Engineering, KNUST for her good supervisory skills, dedication, encouragement and timely comments. Mrs. Momade has, during the course of this thesis, provided input, guidance and feedback of immense value. She has also been exemplary, as an academic role model to me, upholding the true spirit of science and academic research. She has also assisted me in becoming properly familiar with the relevant engineering background knowledge, vital to the completion of this thesis.
2. Mr. Jan van Graan, Senior Consulting Geologist, ArcelorMittal Liberia for his comments, reviews and suggestions.
3. Mr. Desmond Raymond Edifor, Geology Superintendent, ArcelorMittal Liberia for map preparation.
4. Mr. John Osei Bonsu, Senior Geologist, ArcelorMittal Liberia for map preparation.
5. Ms. Jennifer Judy Ayaam, my wife and children Laud Amikiya and Leonard Amikiya for their support throughout the period of this research work.
6. Mr. Mark Wynn, Vice President, DSO Project, Essar Infrastructure Zimbabwe (Pvt) Limited, for granting me access and approval to use some ArcelorMittal Liberia data and information.

CHAPTER ONE

INTRODUCTION

1.1 Overview

Iron constitutes about 5% of the Earth's crust, making it the fourth most abundant element. Iron oxides and hydroxides form the principal iron ore minerals, due to their high iron content and occurrence as large tonnage surface deposits (Ferenczi, 2001). The presence of the amount of iron varies from an average of 2-3% in sedimentary rocks to 8.5% in basalt and gabbro (US EPA, 1994). Iron is, however, present in low concentration in most parts of the earth, thus a deposit must have a high percentage of the metal to be considered ore grade for economic purposes. Typically, a deposit must contain at least 25% iron to be considered economically recoverable. Exploitation of large, low grade iron ore deposits can be achieved through concentration of the iron.

The iron itself is usually found in the minerals of magnetite (Fe_3O_4), hematite (Fe_2O_3), goethite ($\text{FeO}(\text{OH})$) or limonite ($\text{FeO}(\text{OH}) \cdot n(\text{H}_2\text{O})$), siderite (FeCO_3), chamosite ($(\text{Mg,Fe,Al})_6(\text{Si,Al})_{414}(\text{OH})_8$), ilmenite (FeTiO_3) and pyrite (FeS). Despite the existence of iron in many minerals, five of them are the primary sources of iron: magnetite (Fe_3O_4), hematite (Fe_2O_3), goethite/limonite ($\text{FeO}(\text{OH})$), siderite (FeCO_3), and pyrite (FeS) (US EPA, 1994).

Iron ores are rocks and minerals from which metallic iron can be extracted. An iron ore deposit is a mineral body of sufficient size, iron content, and chemical composition with physical and economic characteristics that will allow it to be a source of iron either immediately or potentially (Kennedy, 1990). Iron ore is the raw material used to make pig iron, which is one of the main raw materials to make steel. Nearly 98% of the mined iron ore is used to make steel (MII, 2006). There are four main types of iron ore deposits worked currently, depending on the mineralogy and geology of the ore

deposits. These are magnetite, titanomagnetite, massive hematite, and pisolitic ironstone deposits (Kennedy, 1990).

ArcelorMittal Mining Liberia has acquired Mt. Tokadeh iron ore deposit in Liberia, which offers a potential for establishing sustainable iron ore production. Although this deposit has considerable reserves of iron ore, lack of consistency with respect to the ore quality makes it unsuitable to use directly in a blast furnace without prior beneficiation. Beneficiation by magnetic concentration method has been proposed to enrich the iron content and reduce gangue minerals to make it a better feed for blast furnace (Heneghan, 2010).

1.2 Problem statement

- i. Hematite and other non-magnetic iron minerals present in the Tokadeh iron ore deposit in Liberia would be lost to tailings during magnetic separation.
- ii. Chemical data generated from the ArcelorMittal project in Liberia so far indicate inconsistencies in the magnetic mineral content results from the Davis Tube and Saturation Magnetization Analyzer (SATMAGAN) measurement methods, which are used to predict the magnetic separation characteristics of magnetic iron ores in plant operation.

1.3 General objective

The main objective of this research is to determine the total amount of non-magnetic iron minerals that would be lost to tailings during magnetic separation of the iron ore from the Mt. Tokadeh deposit in Liberia.

1.4 Specific objectives

To achieve the general objective, the following specific objectives have to be fulfilled:

- i. to determine the ferromagnetic and non-magnetic content in the ore,

- ii. to predict the quality of plant concentrate and tailing in the proposed concentrating plant,
- iii. to establish correlation between magnetic susceptibility as measured by a Saturation Magnetization Analyzer (SATMAGAN) and percent magnetic iron (magnetite) content as measured by Davis Tube, and
- iv. to determine the amenability of the Tokadeh iron ore deposit to magnetic separation.

KNUST



CHAPTER TWO

LITERATURE REVIEW

2.1 Formation of iron ore deposits

Mineral deposits represent the result of processes that act to concentrate the elements in mineral form or in anomalous concentration in other minerals. In those places where the concentration is sufficiently high that such rocks or minerals can be extracted from the earth at a profit, these deposits are called ores (Howard, 1987). An iron ore deposit is a mineral body of sufficient size, iron content, and chemical composition with both physical and economic characteristics that will allow it to be a source of iron either immediately or potentially (Kennedy, 1990).

Iron ore deposits are formed by three geological processes: direct sedimentation; forming bedded sedimentary deposits, igneous activity; forming segregation or replacement deposit and enrichment due to surface and near surface weathering (US EPA, 1994). Geological processes of iron ore deposit formation and the resulting type of iron ore formed with its principal iron minerals are illustrated in Table 2.1.

2.1.1 Processes of iron ore formation

Chemical and physical processes are the most widespread and common process of metal or mineral concentration is the dissolution of chemical components of rocks, their transport in solution and the precipitation of those components as ore minerals at some specific sites of deposition, usually controlled by chemical contrast or change in chemical environment. In the process of crystallisation from solutions, the heavier iron bearing minerals segregate by gravity to form iron-rich deposit. When surface water descends or when underground water ascends through rock strata, iron-bearing minerals may be deposited or gangue minerals such as silica may be leached out (Howard, 1987).

Table 2.1: Geological processes of iron formation

Geological type	Principal iron mineral
Sedimentation	
Banded iron formation	Magnetite, Hematite, Siderite, Iron silicate
Iron stones	Chamosite, Limonite, Hematite, Siderite
Igneous Activity	
Magmatic segregations	Titaniferous, Ilmenite, Magnetite, Iron silicates
Pyrometasomatic	Magnetite
Surface or Near-Surface Weathering	
Secondary enrichments of low grade iron deposits	Magnetite, Limonite, Siderite

(Source: US EPA, 1994)

Mechanical processes involve erosion, transportation and deposition of generally dense and insoluble rich iron weathered rock material. The higher specific gravity of the iron-bearing minerals causes them to be deposited earlier than other lighter materials. This method of formation is responsible for certain sedimentary hematite deposits and magnetite beach sands (Robb, 2004).

2.1.2 Classification of iron ore deposits

Iron ore deposits are widespread and have formed in a range of geological environments throughout geological time. These deposits can be divided into four major categories based on their mode of origin (Pratt, 1993), using aspects of previous classifications by Gross, (1970) and Klemic *et al.*, (1973):

- sedimentary (banded iron formation, oolitic, placer, swamp),
- igneous (magmatic segregations and skarn),
- hydrothermal (proximal and distal), and
- surficial enrichment (laterite and supergene).

Sedimentary deposits, particularly those in banded iron formation (BIF), contain the bulk of the world's iron ore resources. Sedimentary deposits include a family of layered silica-rich and iron-rich sediment and meta-sedimentary rocks predominantly composed of cherts or fine-to-medium to coarse-grained quartz and iron minerals as oxides, carbonates, or silicates (Kennedy, 1990). Sedimentary iron formations generally form in a variety of marine environments and rarely in continental (coal) swamps (Kimberley, 1989).

BIF-hosted deposits are almost exclusively of Precambrian period (1.8-2.6 billion years ago) and are distributed worldwide. BIFs are metamorphosed sedimentary rocks composed predominantly of thinly bedded iron minerals and silica (as quartz). The iron mineral present may be the carbonate siderite, but those used as iron ores contain the oxides magnetite or hematite (Harry *et al.*, 1973).

An extensive body of data indicates that BIFs are formed by volcanogenic or hydrothermal effusive processes (Gross, 1993). BIFs are classified into two types: (1) the Superior-type, which formed in a near-shore continental-shelf environment in association with dolomite, quartzite and shale, and (2) the Algoma-type, which is associated with volcanic activities (Edwards and Atkinson, 1986).

Oolitic sedimentary deposits are massive stratiform oolitic ironstones within marine terrigenous clastic sediments. They are Proterozoic to Cretaceous in age and were an important source of iron ore before 1970. They are lower in iron content (30-50% Fe) relative to BIF-hosted deposits (55-65% Fe) (Ferenczi, 2001). Two types have been identified: (1) the Clinton-type which consists of deep red to purple ores composed of hematite, chamosite and siderite, and (2) the Minette-type consisting of brownish to dark greenish-brown ores composed mainly of siderite and iron silicates (berthierine and chamosite).

These deposits were formed in shallow marine environments and accumulated along passive continental margins during times of quiescence, extension and global sea level change (Van Houten and Hou, 1990).

Igneous deposits are formed either by magmatic segregation of an immiscible magnetite-rich melt in association with layered mafic-ultramafic intrusions or by injection of magnetite-rich fluids into surrounding rocks (e.g. iron skarns). The former occur as massive cumulate-textured seams and are often mined for their economic concentrations of titanium and/or vanadium (e.g. Bushveld Complex, South Africa). Iron skarns (or pyrometasomatic deposits) are mainly derived from granitic to mafic intrusive and can be hosted in a variety of rock types. These deposits are massive, irregularly shaped to tabular bodies that continue to be a source of iron ore in some countries (e.g. Peru and Russia) (Ferenczi, 2001). The mineral concentrations in igneous rocks occur as distinctive flows in volcanic successions, or as layers within magmas that cooled at deep crustal levels (Howard, 1987).

Hydrothermal deposits are formed by the circulation of heated, iron-rich aqueous solutions of magmatic, metamorphic or sedimentary parentage. These deposits form the basis of most iron oxide copper gold (IOCG)-style deposits (Hitzman *et al.*, 1992, and Porter, 2000). Proximal hydrothermal deposits (also known as volcanic hosted magnetite deposits) are essentially magnetite-hematite bodies that have replaced non-ferruginous host rocks (e.g. Kiruna iron ores). These deposits usually have obvious magmatic signatures and adjacent wall rocks are generally intensely altered (Pollard, 2000). Hematite-bearing quartz veins within fault zones are also part of this group. Distal hydrothermal deposits are tabular to podiform, stratabound, specular hematite with or without magnetite bodies that formed by the enrichment of an iron-rich protolith (Ferenczi, 2001).

Surficial enrichment of iron ore deposits results from sub-aerial weathering processes of generally low-grade ferruginous protore, commonly BIF. Surface and near-surface weathering causes certain dense or hard and chemically inert minerals, which occur in rocks, to survive chemical weathering and be transported in hydrological systems and re-concentrate in different environments. Mature laterites develop under a wet tropical climate and can form extensive duricrust horizons (ferricrete), rich in iron oxyhydroxides.

Supergene enrichment involves weathering and leaching of the upper parts of a mineral deposit (zone of oxidation) and re-deposition of the ore-minerals at lower levels (zone of secondary or supergene enrichment). Fine earthy hematite and iron oxyhydroxides such as goethite, limonite and lepidocrocite are the principal iron minerals produced from surface and near surface enrichment processes (Ferenczi, 2001). Chemical and physical weathering by soil forming processes of pre-existing iron-bearing minerals resulted in progressive concentration of iron oxides to form iron-rich deposits (US EPA, 1994).

2.2 Types of minerals in iron ore

Almost 300 minerals contain some iron, but only a few are considered to be important iron ore minerals. The major iron ore minerals are presented in Table 2.2.

Table 2.2: Properties of major iron minerals

Mineral	Chemical formula	Theoretical iron content, %	Specific gravity	Mohs hardness
Hematite	Fe ₂ O ₃	70	5.1	5-6
Magnetite	Fe ₃ O ₄	72	5.2	5.5-6
Martite	α -Fe ₂ O ₃	70	5.3	5.5-6.5
Goethite	FeO(OH)	63	3.3-4.3	5-5.5
Siderite	FeCO ₃	48	4	4
Chamosite	(Mg,Fe,Al) ₆ (Si,Al) ₄ O ₁₄ (OH) ₈	45	3.1	3
Pyrite	FeS ₂	47	4.9	6-6.5
Limonite	FeO(OH).n(H ₂ O)	63	3-4	5-5.5
Lepidocrocite	γ -Fe ₂ O ₃ .H ₂ O	60	4.1	5
Greenalite	Fe ₃ Si ₂ O ₅ (OH) ₄	45	2.9	3
Ilmenite	FeTiO ₃	37	4.7-4.79	5-6

(Source: Ferenczi, 2011)

The major iron bearing minerals within the Mt. Tokadeh deposit include hematite, magnetite, martite (pseudomorphs of hematite after magnetite), goethite and limonite (Edifor, 2009). Gangue minerals identified within the deposit include quartz, and aluminum minerals.

2.2.1 Types of iron minerals

Hematite (Fe₂O₃) is also known as "natural ore", a name which refers to the early years of mining, when certain hematite ores containing up to 66% iron could be fed directly into iron-making blast furnaces (MII, 2006). Hematite deposits are mostly sedimentary in origin, such as the banded iron formations (BIFs). BIFs consist of alternating layers of chert (a finely grained re-crystallised quartz), hematite and magnetite. Their formation is not fully understood, though it is known that they formed by the chemical precipitation of iron from shallow seas about 1.8-2.6 billion years ago, during the Precambrian period (Harry *et al.*, 1973).

Magnetite (Fe_3O_4) is a naturally occurring metallic mineral that is occasionally found in sufficient quantities to be an ore of iron. It contains both iron (II) oxide (FeO) and iron (III) oxide (Fe_2O_3) (Norman and Alan, 1997). High grade magnetite ore normally contains more than 60% iron with some impurities such as silica, alumina and phosphorus. Magnetite is beneficiated by crushing and then separating the magnetite from the gangue minerals with a magnet. This separation is usually so efficient that a lower grade magnetite ore can be treated easily than a comparable grade of hematite ore.

Martite (Fe_2O_3) is a secondary hematite formed by chemical replacement of magnetite produced at depth and pressure. The replacement proceeds from the outer edges towards the center of the magnetite grains commonly along crystallographic planes (Petruk, 2000).

Goethite and Limonite ($\text{FeO}(\text{OH})$) are secondary minerals formed by oxidation of Fe-carbonates, hematite, martite and magnetite. Goethite masses are present in quartz where the goethite has replaced hematite. Goethite that replaced hematite does not contain manganese, whereas goethite that replaced carbonates and martite contains significant amounts of Mn (up to 27% wt. Mn) (Petruk, 2000). They are hydrated iron oxides containing up to 60-63% iron. They can occur as primary minerals and always formed relatively near to the surface as a result of weathering of the exposed ore.

Siderite (FeCO_3) ore constitutes only a small proportion of the total world iron ore reserves. When pure, it contains 48.3% iron, but it is easily decomposed by heat to hematite with 70% iron.

Chamosite $\{(Mg,Fe,Al)_6(Si,Al)_4O_{14}(OH)_8\}$ ore occurs, together with limonite and siderite, in the relatively low concentration. This ore usually contains some sulphur and phosphorus and other minerals such as quartz and calcite (Harry *et al.*, 1973).

2.2.2 Gangue minerals

All iron ores contain impurities, which are collectively known as gangue. The presence of small amounts of some elements can have either bad or good effects on the characteristics of an iron ore or on the operation of a steel plant. Flux is normally added to iron ore feed in the blast furnace to increase the furnace efficiency, while other chemicals are added to improve the end product qualities. Ideally, iron ore contains only iron and oxygen, but typically, iron ore contains a lot of elements which are often unwanted in modern steel.

There are four main slag forming constituents in iron ores, which include the acidic oxide silica (SiO_2) and the basic oxides lime (CaO) and magnesia (MgO) as well as the neutral alumina (Al_2O_3). Most iron ores have an excess of SiO_2 and Al_2O_3 and the ash of the coke used for fuel is mainly composed of these oxides, so a basic flux, e.g. limestone must be added (Taylor *et al.*, 2001).

Most iron ores contain silica, which is normally removed in the form of slag during the smelting process. Silica is reduced to silicon above $1300^\circ C$, which form alloy with iron. The major effect of silicon is to promote the formation of gray iron, which is less brittle and easier to finish than white iron and thus preferred for casting purposes. The presence of silica has been reported to reduce shrinkage and the formation of blowholes, lowering the number of bad castings (Strassburger *et al.*, 1969).

Most iron ores contain small amounts of alumina in the form of clays and magnesium aluminum carbonate hydroxide ($Mg_6Al_2CO_3(OH)_{16}.4H_2O$). The presence of alumina

increases the viscosity of the slag. This will result in slow descent of the charge due to thickening of slag and consequently prolonged processes in the furnace. High alumina content will also make slag recovery more difficult, which could lead to a frozen furnace. Increasing the ratio of lime flux will decrease the viscosity (Rosenqvist, 1983).

2.2.3 Metal oxides

Iron ores generally contain metallic oxides, which are reduced to metal in the process of iron making. Some of the metallic oxides, such as nickel, are easily reduced compared to oxides of iron, while others, such as manganese and chromium, are less easily. When the reduction of these metallic oxides occurs in the blast furnace, a proportion of the reduced metals contaminate the final steel produced. A manganese content of about 1% in steel is advantageous but small proportions of other metals, such as zinc, are undesirable. Most deposits of lateritic ores, which consist predominantly of hydrated oxides, contain appreciable quantities of chromium, nickel, and cobalt (Taylor *et al.*, 2001).

2.2.4 Deleterious elements

Common deleterious elements in iron ores include phosphorus, sulphur, and titanium. Uncommon deleterious elements include vanadium, copper, zinc, chromium, nickel, arsenic, lead, and tin.

Phosphorus has five major effects on iron; increases hardness and strength, lowers solidus temperature, increases fluidity and cold shortness. Depending on the use intended for the iron, these effects are either good or bad (Gordon, 1996). The strength and hardness of an iron increases with the increasing concentration of phosphorus. At concentrations higher than 0.2%, iron becomes increasingly cold short, or brittle at low temperatures.

Phosphorus lowers the liquidus temperature, allowing the iron to remain molten for longer, and increases fluidity. The additions of 1% can double the distance molten iron will flow. Remedies for high phosphorus content in iron ores include avoiding high phosphorus content ores or oxidizing the phosphorus during the fining process (removal of bubbles) by adding iron oxide (Rostoker and Bronson, 1990).

Sulphur is also present in small quantities in many ores. It dissolves readily in both liquid and solid iron at the temperatures of iron smelting. The effects of even small amounts of sulphur are immediate and serious. Sulphur causes iron to be red or hot short (Gordon, 1996). Hot short iron is brittle when hot and the degree of hot shortness is in direct proportion to the amount of sulphur present. Iron with over 0.03% sulphur content is avoided.

Sulphur can be removed from the ores by roasting and washing, and by addition of manganese. Roasting oxidizes sulphur to form sulphur dioxide (SO_2), which either escapes into the atmosphere or can be washed out. Addition of manganese removes sulphur in iron ores because manganese forms a high melting sulfide at high temperatures (1610°C) and therefore, prevents the formation of a liquid iron sulfide at the grain boundaries (Verhoeven, 2007).

2.3 Global iron ore production and consumption

The world resources of iron ore are estimated to exceed 800 billion tons of crude ore containing more than 230 billion tons of iron (Jorgenson, 2011). The annual world production of iron ore is usually about one billion tonne and, although iron ore is produced in about fifty countries, the eight largest of these countries produce more than 80% of the world total. Table 2.3 presents the iron ore production distribution of the world.

Table 2.3: Iron ore production

Country	Production, Mt		
	2009	2010	2011 ^e
China	880	1070	1200
Australia	394	433	480
Brazil	300	370	390
India	245	230	240
Russia	92	101	100
Ukraine	66	78	80
South Africa	55	59	55
USA	27	50	54
Other countries	181	199	201
World total	2240	2590	2800

e – estimated values.

(Source: Jorgenson, 2011 and 2012)

Iron-ore trade climbed to a record level of 955 Mt in 2009. China imported 628 Mt and is currently the largest importer of iron ore, accounting for two-thirds of world imports in 2009 and produced about 60% of the world's pig iron (Jorgenson, 2011). Australia is the largest exporting country and sent 363 Mt of iron ore overseas. Exports from Brazil decreased by 3% to 266 Mt and India exported 116 Mt (Prinsloo, 2010).

Steel is the world's most commonly used metal primarily in structural engineering works, in maritime purposes, automobiles, and general industrial applications (machinery). About 98% of iron ore is used to produce pig iron, which is, therefore, the best indicator of iron ore consumption worldwide. The World Apparent Steel Consumption (ASC) is presented in Table 2.4.

Table 2.4: Apparent steel consumption

Region	Apparent Steel Use, million tonnes						
	2005	2006	2007	2008	2009	2010	2011
European Union	165.5	188.4	198.4	182.9	119.8	144.9	152.8
Other Europe	24.8	29.4	31.6	28.8	23.9	29.6	33.0
CIS	41.5	48.9	56.3	50.0	36.0	48.2	54.0
NAFTA	137.5	154.9	141.7	130.5	83.5	111.2	121.2
Central and South America	32.3	37.2	41.1	43.9	33.7	45.1	46.0
Africa	19.4	20.0	20.7	24.3	26.9	24.8	22.7
Middle East	34.0	34.4	43.6	45.6	41.6	46.9	48.1
Asia	579.6	617.6	676.0	703.6	768.6	842.2	888.5
Australia and New Zealand	7.9	7.9	8.4	8.5	6.0	7.9	7.0
World total	1042.5	1138.7	1217.9	1218.1	1140.0	1300.8	1373.3

(Source: World Steel Association, 2012)

The major constraint to economics for iron ore deposits is not necessarily the grade or size of the deposits, because it is not particularly hard to geologically prove enough tonnage of the rocks existence. The main constraint is the position of the iron ore relative to market, the cost of rail infrastructure to get it to market and the energy cost required to do so (Rao *et al.*, 2009).

2.4 Iron ore requirement for steel industry

It has been established that the adverse effects of impurities present in the ore is detrimental to blast furnace and sinter plant productivity. Iron ores are generally beneficiated to enrich the iron content and reduce gangue minerals to make them a better feed for steel plants. The quality specifications of iron ores required by steel makers are significantly different from the ore mined. Iron ore with high amount of hematite is mostly desirable due to its good reducibility and narrow/low softening and melting temperature range as compared to magnetite (Rao *et al.*, 2009).

Generally, close sized lumps, mostly 1-4 cm, with high iron content, and low in gangue minerals are required for steel plants. However, iron ore fines (< 1 cm) are also used

after sintering (Rao *et al.*, 2009). The sintering technique involves the partial fusion of fine iron ore material at high temperature (1150-1250°C) to produce clustered lumps. Iron ore sinter is typically 0.5-4 cm in size and has the following chemical composition: 55% Fe (71% in the form of Fe₂O₃ and 7% as FeO); 10% CaO; 2% MgO; 1% Al₂O₃; and 4% other (Kogel *et al.*, 2006).

Iron ore fines below 150 µm size are used to make pellets often after beneficiation to increase the iron content to over 65%. Pelletising is a size enlargement technique employed to process fine-grained iron-bearing concentrates and powder ores into spheres of about 1-1.5 cm in diameter. It involves mixing very finely ground particles of iron ore of less than 45 µm sizes with fluxes such as limestone, lime, dolomite etc. as fines, and a binder like bentonite (0.5-1%) (Ghosh and Chatterjee, 2008).

Pelletising is carried out either in a 3.5-5.5 m diameter rotating disc inclined at 45°, or in a drum, typically 9-10 m long and 2.5-3 m in diameter, rotating at 10-15 rpm. Typical properties of pellets suitable for use in blast furnaces are presented in Table 2.5 (Ghosh and Chatterjee, 2008).

Table 2.5: Typical properties of pellets suitable for use in blast furnaces

Parameter	Target
Fe, %	> 65
SiO ₂ , %	2.8 + 0.1
CaO/SiO ₂ ,	2.1 + 0.1
MgO, %	2.1 + 0.1
(Na ₂ O + K ₂ O), %	< 0.075
Mean diameter, mm	11.2 + 1
4 mm undersize, %	< 0.5
Porosity, %	26.5 + 0.3
Compressive strength, kg/pellet	> 260
Compressive strength above 210 kg/pellet, %	< 80
Reduction degradation index (< 3 mm), %	< 5.5
Swelling index, %	< 12
Contraction, %	< 9

(Source: modified from Ghosh and Chatterjee, 2008)

Marketable iron ore has high iron (> 64% Fe is considered export-grade) and low silica (< 10%), alumina (< 5%) and phosphorus (< 0.08%) content. However, low-grade magnetite deposits can be beneficiated to produce export-grade ore. Approximate tolerance limits for minor elements in iron ore have been quoted as Cu 50 ppm, Pb 500 ppm, Zn 200 ppm, S 1000 ppm, As 50 ppm, Cr 300 ppm, Ni 300 ppm, Sn 100 ppm, V 60 ppm, and TiO₂ 100 ppm (Gross, 1993).

Cumulative content of minor elements in ore material supplied to the furnaces greatly influence and may determine the metallurgical processes that can be used to convert iron ore to iron and steel. The evaluations of the iron ore materials involve chemical and mineralogical analyses, physical testing (e.g. size distribution and strength) and pilot plant trials to assess the product properties (Cripps-Clark and Pepper, 1981).

2.5 Location of the study area

ArcelorMittal Liberia's exploration area is located to the East-Northeast of Monrovia, in Nimba County, Yekepa, near the international boundary with Guinea and the Ivory Coast as it is shown on Figure 2.1.



Figure 2.1: Map of Liberia showing location of ArcelorMittal concession area
(Source: Hadden, 2006)

The Tokadeh iron ore deposit covering a total area of about 12 km² on longitude 4°48'41"; 4°50'49" and latitude 7°25'58"; 7°23'08" is located to the west of the Nimba Range and approximately 19 km to the southwest of Yekepa. The Nimba Range is a 45 km long, narrow northeast-southwest oriented ridge extending within Guinea and Liberia. Satellite imagery of the Nimba area clearly shows that Mt. Tokadeh is part of the Nimba mountain range, although it is located west of the 'Main' Nimba mountain range due to major folding as shown in Figure 2.2.

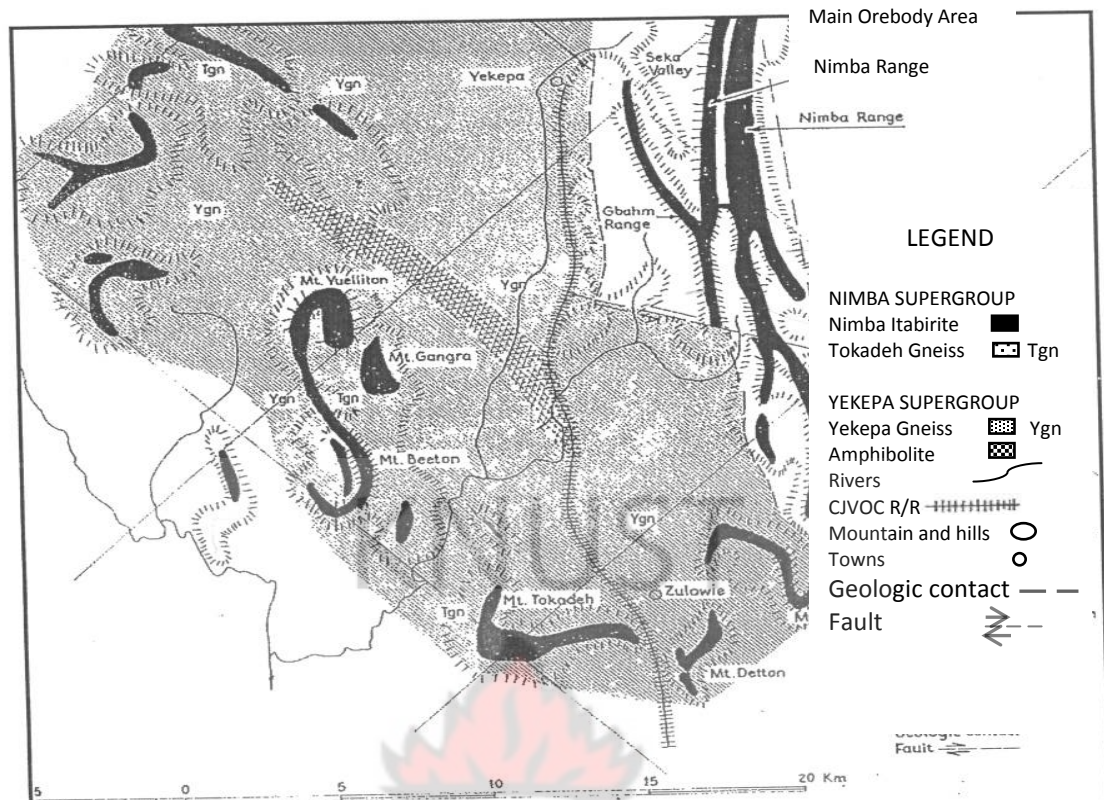


Figure 2.2: Iron ore mineralisation at the Nimba Range and “Western Area”
 (Source: Berge, 1974)

The mountains within the Western Nimba Area dominate, from an altitude of 1050 m, the undulating low-lying area at 450 m mean sea level (MSL). The Nimba Range forms part of the Eastern Area in Liberia, whereas Mount Tokadeh forms part of the Western Area which also includes Mount Beeton, Mount Gangra, and Mount Yuelliton (Buro and Alain, 2009b). The Tokadeh Mountain has an altitude of 985 m mean sea level (MSL) and consists of a ridge in the shape of an east-facing horse-shoe (Edifor, 2009).

2.5.1 History of exploration and mining of iron ore in Liberia

Liberia is a country with a history of iron ore mining and is currently viewed as one of the most prospective locations for exploration since its emergence from civil war in 2003. Liberia’s political environment has been stable for seven years and is currently attracting significant international investment, with major mining companies including BHP Billiton active in the country (Tomlinson, 2004).

The Liberia Mining Company (LMC) was the first of four iron ore companies, which produced and shipped large quantities of iron ore in the 1960s and 1970s making Liberia Africa's largest iron ore exporter and third on the world list at that time. In 1958 the National Iron Ore Company (NIOC) signed a concession agreement for the exploitation of the Mano river iron ore deposits. The Liberian American-Swedish Minerals Company Joint Venture (LAMCO JV) became operational and commenced iron ore production in 1960/61. LAMCO JV exploited the extremely rich Nimba mountains iron ore deposits. The fourth mining company, Bong Mining Company (BMC), was created following a concession agreement with German investors in 1958. The mine opened in 1965. 'Bong mine' as the company was and still is colloquially called in Liberia, was then the largest German investment in Sub-Saharan Africa (Van der Kraaij, 2010). The locations of the four mining companies that operated in Liberia at that time are shown in Figure 2.3.



Figure 2.3: Map of Liberia showing locations of past four major iron ore mining companies (Source: Van der Kraaij, 2010)

Airborne reconnaissance work done in 1957 by LAMCO JV provided the first indication of the existence of iron formations in the Western Area of Liberia which was later confirmed by field work in 1958. The deposit in Mt. Tokadeh was discovered in 1965 after conducting a comprehensive field mapping program by LAMCO geologists. The first exploration hole drilling commenced in 1966 in Mt. Tokadeh by LAMCO (Goldschmidt *et al.*, 2006). Table 2.6 presents the summary history of exploration and mining activities carried out by LAMCO JV in the Yekepa area (Buro and Alain, 2009a).

Currently, advanced exploration is being carried out in Mt. Tokadeh, to re-evaluate the iron ore deposit and re-establish iron ore production by an intensive drilling program (Chilson and Horlacher, 2008). AcelorMittal Liberia has drilled a total of 26,886 m of diamond drill core and 11,754 m of reverse circulation (RC) drill ore by the end of 2009 (Buro, 2009a).

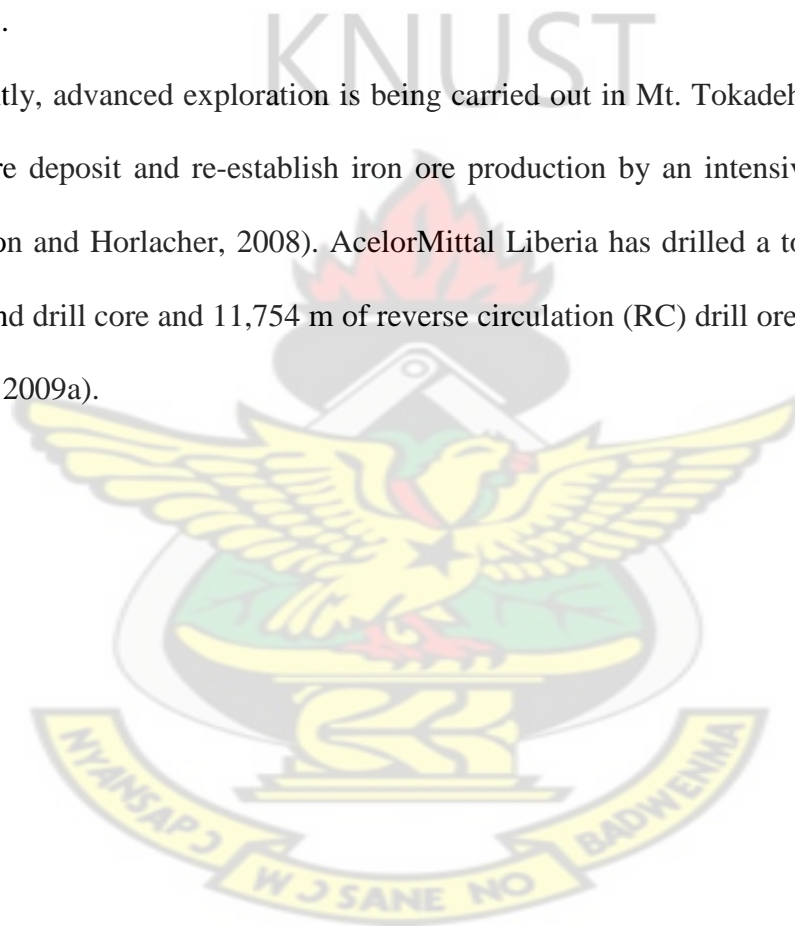


Table 2.6: Summary history of exploration and mining in the Yekepa area

Year	Activity
1953	The Liberia-American-Minerals Company granted 70 years concession for exploration
1955	Swedish Grangesbergsbolaget joins the project; company renamed Liberia-American-Swedish-Minerals Company – LAMCO Joint Venture. Iron deposit discovered in the Nimba area
1956-1957	Exploration, reserves estimate at Nimba area
1957	Airborne reconnaissance survey; discovery of iron formation in the western area
1958-1959	Bethlehem Steel company acquires participation in the project, shared with the Government of Liberia and LAMCO JV
1960-1963	The building of Yekepa community. Production of iron ore commenced at Mt. Nimba in 1963
1965	Phase I: Exploration: mapping, trenching of the Western Nimba Area including Mt. Tokadeh
1969-1979	Phase II: Core drilling (300 x 300 m) at Tokadeh, Gangra, Yuelliton, Beeton and occurrences in West Area and Northwest Extension tested. Phase III: Core drilling (100 x 100 m) on the four main deposits, tunneling, Close to 54,000 m of drilling, 3,300 m tunnels/adits (35,000 t material removed), 6,400 bulk samples
1967	Processing and pellet plant constructed by LAMCO JV
1973	Mining starts at Tokadeh (3Mt/year crude ore)
1975	Exploration starts at Gangra, Yuelliton and Beeton, resource estimate
1976	Start of engineering work on concentrator to develop Tokadeh deposit
1989-1992	Depletion of ore reserves at Nimba, start of civil war, mine closure, concession relinquished
1992-2003	No production of iron ore due to civil war
2004-2011	ArcelorMittal acquires concession and re-establishes iron ore production

(Source: Edifor, 2009)

2.5.2 Geology of the study area

The Western Nimba Area deposit is part of the Nimba Mountains straddling Liberia, Guinea and the Ivory Coast. The iron ore deposits of the Nimba Mountains are Achaean age iron formations of itabirite type and are associated with metavolcano-sedimentary formations overlying and tightly infolded into the predominantly gneissic basement complex (Coakley, 2004). The Achaean age iron formations at Western Area lie within the West African craton (Heneghan, 2010).

The Nimba Itabirite is metamorphosed to the epidote-amphibolite facies in the northeastern Liberian Nimba range and to upper amphibolite-lower granulite facies in the Tokadeh-Yuelliton ridge. Magnetite oxide-facies iron-formation is recrystallized to gray itabirite on northeastern Mt. Nimba (Berge, 1974). Facies are a body of a rock with specified characteristics and usually a distinctive unit that forms under certain conditions of sedimentation, reflecting a particular process or environment (Reading, 1996).

Chemical balances indicate that the iron-formation could have been derived by chemical weathering of the basaltic meta-volcanic rocks, which are dominant in the lower 700 m of the Nimba Supergroup (several associated formations with significant and diagnostic lithologic properties in common). The residue from such weathering would be a siliceous kaolinite $(\text{Si}_2\text{O}_5)(\text{OH})_4\text{Al}_2$, which, when transported to and deposited within a marine basin, would form an argillite (Berge, 1974).

An argillite is a fine-grained sedimentary rock composed predominantly of indurated clay particles. These rocks, although variable in composition, are typically high in alumina and silica with variable alkali and alkaline earth cations. Chemical weathering of the basaltic landmass is believed to have occurred under swampy stagnant kaolin-

forming conditions in a climate (either CO₂ -rich or reducing), which encouraged liberation of iron during weathering (Berge, 1974).

Four horizons of iron formations separated by schist-gneiss bands were recognized from the drilling and mapping program by LAMCO JV geologists. The iron formation is mainly a metamorphosed, oxide-type banded iron formation made up of an assemblage of quartz and magnetite, with ubiquitous, locally abundant iron silicates (amphibole, pyroxene). Weathering reaches depths varying from 40-70 m depending on the location. The iron formations predominantly consist of quartz and hematite/magnetite, with widespread iron silicates and minimal secondary calcite stringers in a breccia zone (Heneghan, 2010).

2.5.3 Geology of Mt. Tokadeh

The highest point of Mt. Tokadeh is 985 m mean sea level (MSL) (Edifor, 2009). The Tokadeh deposit forms part of the Nimba itabirite of about 250-450 m thick formation consisting of re-crystallized iron formation. Itabirites are laminated metamorphosed oxide-facies iron formations in which the original chert (finely grained re-crystallised quartz) or jasper bands have been re-crystallised into granular quartz and in which the iron is present as hematite (Fe₂O₃), magnetite (Fe₃O₄) or martite (pseudo morphs of Fe₂O₃) (Goldschmidt *et al.*, 2006).

High and medium grade ores are the result of tropical weathering (laterization) and the action of meteoric waters, which have leached silica with consequent enrichment of iron. Weathering alters magnetite to hematite and also produces hydrated iron oxides, such as limonite. Usually the high grade (weathered) mineralization is located on top of the iron formation (GIBC, 2011). The iron ore formation in Tokadeh consists of an oxidised top layer as well as a transitional material in the middle zone and primary ore

located at the bottom zone. Some core samples for each of the three zones are shown in Figure 2.4.

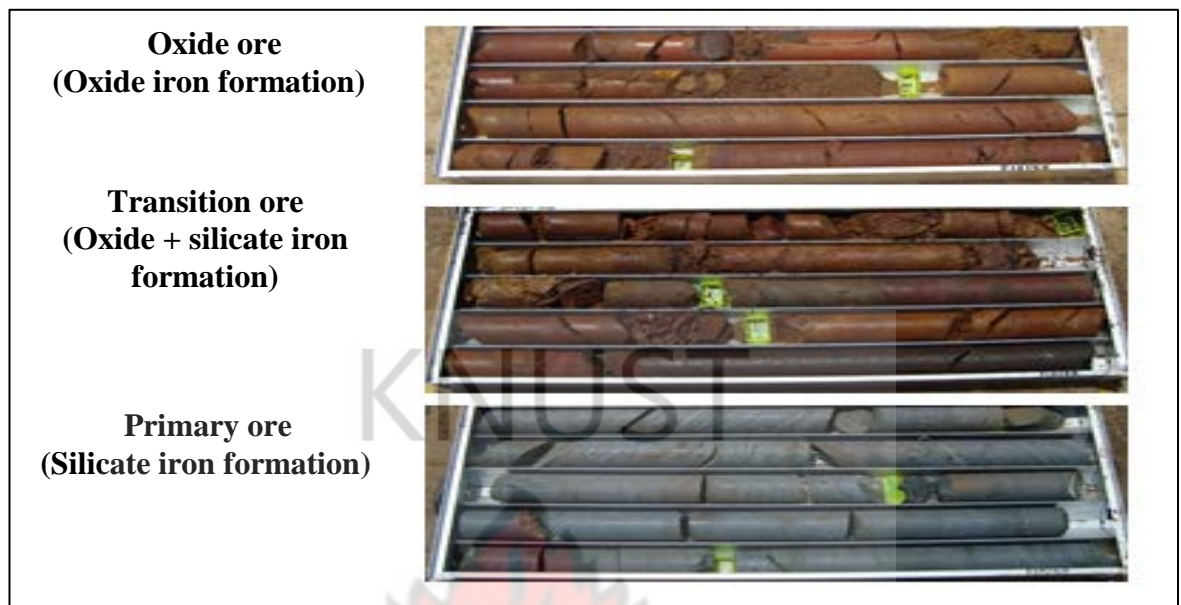


Figure 2.4: Types of iron formation in Mt. Tokadeh (Source: Edifor, 2009)

2.5.4 Mineralogy of Mt. Tokadeh iron ore deposit

The gradual depletion of high-grade iron ores has necessitated the exploitation of low grade iron ore reserves all over the world. The role of geochemical and mineralogical characterization is paramount to arrive at the process flow sheet for beneficiation such ores (Roy and Das, 2008).

According to Force (1983, citing Berge, 1966, 1968, 1971-1972, 1974) the Nimba supergroup contains the oxide facies Nimba itabirite. Different depositional conditions produced both a simple oxide and a carbonate- and silicate-bearing oxide facies. Metamorphic grade ranges from greenschist facies to pyroxenegrnulite facies, as indicated by the assemblages of actinolite-chlorite and orthopyroxene-garnet (Force, 1983).

The iron formation in Mt. Tokadeh deposit consist of itabirite, a fine grained banded quartz-hematite rock of Precambrian age and sedimentary origin, formed as precipitates

in shallow off-shore basins. Fine grained quartz chlorite-mica schists (called phyllites) are in contact with the itabirite. The deposit is flanked on the sides by other metamorphous sedimentary rocks and gneiss of the Liberian-Guinean Precambrian Shield (ATKINS, 2005).

Medium-hard and hard ores are distinguished from soft ores on the basis of mineralogical, structural, and physical characteristics. Medium-hard ores consisting of compact but uncemented euhedral magnetite and hard ores consisting of compact cemented subhedral magnetite are of synmetamorphic origin. (Berge *et al.*, 1977). The three ore zones formations in Mt. Tokadeh have been defined as 'soft' (with density of 2700 kg/m^3), 'medium-hard' (density 2700 kg/m^3) and 'hard' (density 3500 kg/m^3), in order of increasing depth from the surface (ATKINS, 2005). Iron content distribution of each of the ore zones within the deposit decreased with increasing depth, with the soft oxidised iron formation containing relatively the highest amount of iron and the hard iron formation with the relatively lowest iron content. The general stratigraphy of Mt. Tokadeh is presented in Table 2.7.

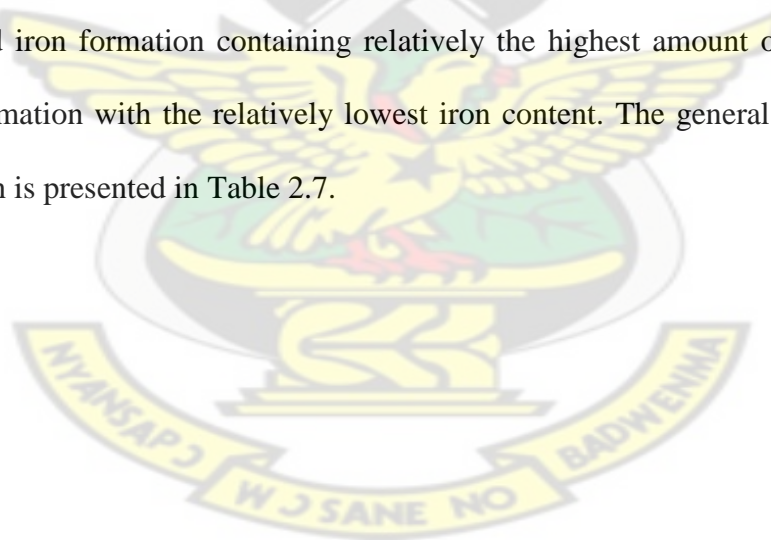


Table 2.7: Mt. Tokadeh general stratigraphy

Stratigraphic position	Formation	Approximate thickness, m
Highest	Oxide iron formation	Unknown
	Gneiss	30
	Oxide iron formation	40
	Gneiss	10-40
	Oxide iron formation	30-90
	Silicate iron formation	0-50
	Gneiss	10-60
	Silicate iron formation, interbedded with schist	0-90
	Oxide iron formation	40-135
	Silicate iron formation, interbedded with schist	0-60
	Tokadeh Gneiss	Unknown
Lowest		

(Source: ATKINS, 2005)

The 'hard ore' is steel grey coloured fresh iron ore formation with iron content between 30-42%, while the 'medium hard' ore is a partially weathered hard ore, which contains both loose and hard material. The 'medium hard' ore is inherently soft and powdery in nature and contains very high percentage of fines with iron content of 42-48%. The 'soft ore' is soft, light grey in colour, earthy, has low specific gravity and non-crystalline in nature. Typically it has high iron content, extremely weathered and contains mixtures of oxy-hydroxides of iron and silicate gangue material (Buro and Alain, 2009a).

Detailed mineralogical studies conducted on samples from the Mt. Tokadeh iron ore deposit using particle mineralogical analysis (PMA) techniques; quantitative evaluation of minerals by scanning electron microscopy (QEMSCAN) and x-ray diffraction (XRD) indicate magnetite as the major iron oxide mineral with minor amounts of hematite, goethite, martite, limonite and iron silicate with quartz as major gangue. Trace amounts

of pyrite, and iron carbonates have also been reported from the microscopic study with the quartz grains only present as inclusions within the hematite and magnetite grains (Boudrias-Chapleau, 2009).

Qualitative mapping and quantitative particle mineralogical analysis on these ores indicated the presence of gibbsite $[Al(OH)_3]$ as the only aluminium bearing phase and apatite $[Ca_5(PO_4)_3(F,Cl,OH)]$ as phosphorous bearing mineral. Traces of alumina, present as solid solution in the iron oxide minerals, has also contributed Al_2O_3 to the ores. Electron microscopic studies revealed the gibbsite grains are in the size range of 10-50 μm and are intimately and intricately associated with the iron oxide phases (Boudrias-Chapleau, 2009).

The economical minerals present in the weathered and transitional zones are mainly iron oxides containing more than 50% hematite and magnetite. They also contain more than 20% of goethite. The gangue minerals correspond to variable quantities of quartz and traces of aluminium oxides/hydroxides, clay minerals and chlorite. The distribution of the economical iron minerals (iron oxides and iron oxy-hydroxide/hydroxide) is 84% and 95% for the transition and oxide ores, respectively (Buro and Alain, 2009b).

The gangue minerals in the primary zone are mainly quartz and iron-magnesium silicates or calcium-iron-magnesium aluminium silicates. The iron-magnesium silicates mainly correspond to amphibole (assumed grunerite-cummingtonite) and/or orthopyroxene. The calcium-iron-magnesium (aluminium) silicates mainly correspond to actinolite. Other gangue minerals in minor and in trace quantities are feldspars, mica, iron-magnesium-potassium silicates and carbonates. The amount of economical iron minerals (iron oxides and iron oxyhydroxide/hydroxide) in the primary ore zone is 64% (Buro and Alain, 2009b).

2.6 Iron ore mining

The two main mining techniques used to extract iron ores from their deposits are surface and underground methods. The decision to employ underground or surface mining techniques depends on the proximity of the ore body to the surface (US EPA, 1994).

Surface mining is the predominant of the two mining techniques. It consists of the open-pit and open-cut methods. Open pit and open cast mining accounts for about 96% of non-metal minerals, 87% of metallic ores and 60% of coal production in the world. Surface mining is the most common exploitation method producing nearly 85% of all minerals, excluding petroleum and natural gas. Surface mines of iron ore extract 0.5-30 Mt/year.

Underground methods are employed when the depth of the deposit, the stripping ratio of overburden to ore or both become excessive for surface exploitation. Underground mining of iron ore is still being carried out in a few large, well established deposits in some parts of the world, for example in the Kiruna Mine in Sweden (Ferenczi, 2011) and Kumba's Thabazimbi Mine in South Africa (Howard, 1987).

2.7 Iron ore processing

Iron ore is converted into iron through processes of beneficiation and extraction. Most high grade iron ores can be sent directly to iron extraction plants without beneficiation activities other than crushing and washing, but low grade ores must be beneficiated to upgrade the iron content.

Methods of ore and mineral treatment generally involve mechanical and chemical processes. Mechanical methods include hand-picking, wet concentration, dry concentration, amalgamation, magnetic separation, electrostatic separation and flotation (Ferenczi, 2011). Chemical methods include smelting and the use of solutions of

chemical agents to dissolve valuable minerals from ore material. Beneficiation improves both physical and chemical characteristics of the final iron concentrate.

The ore excavated from the mine site is usually crushed using different types of crushers, followed by screening to obtain three basic products as follows: (1) 1-4 cm size fraction, which is used as lump ore in blast furnaces, (2) an intermediate fraction (<1 cm) for sintering, and (3) fines below 150 μm size, that is either rejected or used to make pellets, often after beneficiation to increase the iron content to over 65%, since the gangue in iron ore gets concentrated in the 'fines' fraction (Ghosh and Chatterjee, 2008).

High-grade iron ore is usually crushed and screened to provide direct lump feed of 6-30 mm in size and sometimes fines feed of less than 6 mm in size. The fines can be processed to produce either high-grade sinter (agglomerated fines) or pellets. Low-grade iron ore (e.g. magnetite BIFs, some iron skarns, proximal hydrothermal and oolitic deposits) is usually beneficiated and upgraded by gravity separation, magnetic separation, and/or floatation of the ore minerals, followed by sintering or pelletising (Ferenczi, 2011).

Iron ore is being beneficiated all around the world to meet the quality requirements of iron for the steel industries. However, each source of iron ore has its own peculiar mineralogical characteristics and requires the specific beneficiation and metallurgical treatment to get the best product out of it. The choice of the beneficiation treatment depends on the nature of the gangue present and its association with the ore structure (Taylor, 1997).

2.7.1 Crushing and grinding

The 1-1.25 m lumps excavated at the mine are reduced to a maximum size of 2-4 cm for rich ores and to a size which may be as small as 45 μm for certain low grade ores, to enable high grade concentrate to be obtained. The first stage of crushing produces particles of 15-25 cm in size. Both gyratory and jaw crushers can be used as primary crusher. Factors considered in determining the degree of ore crushing include the concentration of the iron in the ore, its mineralogy, hardness, and moisture content (Taylor, 1997)

The second stage of crushing, which is usually carried out using cone or gyratory crushers, may be carried out in a single operation if the aim is to produce a material in the size range of 3-5 cm. If the ore must be ground fine for concentration, it is usually done by rod or ball mills or combination of both down to particle size of approximately 1-2.5 cm. Rod mills grind the larger particles preferentially and so produce a smaller proportion of very fine particles, followed by an initial concentration, after which further grinding in ball mill is carried out.

Grinding systems employed in most operations include, autogenous or semi-autogenous (SAG) grinding systems. Autogenous grinding uses coarse pieces of the ore itself as the grinding media in the mill. Semi-autogenous operations use metallic balls and/or rods to supplement the grinding action of the ore pieces. Autogenous grinding is best suited to weakly cemented ores containing some hard material (Taylor, 1997).

2.7.2 Concentration methods

There are many methods normally used to separate iron oxide from gangue minerals such as, gravity method, magnetic separation, and reduction roasting followed by magnetic separation, floatation and electrostatic separation. In addition to these methods, some degree of concentration can be achieved by washing (DeVaney *et al.*,

1985). Concentration of valuable minerals from gangue involves exploitation of the differences in the mineral properties of the ore after effective comminution (Olubambi and Potgieter, 2005).

Washing

Sometimes ores can be enriched by the simple process of washing such ores that consist of coarse and fine particles of clean ore minerals mixed with either barren sand or clay. In general, clay minerals increase the alumina in iron ore which is easily reduced by washing. Separation of clay minerals consists of a simple scrubbing operation in a log-washer or classifier followed by a screening operation to remove the coarser iron ore particles, whereas the overflow usually is the waste product.

Gravity separation

The common iron oxides are usually heavier than the waste minerals, so they can be separated by their differences in specific gravity. Jigging is one of the oldest methods of gravity concentration in which the feed is kept in motion by water pulsing vertically through it. The heavier grains move downwards to the bottom of the bed and are removed. Since the weight of the grain is governed by its size as well as its density, it is necessary for the feed to be sized within close limits (DeVaney *et al.*, 1985).

Many kinds of jigs exist according to the size and the nature of the ore. For fine ore with particle size of 1-1.5 mm, Humphrey's spirals are now largely used and have taken the place of the shaking tables; because they have relatively high capacity and also low maintenance requirements. The ore is washed down a spiral launder with a curved bottom. The valuable fine concentrate moves to the bottom of the curved track whilst the lighter tailings climb toward the outer rim (Mular *et al.*, 2002).

Magnetic separation

Magnetic separators exploit the difference in magnetic properties between the ore minerals and are used to separate the magnetic minerals (magnetite, in some application hematite) from non-magnetic gangue such as quartz. Magnetic separators can be classified into low- and high-intensity machines, which may be further classified into dry-feed and wet-feed separators (Mular *et al.*, 2002).

When the mineral is magnetite, low-intensity (500-1200 G) separation is normally practiced because it is relatively cheap and effective. If the particles are of comparatively large size (greater than 6 mm), dry magnetic separations is used. When the particles are less than 100 μm in size, wet magnetic separation is used. If the size of the ore is intermediate, it is possible to use either method. High-intensity (1200-22000 G) separators can be used to separate weakly magnetic materials, such as hematite and hydrated hematite from gangue materials, for both wet and dry iron ores (Mular *et al.*, 2002).

Wet high-intensity magnetic separation has its greatest use in the concentration of low grade iron ores containing hematite, which frequently replaces flotation methods, although the trend towards magnetic separation has been slow in North America, mainly due to the very high capital cost of such separators (DeVaney *et al.*, 1985). Magnetic separation techniques are used to beneficiate over 90% of all iron ores in the world, but 20-35% of all the iron ores being beneficiated today is lost to tailings because hematite is only weakly magnetic (US EPA, 1994).

Froth flotation

Froth floatation is a selective process and can be used to achieve specific separation from complex ores. This process utilizes the differences in physicochemical surface properties of particles of various minerals. After treatment with reagents, such

differences in surface properties between the minerals within the floatation pulp become apparent and, for floatation to take place, an air-bubble must be able to attach itself to a particle, and lift it to the water surface.

Froth floatation can effectively be used to upgrade low grade iron ores to high iron ore concentrates. For floatation to take place, the particle size should be at least 250 μm . Fatty acids or petroleum sulfonates can be used as collector in anionic floatation to float fine iron oxides, such as magnetite, hematite, or siderite away from waste minerals such as quartz or chert. Cationic floatation may be used to upgrade fine concentrate by floating the gangue minerals away from the iron minerals (Kelly and Spottiswood, 1989).

The efficiency of froth floatation process decreases when slime is apparent. Magnetic separation and floatation are the most widely accepted technologies for the concentrating of iron ore particles, however, these processes result in iron concentrate with high amounts of very fine and/or interlocked silica particles (Kelly and Spottiswood, 1989).

Electrostatic separation

Electrostatic separation is limited to relatively few iron ores. The major process makes use of the differences in electrical conductivity between iron oxides and gangue minerals. It works best on crystalline, nonmagnetic iron oxides finer than about 1.7 mm and coarser than 75 μm . The minerals surfaces should be free from slime or dust coating (DeVaney *et al.*, 1985).

2.7.3 Fine iron ore processing

Fine iron ores are not suitable as direct feed to the blast furnace because they tend to pack into a non-permeable bed or their fine particles are likely to be carried away as dust by the high gas flow rates. Fine iron ores must therefore be agglomerated into

larger particles that will improve permeability of the furnace burden, increase throughput, and reduce the amount of material blown out of the furnace as dust.

Agglomeration is a size enlargement process which involves combining small size particles to create products with new larger particle sizes. Products can come in many different forms such as granules, tablets, briquettes, pellets, sinters, bricks, or compacts. The resulting entity is only apparently a new unit but the original solid particles are still present in the structure, often with completely unaltered shape and size, and are held together by binding mechanisms. Agglomeration processes may involve the application of pressure or thermal methods to iron ore fines with materials such as bentonite, limestone and dolomite (Pietsch, 2008).

2.8 Iron ore characterisation

Until the 1970s, the raw materials for steel plants were statistically and empirically determined. The control on iron ore blends was exercised only by chemical composition, especially SiO_2 , Al_2O_3 and alkali contents. Other properties of iron ore like, porosity and pore size distribution, pseudo-particle formation characteristics, fusibility or assimilation characteristics were not being considered. Superior requirements on iron ore characteristics and several abnormalities in plant operation necessitated detailed examination of iron ores.

Iron ore characterization is a very important method in quantitative classification of mineral deposits and all other steps in process flow sheet development. Without proper understanding of the ore characteristics of the deposit, it may be impossible to develop a successful process flow sheet. Iron ore characterization provides information for proper understanding of the mineralogical as well as the chemical nature of the ore (Venugopal *et al.*, 2005).

2.8.1 Chemical characterisation

Samples are subjected to chemical analyses to determine their quantitative chemical composition (Mishra *et al.*, 2007). Wet chemical methods of analysis are destructive methods used in chemical mineral assay. Some of the wet chemical methods include classical volumetric, gravimetric, and colorimetric analysis. Classical volumetric and gravimetric methods of analysis are used principally for the determinations of the higher concentrations of various elements in ores and concentrates. Colorimetric methods of analysis are used for trace element analysis.

X-ray fluorescence (XRF) analysis is a nondestructive analytical technique used for the determination of elemental concentration of samples. It provides rapid elemental identification and quantification of solids, liquids and loose powders. XRF spectrometers are capable of measuring elements from beryllium (Be) to uranium (U) and beyond at trace levels, often from below 1 ppm up to 100%. XRF spectrometers measure the characteristic wavelength of the fluorescent emission produced by a sample when irradiated with X-rays. ISO 9516 is an international standard method that describes the calibration and elemental analysis of iron ore using the fusion method. The method focuses on the determination of a full range of major, minor and trace elements. Some of the elements, which are usually determined in iron ores include iron (Fe), silicon (Si), aluminum (Al), magnesium (Mg), calcium (Ca), sodium (Na), potassium (K), titanium (Ti), manganese (Mn), phosphorus (P), chromium (Cr) and sulphur (S) (Kamarudin and Ibrahim, 2012)

2.8.2 Physical and mineralogical characterisation

Physical and mineralogical characterization of iron ore identifies major minerals, gangue minerals and their association as well as grain size in the different ore phases. The mineralogy of iron ore varies from quite simple hematite and quartz with little of

aluminum mineral to hydrated hematite along with complex gangue minerals like hydrated aluminum silicate or kaolinite ($\text{Al}_2\text{Si}_2\text{O}_5(\text{OH})_4$) and trihydrated aluminium oxide or gibbsite ($\text{Al}(\text{OH})_3$).

The hematite can be partially hydrated as in goethite $\text{FeO}(\text{OH})$ or deoxidized as in magnetite Fe_3O_4 . In some ore bodies the quartz is the predominant gangue mineral and for all practical purposes aluminium minerals are absent. Some ore bodies, on the other hand, may contain mainly magnetite and only very little hematite. The gangue minerals may vary from simple to complex types as above. The extend of hematite or magnetite, total iron content, and any of the impurities vary from source to source (Venugopal *et al.*, 2005)

Macroscopic study is done with unaided eye, with hand lens and/or with stereomicroscopy to gather information on the ore deposit. Physical characteristics, which can be obtained from macroscopic study include crystalline or amorphous nature of the ore, whether it is soft, hard and flaky, or dust ore material. The magnetic characteristics of an iron ore deposit can also be determined using a magnetic pen.

Microscopic study is done with a microscope to gather information of the mineral composition of the ore deposit. Microscopic study identifies the major minerals present in the ore body and grain size of each component, which is useful for metal liberation studies.

Thermal analysis involves the study of the changes in the weight of the sample as a function of time and temperature. Thermal analysis of iron ore gives an indication of its thermal stability, composition of intermediate compounds that may be formed, and the final residue that is left behind after exposure to any given temperature for a given duration. Thermal methods are used for characterizing a system (element, compound or

mixture) by measuring changes in physico-chemical properties at elevated temperature as a function of increasing time.

Two main thermal analysis techniques, differential thermal analysis and thermogravimetric analysis, provide information about physical phenomena, such as second-order phase transition, including vapourisation, sublimation, absorption, adsorption, and desorption. Likewise, thermal analysis can provide information about chemical phenomena including chemisorptions, desolvation (especially dehydration), decomposition, and solid-gas reactions (for example, oxidation or reduction). Thermogravimetric analysis is commonly used to determine selected characteristics of materials that exhibit either mass loss or gain due to decomposition, oxidation or loss of volatile matter (such as moisture) (Coats and Redfern, 1963).

2.9 Magnetic material content determination by Davis tube method

The Davis tube tester provides separation based on magnetic susceptibility of the sample, which measures the amount of ferromagnetic mineral present in the iron ore. Magnetite content measurement by the Davis tube method is used for the assessment of the separation characteristics of magnetic ores, which measures the performance of wet drum magnetic separators (Mular *et al.*, 2002). Since the Davis tube method provides essentially perfect separation, any diluents (silica and alumina) in the magnetite concentrate occur as locked particles.

The Davis tube tester shown in Figure 2.5 is a laboratory-size instrument designed to separate samples of magnetic ores into strongly magnetic and weakly magnetic fractions. The magnetic content of both fractions is determined after the separation. The Davis tube tester consists of an extremely powerful electromagnet, which can generate a magnetic field intensity of up to 4000 Gauss, a glass separation tube and a motor driven

agitation mechanism. The tube is positioned between the poles of an electromagnet at an adjustable angle of approximately 45°.



Figure 2.5: Davis Tube Tester (Source: Own photograph)

During operation, a small electric motor drives the agitating mechanism that supports the water filled glass tube. The tube moves forward and backward while it rotates simultaneously. Any magnetic particles present in the sample inside the tube are collected in the zone of intense magnetism. A vigorous washing action by agitation is applied to these magnetic particles. Eventually all non-magnetic particles are flushed from the tube and a clean concentrate of magnetic particles is collected for further determination. The total iron content of the magnetic material concentrate is determined by chemical analysis but this does not represent total iron content of an ore (Mular *et al.*, 2002).

2.10 Magnetite content measurement by SATMAGAN

Accurate measurement of ferrous material content in iron ores is extremely difficult and time-consuming by conventional chemical methods. Ferrous material content in iron ores can be measured by measuring the total magnetic moment of the sample in a high

magnetic field, thereby measuring the total magnetic material content in the sample. The magnetic material present in the iron ore is determined as magnetite content of the ore.

The principle behind the Saturation Magnetization Analyzer (SATMAGAN) is to measure the force acting on the sample in a magnetic field with a spatial gradient. Figure 2.6 presents a photograph of the equipment. SATMAGAN is a magnetic balance in which the sample is weighed in gravitational and magnetic fields. If the field is strong enough to saturate the magnetic material in the sample, the ratio of the two weights is linearly proportional to the amount of magnetic material present in the sample.

SATMAGAN has been used in the mining industry around the world, and has been proven to be a fast, accurate and reliable instrument with a measuring time of about 1 min and accuracy of 0.4% or less (Sarangi and Sarangi, 2011). The analyser can be used to measure the magnetite content in iron ores, concentrates and tailings. SATMAGAN can also be used to measure any sample with only one magnetic component as well as component with dominant concentrations and/or dominant specific magnetic moment.



Figure 2.6: Saturation Magnetization Analyser (Source: Instrument user manual)

The operation of the SATMAGAN is based on measurement of the magnetic moment m after the magnetic component in the sample has been magnetized for saturation. The total magnetic moment is:

$$m = VM_{\text{sat}}$$

where V = volume of the magnetic component in the sample, m^3

M_{sat} = saturation magnetization of the magnetic component, J/Tm^3 (T = Tesla)

In the SATMAGAN, the magnetic moment is determined by measuring the force acting on the sample in a non-homogeneous magnetic field, a field having a vertical gradient of (dH/dz) , and comparing it with the gravitational force acting on the sample:

$$\frac{F}{G} = \frac{M_{\text{sat}} \left(\frac{dH}{dZ} \right) M_m}{\rho g M_{\text{tot}}}$$

where F = magnetic force, N

G = gravitational force (weight), N

g = gravitational acceleration = 9.81 m/s^2

M_{tot} = total mass of the sample, kg

M_m = mass of the magnetic component in the sample, kg

ρ = density of the magnetic component, kg/m^3

dH/dz = spatial gradient (magnetic field that varies in intensity over distance)

The percentage of magnetic material in the sample is thus: (Malley, 2002)

$$\left(\frac{M_{\text{sat}}}{M_{\text{tot}}} \right) \times 100 = \frac{F \rho g}{M_m \left(\frac{dH}{dZ} \right) G} \times 100$$

2.11 X-ray diffractometric analysis

X-ray diffraction (XRD) analysis is used to identify the minerals and crystalline phases present in geological specimens and processed materials. About 95% of solid materials are crystalline, which means that they have a regular three-dimensional distribution (lattice) of atoms.

When an X-ray beam of a particular wavelength (usually Cu K_{α}) hits a set of planes in a lattice, it is diffracted at a particular angle and produces a peak in the diffraction pattern. The set of peaks produced for a particular phase can be used to identify it. Multiple phases can exist in one sample simultaneously.

An XRD pattern of a sample is the summation of diffraction patterns from each phase in that sample. This allows the identification of phases in the sample from their diffraction patterns. The amount of each phase in a mixture will relate to the strength of its signal in the final pattern and this allows the quantification of phases in mixtures. XRD is an important technique in mineral processing because it is the mineralogy rather than the chemistry that in general controls the mineral processing. (Madsen and Scarlett, 2010)

2.12 ArcelorMittal proposed iron ore beneficiation plant

The ArcelorMittal proposed concentrating plant is designed to produce 15 Mt/year of concentrate, which requires treating 23 Mt/year (2015-2017) of oxide and 30 Mt/year (2018-2026) of transition crude ores, respectively, from the Tokadeh-Gangra deposits. A relatively fine particle size (< 1 mm) of the ore is required to achieve a marketable concentrate grade of 65% Fe, and hence concentrate production will consist entirely of washed fines. The product specification for the proposed plant is presented in Table 2.8

Table 2.8: Final product specification for the proposed magnetic separation plant

Component	Concentration, %
Fe	> 66.5
SiO ₂	< 3.0
Al ₂ O ₃	< 1.0
Mn	< 0.02
P	< 0.07

(Source: Boudrais-Chapleau, 2009)

The ore minerals are a mixture of magnetite, martite and hematite. In addition, hydrated minerals, i.e. goethite and limonite, are also identified to a greater extent in the oxide ore. The gangue minerals are predominantly quartz and different aluminum minerals of which hydrargillite (Al(OH)₃) and boehmite (γ -AlO(OH)) are identified and other silicates such as amphiboles, biotite and feldspars. Most significantly, much of the iron in magnetite is also bound to hematite, therefore, the appropriate beneficiation flow sheet is a combination of grinding the ore and low or medium intensity magnetic and gravity separation (Buro and Alain, 2009c).

2.12.1 Process description

A simplified overall block diagram of the ArcelorMittal proposed beneficiation process is shown in Figure 2.7. The ore will be delivered to the primary crusher dump hoppers by mine trucks. An apron feeder will withdraw the ore to a scalping grizzly ahead of a jaw crusher. The crushed ore with particle size of about 175 mm will be feed to the primary ball mill by apron feeders and a conveyor belt. Primary grinding will reduce the ore particle size to about 6 mm by wet milling.

The product from the primary ball mill will be passed through 6 mm screens and the oversize will be returned to the primary ball mill by means of a lifter and a return trough with a water jet. The undersize will be pumped to the primary low intensity magnetic

separators (LIMS). The primary LIMS concentrate will flow by gravity to a secondary ball mill. The primary LIMS tailings will go to a hydrocyclone, which will separate and send the 200 μm oversize particles to the tailing thickener, while the underflow ($< 200 \mu\text{m}$) will be pumped to the process water reservoir.

The primary LIMS concentrate will be ground in a ball mill to its final liberation fineness of about 80% below 44 μm . The ball mill will operate in closed circuit with secondary low intensity magnetic separators and classifying hydrocyclones. The ball mill discharge will flow to a pump-box from where it will be pumped to the secondary LIMS. The pumps will have variable frequency drives. Pump box level will be controlled by water addition. Slurry density will be monitored by a density meter in the pump discharge line, which will vary pump speed. The secondary LIMS tailings will flow by gravity to the tailings thickener. The secondary LIMS concentrate will flow by gravity to the respective classifying hydrocyclone feed pump-box. The hydrocyclone underflow will flow by gravity back to the ball mill. The hydrocyclone overflow is the secondary grinding circuit product and will flow to the respective de-sliming hydro-separator.

The de-slimer is a tank where siliceous slimes are separated from the fine magnetite particles based on the difference of their specific gravity. The de-slimer is controlled to overflow only the slimes leaving only the magnetite, which moves to the tertiary magnetic separator for the removal of non-magnetic fine particle.

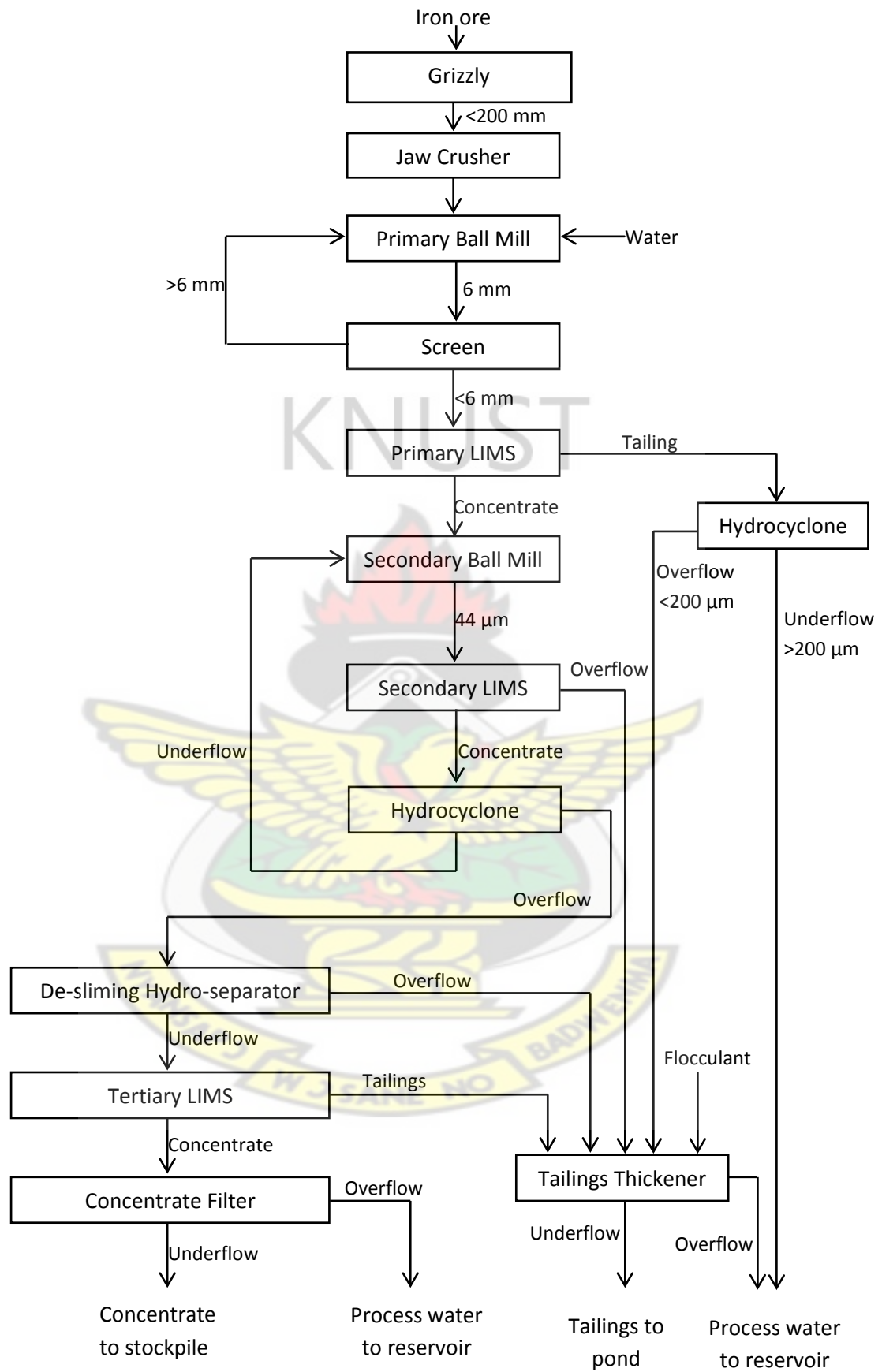
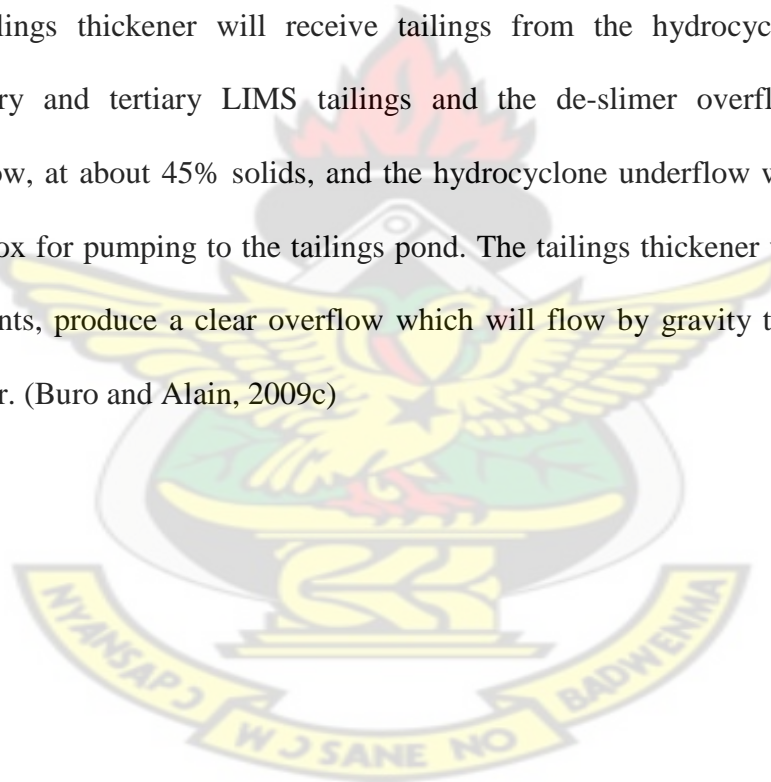


Figure 2.7: Proposed process block diagram

The tertiary magnetic separator tailings will flow by gravity to the tailings thickener. The tertiary magnetic separator concentrate is the final product and will flow to the concentrate thickener.

The tertiary magnetic separator concentrate will be thickened to 70% solids in the concentrate filter using disc filters. The density of the underflow will be controlled by recirculation. The thickener overflow will flow by gravity to the process water reservoir. The filter cake, at about 9% moisture, will drop onto a belt conveyor and will be transported to a stock pile ahead of train loading.

The tailings thickener will receive tailings from the hydrocyclone overflow, the secondary and tertiary LIMS tailings and the de-slimmer overflow. The thickener underflow, at about 45% solids, and the hydrocyclone underflow will be pumped to a pump-box for pumping to the tailings pond. The tailings thickener will, with the aid of flocculants, produce a clear overflow which will flow by gravity to the process water reservoir. (Buro and Alain, 2009c)



CHAPTER THREE

MATERIALS AND METHODS

3.1 Sampling

Sample collection from the study area of Mt. Tokadeh for this research conformed to the ASTM E877-08 “Standard practice for sampling and sample preparation of iron ores and related materials for determination of chemical composition”. This practice covers procedures for mechanical sampling of iron ores and related materials, and preparing the gross sample to the various test samples required for each characteristics to be measured. Design criteria to prevent bias during sampling and statistical methods to determine quality variation and precisions were used (ASTM, 2008).

Samples were collected, dried, blended, divided, crushed, pulverized, and ground as required. Sample analysis was performed in the laboratory of ArcelorMittal Liberia and SGS geochemical laboratory in Monrovia, which were both well equipped for iron ore sample preparation and analysis.

3.2 Drilling for sample collection

Drilling is a critical important activity in the exploration and evaluation of an iron ore deposit. Basic information on potential valuable occurrence of iron ore deposits can be established through drilling and analysis of drill samples. Ore dimension, grade distribution, chemical, and physical nature of ore can also be determined, which is useful in evaluating ore processing needs of the ore deposit (Kennedy, 1990). Other methods that can be used to generate samples for iron ore testing include trenching, test pitting, adits/tunnels and shafts. Sampling intervals for drill hole material can be 0.5–2 m, depending on the average thickness of the ore zone.

Diamond drill rigs equipped with wire line system to retrieve, mostly conventional core size (HG=71 mm diameter) and wireline core sizes (HQ=63.5 mm and NQ=47.6 mm), core samples using single tube core barrels were used at Mt. Tokadeh to drill ore sites for sample collection (see Figure A1 in the Appendix). A total of 10 holes at varying depths were drilled. The minimum and maximum drill hole length was 30 and 275 m, respectively.

The cylindrical core samples were divided for 1 m lengths and stored in a variety of 2, 3 or 4 m long plastic, wooden or metal trays. Physical properties such as core recovery, rock type, colour, hardness, structural data, weathering, mineralogical assemblage, textural profile and grain size of the core sample were examined and recorded. Tables A1-A5 in the Appendix present physical data of the core recovered from the drilled holes, while Tables A6-A13 present the codification system adopted by ArcelorMittal Liberia. The drill holes were labeled serially and the location coordinates were measured in the Universal Transverse Mercator (UTM) system.

The azimuth is the angle formed between a reference direction (usually north) and a line from the observer to a point of interest projected on the same plane as the reference direction. The intervals for the oxide, transition and primary ore zones were identified and marked appropriately for each drill hole. A map of Mt. Tokadeh showing location of sample collection points is shown in Figure 3.1 and the drill hole data is presented in Table 3.1. The total core length for each of the oxide, transition and primary ores recovered from each drill hole was measured and presented in Figure 3.2.

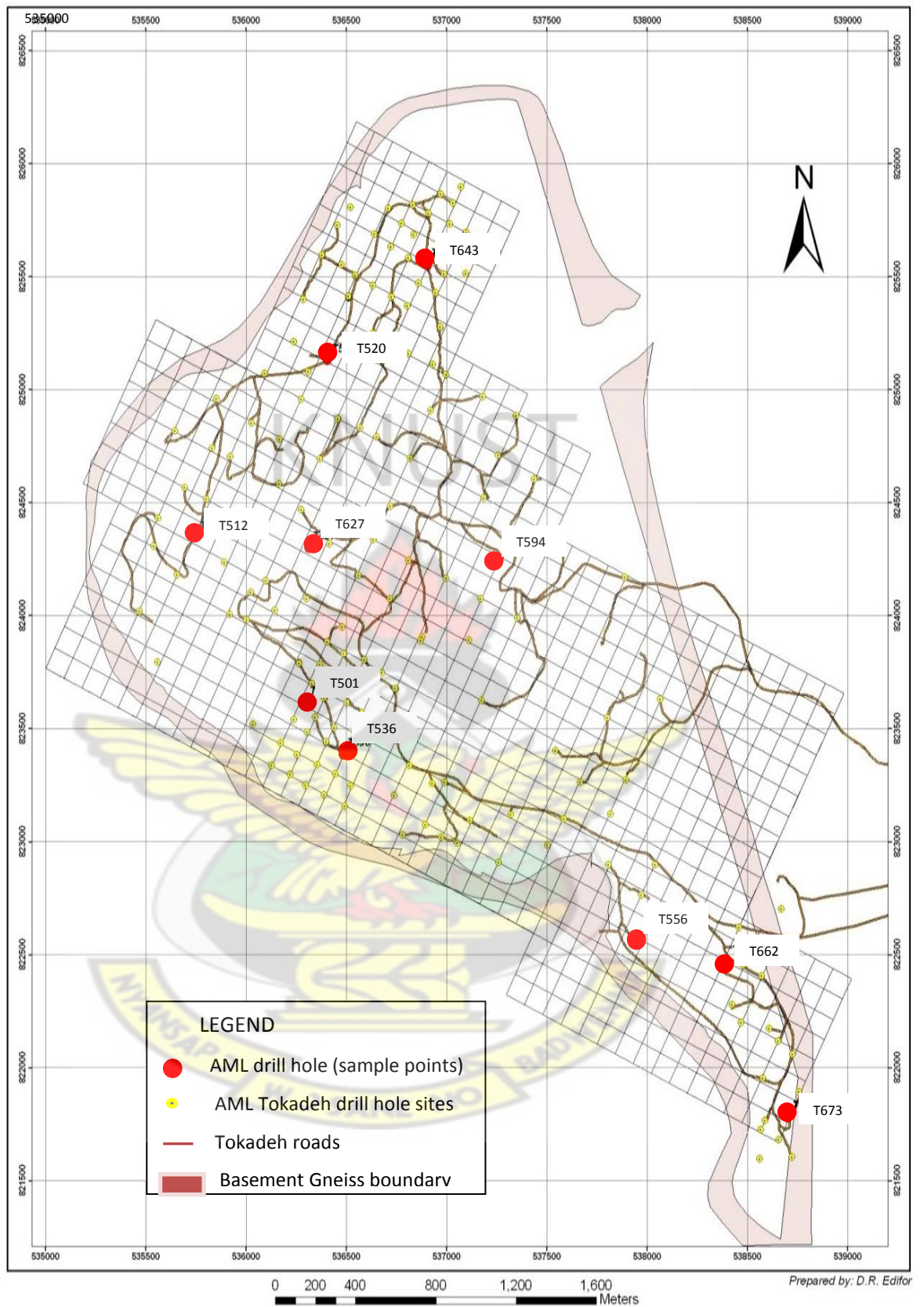


Figure 3.1: Map of Mt. Tokadeh showing sample collection points

(Source: Edifor, 2012)

Table 3.1: Drill hole data

Drill hole ID	Coordinates			Dip, °	Azimuth, °	Total depth, m	Oxide ore			Transition ore			Primary ore		
	X (UTM)	Y (UTM)	Z				From, m	To, m	Interval, m	From, m	To, m	Interval, m	From, m	To, m	Interval, m
T501	536297	823614	832	-60	207	100	0	25	25	25	52	27	52	100	48
T512	535750	824345	765	-90	0	249	0	10	10	10	28	18	28	249	221
T520	536407	825128	705	-90	0	275	0	53	53	53	95	42	95	275	180
T536	536486	823385	824	-90	0	113	0	53	53	53	73	20	73	113	40
T556	537970	822560	709	-90	0	88	0	42	42	42	58	16	58	88	30
T594	537263	824254	537	-90	0	30	0	6	6	6	25	19	25	30	5
T627	536314	824299	653	-90	0	54	0	30	30	30	49	19	49	54	5
T643	536903	825550	682	-90	0	66	0	34	34	34	60	26	60	66	6
T662	538402	822468	551	-90	0	44	0	34	34	34	42	8	42	44	2
T673	538703	821778	596	-90°	0	74	0	26	26	26	59	33	59	74	15

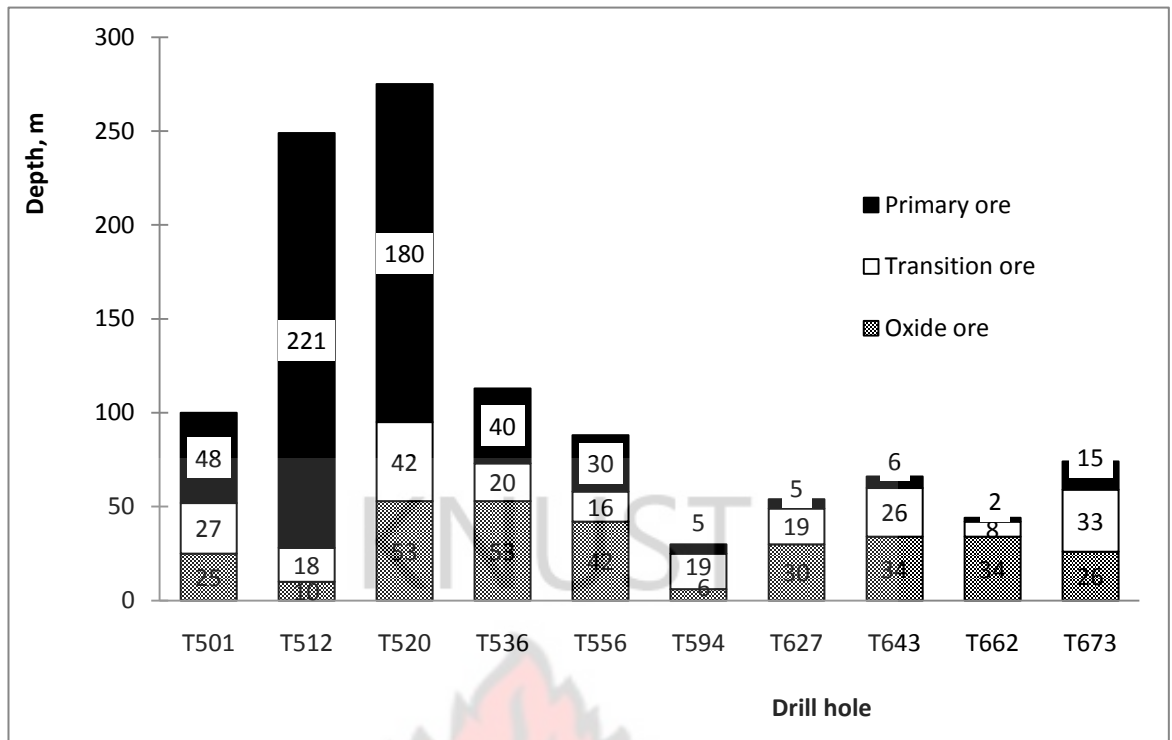


Figure 3.2: Drill hole chart

3.3 Core sample splitting

The cylindrical core samples were split into two mirror-image halves with a Corstor Core Splitter. One of the split halves was broken down to particle size of about 5-7 cm with a geological hammer and sampled at 2 m intervals, avoiding physically identified waste, to form one sample of between 10-15 kg. Summary of resulting samples for the 10 drill holes is presented in Table 3.2.

Table 3.2: Core lengths and number of samples

Drill hole ID	Core length, m				Number of samples			
	Oxide ore	Transition ore	Primary ore	Total	Oxide ore	Transition ore	Primary ore	Total
T501	25	27	48	100	12	14	24	50
T512	10	18	220	249	5	9	110	124
T520	53	43	180	275	26	21	90	137
T536	53	20	40	113	27	10	20	57
T556	42	15	30	88	21	8	15	44
T594	6	19	6	30	3	9	3	15
T627	30	19	5	54	15	10	2	27
T643	34	26	7	66	17	13	3	33
T662	34	8	2	44	17	4	1	22
T673	26	33	14	74	13	17	7	37
Total	313	228	552	1093	156	115	275	546

3.4 Sample grinding

Sample grinding is the process of converting sample with large particle size from the field or mine into finely divided homogenous powders suitable for chemical analysis or other testing. This is accomplished by the mechanical reduction of the particle size in a stepwise sequence, alternating with the reduction of sample volume or mass by an unbiased splitting process (Howard, 1987).

Each 10-15 kg sample was placed in a 40x30x5 cm stainless steel pan and dried in an ESSA DO2 electric drying oven at a temperature of $105 \pm 5^{\circ}\text{C}$ till constant mass. Constant mass is obtained when an additional hour of drying at $105 \pm 5^{\circ}\text{C}$ did not cause a change greater than 0.05% mass (ASTM, 2008). Each dried sample was crushed to particle size of about 6-8 mm with a Morse 4000, 8"x 8" laboratory jaw crusher. Secondary crushing of each sample was done with an ESSA RC2000 rolls crusher to achieve sample particle size of about 2 mm.

Each 10-15 kg of 2-mm particle size sample was then homogenised and repeat split in a Jones Riffle Splitter, adjustable, 720x360x680 mm to obtain 5 sub-split samples of about 300 g each for further grinding. The split sample remainders were stored in plastic bags for future use. Each sub-sample was put in an ESSA B800 grinding bowl with a disc, well secured with a bowl lid and pulverised in an ESSA LM2-P pulveriser for 2, 4, 6, 8 or 10 min. The pulverised sub-samples were wet screened with 200, 150, 106, 100, 75, 63, 53 and 45 µm sieves. The particle size distribution was determined by measuring the masses retained on each sieve.

3.5 Composite sample preparation

The 300 g pulverised samples for each drill holes were composited for the oxide, transition and primary ore zones according to their grinding time. This resulted in 30 samples for each of the 5 different grinding times of 2, 4, 6, 8 and 10 min as it is presented in Table 3.3. A total of 150 composite samples resulted by this process.

3.6 Loss on ignition determination

About 1 g each the pulverized composite sample was weighed into a ceramic crucible using a Sartorius GK3102 balance with 0.001 g accuracy. The composite sample was then placed in a pre-heated Modutemp SC142BM automatic furnace at 950°C for 1 hour. The sample was removed from the furnace and cooled in a Pyrex glass dessicator containing silica gel for 30 min and weighed. The lost on ignition (LOI) was calculated as a percentage change in mass of the composite sample as follows:

$$LOI = \frac{(W_1 - W_2)}{W_1} \times 100, \quad \%$$

where W_1 = initial mass of the composite sample, g

W_2 = final mass of the composite sample, g

Table 3.3: Composite samples for a particular grinding time

Drill hole ID	Number of core samples				Number of composite samples			
	Oxide ore	Transition ore	Primary ore	Total	Oxide ore	Transition ore	Primary ore	Total
T501	12	14	24	50	1	1	1	3
T512	5	9	110	124	1	1	1	3
T520	26	21	90	137	1	1	1	3
T536	27	10	20	57	1	1	1	3
T556	21	8	15	44	1	1	1	3
T594	3	9	3	15	1	1	1	3
T627	15	10	2	27	1	1	1	3
T643	17	13	3	33	1	1	1	3
T662	17	4	1	22	1	1	1	3
T673	13	17	7	37	1	1	1	3
Total	156	115	275	546	10	10	10	30

3.7 Fused bead preparation

ISO 9516 is an international standard method that describes the elemental analysis of iron ore using fusion method. The method was first proposed by the ISO panel in 1989 as one of an alternative method for the old ISO 2597 – ISO 2599 that utilized a number of conventional analytical techniques (titrimetric and gravimetric) in the determination on the quality of natural iron ore (Kamarudin and Ibrahim, 2012).

About 1 g of each pulverised composite sample and 10 g of pre-mix flux (12:22 of $\text{Li}_2\text{B}_4\text{O}_7:\text{LiBO}_2$) was weighed into a platinum-gold crucible using a Sartorius GK3102 balance with 0.001 g accuracy. The sample was then fused in a pre-heated Modutemp SC142BM automatic furnace at 1200°C for 10 min. The melt from the crucible was poured into a 40 mm diameter pre-heated platinum-gold mould and cooled with in-built fan propelled air.

3.8 Chemical analysis

Two basic classes of assay methods are available for the analysis of geological samples: geochemical and quantitative assays. Geochemical procedures typically are used in prospecting and the early stages of exploration when results of high accuracy and precision are not as necessary, but low levels of detections are required. Quantitative procedures are used during exploration drilling, sampling and analysis for ore reserve estimation, and subsequent stages of mine development and operation.

Elemental composition of the fused samples was determined using a Panalytical Axios^{mAX} X-ray fluorescence spectrometer as shown in Figure A2 in the Appendix. Elements determined were iron (Fe), silicon (Si), aluminum (Al), magnesium (Mg), calcium (Ca), sodium (Na), potassium (K), titanium (Ti), manganese (Mn), phosphorus (P), chromium (Cr), and sulphur (S).

3.9 Magnetic material content determination by Davis tube tester

The magnetic material content of each pulverized sample was measured with an Eriez Davis Tube Tester shown in Figure 2.5. About 20 g of sample was filled into the glass separation tube of the tester. The tube was positioned between the poles of the electromagnet at an angle of approximately 45°. The tube was operated with a magnetic field intensity of 4000 G and 1.0 L/min wash water flow rate, causing all the magnetic particles present in the sample inside the tube to be collected in the zone of intense magnetism. The non-magnetic particles were received from the tube and filtered to obtain the tailing and a clean concentrate of magnetic particles was collected for further chemical analysis. The conditions for the Davis tube operation are presented in Table 3.4.

Table 3.4: Conditions for Davis Tube separation

Parameter	Value
Tube diameter	38 mm
Number of strokes	120/min
Inclination of the Tube	45°
Test time	10 min
Water flow	1.0 L/min
Feed mass	20 g
Current intensity	1.5 A
Voltage	60 V
Field strength	4000 Gauss

The concentrates and the tailings were analysed to determine their Fe, SiO₂ and Al₂O₃ content by XRF method.

The separation efficiency by the Davis tube method can be characterized by the mass recovery. It can be calculated as

$$MR = \frac{M_{conc.}}{M_{sample}} \times 100, \quad \%$$

where MR = mass recovery, %

M_{conc.} = mass of concentrate (magnetic material) obtained, g

M_{sample} = mass of sample, g

Based on the mass recovery, the recovery of the different components can be calculated as well:

$$Fe_{recovery} = \frac{Fe_{conc.}}{Fe_{sample}} \times MR, \quad \%$$

$$(SiO_2)_{recovery} = \frac{(SiO_2)_{conc.}}{(SiO_2)_{sample}} \times MR, \quad \%$$

$$(Al_2O_3)_{recovery} = \frac{(Al_2O_3)_{conc.}}{(Al_2O_3)_{sample}} \times MR, \quad \%$$

where

$Fe_{recovery}, SiO_2_{recovery}, Al_2O_3_{recovery}$ = the amount of components in the concentration, %

$Fe_{conc.}, SiO_2_{conc.}, Al_2O_3_{conc.}$ = concentration in the concentrate, %

$Fe_{sample}, SiO_2_{sample}, Al_2O_3_{sample}$ = concentration of component in the sample, %

3.10 Magnetite content measurement by SATMAGAN

First the sample cell was filled with about 10 g pulverised composite sample and closed with the plug and then inserted into the holder. The sample was weighed by bringing the balance of the equipment into equilibrium with a potentiometer. Then the magnet was turned with a crank handle. The magnetic force acting on the sample was compensated by bringing the balance into equilibrium with the potentiometer again. The reading of the potentiometer is, in the first approximation, directly proportional to the mass fraction of the magnetite in the sample.

A calibration curve was established by measuring three standard magnetite samples with different magnetite concentrations. The output reading from the Satmagan was a linear function of the magnetite content of the sample. After preparing the calibration curve, the mass fraction of magnetite in the ore samples was read from the calibration curve.

CHAPTER FOUR

RESULTS AND DISCUSSION

4.1 Composite sample concentration

The chemical analysis results on the composite samples from the oxide, transition and primary ore zones are presented in Tables 4.1 and 4.2, and Figure 4.1. Figure 4.2 shows the average concentration values for the three ore zones. We can observe that the iron concentration is generally the highest, 39.6-56.0%, in the oxide ore zone and the lowest, 34.4-41.1% in the primary ore zone in each of the core samples. The oxide zone is enriched by continual removal of gangue minerals, such as silica, by downward movement of water, which is also evident in the low silica concentration observed in this zone. An average of 46.6% iron content is observed for the oxide ore zone, 39.1% and 38.3% for the transition and primary ores respectively. The iron concentration increases with decreasing silica content for all the ores.

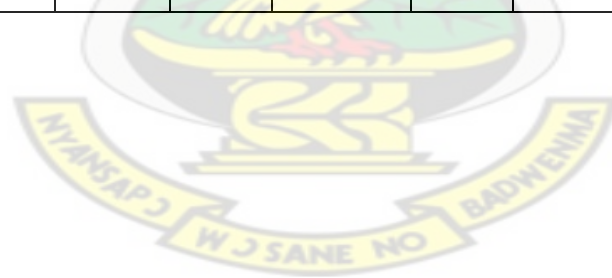
The silica concentration is, however, very high in the primary ore zone as the iron formation is predominantly silicate (Buro, 2009a). The concentration of silica is observed to gradually increase from the oxide ore zone with an average of 22.4% to 40.4% in the primary ore zone. The intense surface weathering causes the lighter silica minerals in the oxide ore zone to be freed from the iron minerals and become available for transport to other destinations. Silica content ranges from 7.6-33.8% in the oxide ore zone to 37.6-43.3% in the primary ore.

Table 4.1: Chemical composition of composite samples

Ore zone	Sample Number	Chemical composition, %												
		Fe	SiO ₂	Al ₂ O ₃	MgO	CaO	Na ₂ O	K ₂ O	TiO ₂	MnO	P ₂ O ₅	Cr ₂ O ₃	S	LOI
Oxide	Ox-T501	56.0	15.9	0.7	0.10	0.01	0.13	0.01	0.02	0.12	0.18	0.02	0.01	3.3
	Ox-T512	42.3	28.6	5.5	0.08	0.03	0.03	0.03	0.27	0.04	0.18	0.06	0.04	5.5
	Ox-T520	39.6	17.7	15.0	0.10	0.08	< 0.10	0.03	0.37	0.02	0.14	0.04	0.04	10.4
	Ox-T536	52.7	21.3	1.0	0.12	0.02	0.04	0.02	0.03	0.09	0.18	0.01	0.01	2.7
	Ox-T556	45.4	33.8	0.8	0.00	0.02	0.02	0.01	0.02	0.05	0.12	0.04	0.01	1.0
	Ox-T594	44.1	22.9	5.3	0.05	0.00	< 0.10	0.01	0.15	0.03	0.11	0.00	0.03	8.3
	Ox-T627	44.2	23.7	6.3	0.07	0.13	0.00	0.44	0.29	0.06	0.16	0.06	0.04	6.2
	Ox-T643	50.2	24.4	0.8	0.02	0.00	< 0.10	0.00	0.00	0.13	0.23	0.00	0.01	2.7
	Ox-T662	44.6	28.6	3.0	0.03	0.00	< 0.10	0.01	0.07	0.06	0.17	0.00	0.03	4.2
	Ox-T673	46.5	7.6	13.5	0.05	0.01	< 0.10	0.04	0.40	0.04	0.20	0.02	0.06	12.8
	Average	46.6	22.4	5.2	0.06	0.03	0.04	0.06	0.16	0.06	0.17	0.03	0.03	5.7
Transition	Tr-T501	44.2	32.4	0.9	0.99	0.65	0.17	0.31	0.03	0.08	0.23	0.02	0.01	3.0
	Tr-T512	44.0	35.9	0.6	0.42	0.22	0.17	0.09	0.01	0.06	0.09	0.06	0.16	0.5
	Tr-T520	30.3	42.3	4.7	1.61	1.72	0.26	0.57	0.11	0.12	0.22	0.02	0.12	5.3
	Tr-T536	37.3	41.8	0.5	0.65	0.16	0.25	0.02	0.08	0.18	0.01	1.00	3.68	0.0
	Tr-T556	39.3	40.6	0.3	0.78	0.30	0.15	0.19	0.01	0.03	0.10	0.00	0.02	2.1
	Tr-T594	44.0	34.0	0.6	0.04	0.01	< 0.10	0.00	0.00	0.01	0.17	0.00	0.02	2.3
	Tr-T627	38.9	38.3	0.4	0.71	0.29	0.15	0.54	0.02	0.04	0.13	0.00	0.04	3.9
	Tr-T643	43.7	29.5	1.4	0.04	0.05	< 0.10	0.25	0.05	0.04	0.33	0.00	0.01	5.8
	Tr-T662	33.3	44.5	2.3	3.77	1.36	0.07	0.31	0.07	0.07	0.22	0.00	0.02	-0.3
	Tr-T673	36.3	43.2	0.5	0.58	0.30	< 0.10	0.51	0.02	0.01	0.09	0.00	0.04	3.2
	Average	39.1	38.2	1.2	0.96	0.51	0.17	0.28	0.04	0.06	0.16	0.11	0.41	2.6

Table 4.2: Chemical composition of composite samples (continued)

Ore zone	Sample Number	Chemical composition, %												
		Fe	SiO ₂	Al ₂ O ₃	MgO	CaO	Na ₂ O	K ₂ O	TiO ₂	MnO	P ₂ O ₅	Cr ₂ O ₃	S	LOI
Primary	Pr-T501	41.1	39.2	0.2	1.51	1.23	0.24	0.15	0.01	0.07	0.18	0.02	0.02	-0.8
	Pr-T512	38.1	41.6	1.0	2.12	1.86	0.46	0.56	0.04	0.08	0.16	0.02	0.05	-1.3
	Pr-T520	38.7	41.2	0.6	2.21	2.08	0.32	0.38	0.02	0.09	0.17	0.03	0.04	-1.5
	Pr-T536	40.2	39.0	0.7	2.11	2.00	0.41	0.37	0.03	0.09	0.17	0.01	0.11	-1.5
	Pr-T556	38.5	41.3	0.6	2.19	2.12	0.27	0.30	0.02	0.09	0.16	0.02	0.03	-1.1
	Pr-T594	39.1	42.2	1.4	2.21	2.11	0.44	0.48	0.06	0.10	0.16	0.03	0.04	-1.4
	Pr-T627	39.1	37.6	0.2	1.57	1.57	0.64	0.57	0.00	0.04	0.10	0.00	0.05	1.8
	Pr-T643	39.0	38.7	5.4	1.17	0.89	0.21	0.57	0.04	0.03	0.24	0.00	0.08	4.3
	Pr-T662	34.8	39.8	2.0	2.97	0.88	< 0.10	0.07	0.06	0.06	0.21	0.00	0.07	4.2
	Pr-T673	34.4	43.3	0.7	0.93	0.55	< 0.10	0.53	0.03	0.05	0.13	0.00	0.05	3.3
	Average	38.3	40.4	1.3	1.90	1.53	0.37	0.40	0.03	0.07	0.17	0.01	0.05	0.6



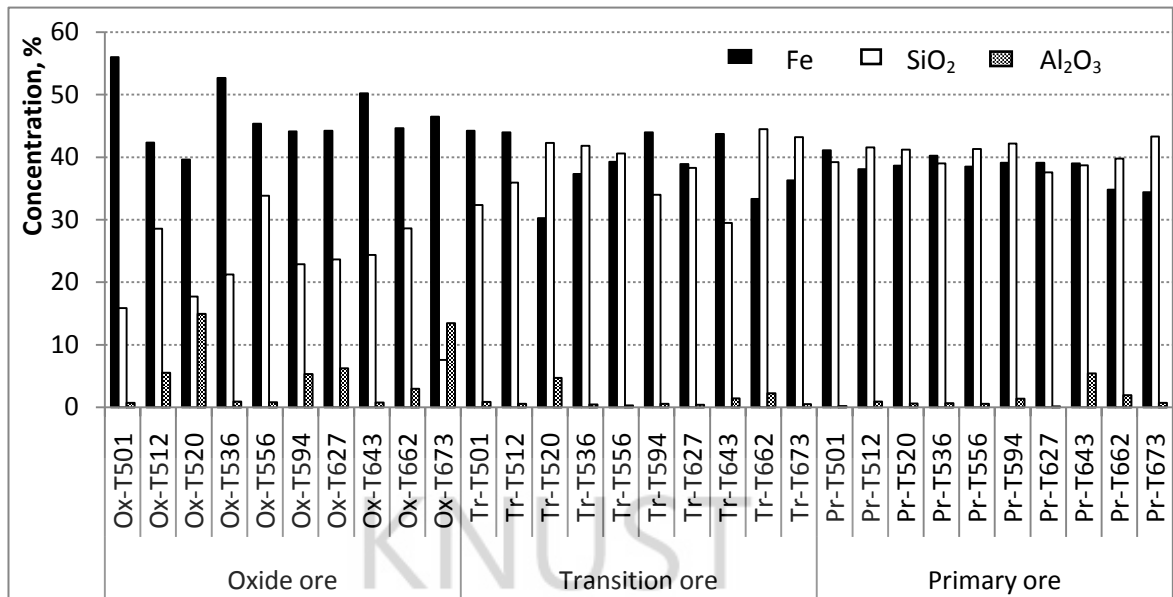


Figure 4.1: Concentration of composite samples

The alumina content varies from 0.8-15% in the oxide ore to 0.2-5.4% in the primary ore. The Al₂O₃ content is relatively high, 3-15% with an average of 6.8% for the following composite samples: Ox-T512, Ox-T520, Ox-T594, Ox-T627, Ox-T662, Ox-T673, Tr-T520, Tr-T662 and Pr-T643. It is suspected that canga, which forms a capping on Mt. Tokadeh deposit may explain the relatively high alumina content in the above samples. Canga is the iron oxide crust deposit that contains variable amounts of cherty iron-formation and iron ore fragments cemented by goethite and hematite. The term canga may also be applied to similar deposits that occur extensively as residual crusts of hematite and goethite on outcropping iron-formation (Kennedy, 1990). The canga formation in Mt. Tokadeh is usually thin (a few meters), which only occurs at the surface and characterized by relatively higher Al₂O₃ content values.

The higher Al₂O₃ values in the canga formation cannot, however, be used to explain the high Al₂O₃ results for the composite sample over a distance of 40 m or greater as in the case of transition and primary ore zones. The higher Al₂O₃ values in some of the composite samples from the transition and primary ore zones are suspected to be caused

by the presence of certain zones within the Mt. Tokadeh deposit, which contain aluminium minerals like biotite $[K(Mg,Fe)_3AlSi_3O_{10}(F,OH)_2]$ and garnet schists. (Boudrais-Chapleau, 2009)

The graphical presentation of the average Fe, SiO₂ and Al₂O₃ concentrations for all composite samples from the oxide, transition and primary ores is shown in Figure 4.2

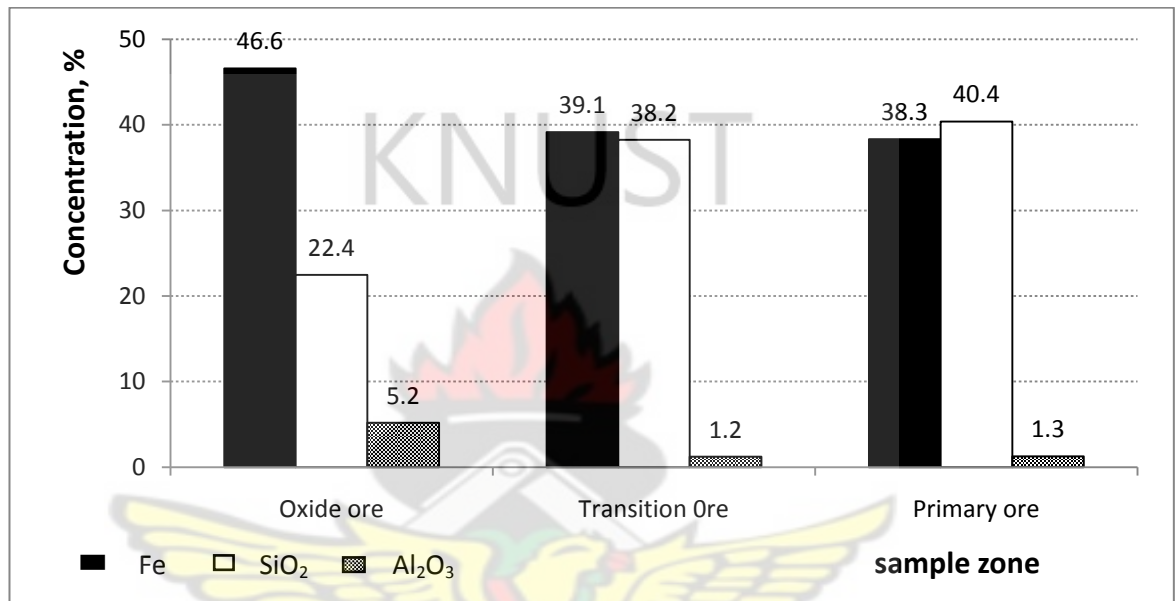


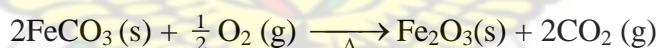
Figure 4.2: Average concentration of composite samples

The concentration of the other elements expressed as oxides in the composite samples is generally very low (< 0.2%) in the oxide ore zone. The concentrations of MgO and CaO in the primary ore zone are observed to be high, averaging 1.90% and 1.53%, respectively. The MgO and CaO content generally increases from the oxide to the primary ore zones (0.06%, 0.96%, 1.90% MgO and 0.03%, 0.51%, 1.53% CaO for the oxide, transition and primary ores, respectively).

Higher loss on ignition (LOI) values is observed for composite samples from the oxide zone compared to those in the transition and primary ores. The oxide ore recorded an average of 5.7% LOI compared with 2.6 and 0.6% for the transition and primary ores,

respectively. From Tables 4.1 and 4.2, it can be observed that LOI results vary from 1-12.8% in the oxide ore to (-1.5)-5.8% in the transition and primary ores. The LOI values are very high for those composite samples, which also have very high Al₂O₃ content in the oxide ore. An increase in sample mass after ignition was however, observed for some samples from the transition and primary ores (Tr-T662, Pr-T501, Pr-T512, Pr-T520, Pr-T536, Pr-T556 and Pr-T594) resulting in negative LOI values. Samples with high MgO and CaO concentrations in the primary ore zone also have GOI (gain on ignition) instead of LOI.

The negative LOI values in these ore zones indicate that the amount of weight loss at ignition is relatively lower than the amount of mass gained by the conversion of lower molecular mass compounds to higher molecular mass compounds during ignition as shown in the reactions below (Norman and Alan, 1997)



Due to the escape of volatiles (such as H₂O⁺, CO₂, F, Cl, S), there will be a decrease in mass among all other oxides, however, by oxidizing FeO to Fe₂O₃, the total number of Fe₂O₃ molecules increases. The resulting increase in the total number of Fe₂O₃ molecules gained from oxidation subsequently increase the mass of the sample after ignition, which thus explains the negative LOI values in some samples from the transition and primary ores. The primary ore, which is predominantly magnetite (FeO·Fe₂O₃), is therefore observed to have weight increase during ignition for 60% of the study samples due to the oxidation of FeO to Fe₂O₃.

4.2 Particle size distribution

Grinding is a very important step in the beneficiation processes since not only the size of the ground particle generated in grinding plays an important role, but also the grinding process is the most energy intensive among all other processes during beneficiation. Due to these reasons, modeling and thereby optimization of grinding operation of industrial scale has been tried very extensively by mineral researchers (Rao and Misra, 2004).

The cumulative particle size distribution for the composited samples (oxide ore, transition ore, and primary ore) are presented in Table 4.3 and Figures 4.3-4.7 for the different grinding times of 2, 4, 6, 8 or 10 min. It can be observed from Figure 4.3 that 2 min grinding time was sufficient to reduce 95% of the particles to pass through a 150 μm sieve. From Figure 4.4, 4 min was needed to achieve the same results for 106 μm size for all the three ore types. The 6 min grinding time was only able to produce 95% of the 90 μm sieve undersize particles. Figures 4.6 and 4.7 show that the 8 and 10 min grinding times were sufficient to reduce 95% of particles to pass through the 75 and 63 μm sieves, respectively.

It clearly shows from the grinding curves, that it is easier to grind the oxide ore than the others and the most difficult to grind is the primary ore. This is due to the fact that the primary ore zone contains high amount of silica and lower amount of iron in a hard rock.

Table 4.3: Particle size analysis of composited samples

Composited sample	Grinding time, min	Cumulative undersize, %							
		200 μm	150 μm	106 μm	100 μm	75 μm	63 μm	53 μm	45 μm
Oxide ore	2	100	96.9	89.7	86.8	56.5	42.2	32.1	23.0
Transition ore		99.7	95.4	86.1	83.2	50.3	38.5	28.0	21.1
Primary ore		99.1	94.7	81.3	78.8	47.3	32.4	21.1	15.0
Oxide ore	4	100	100	96.7	93.7	56.5	42.2	32.1	23.2
Transition ore		100	100	95.9	91.9	50.3	38.5	28.0	21.1
Primary ore		100	99.6	95.7	90.8	40.3	28.3	20.1	15.2
Oxide ore	6	100	100	100	99.7	90.5	80.3	65.2	48.8
Transition ore		100	100	100	99.0	89.6	79.8	50.0	30.6
Primary ore		100	100	100	98.7	88.7	58.2	36.9	20.4
Oxide ore	8	100	100	100	100	96.5	85.3	68.2	49.8
Transition ore		100	100	100	100	95.7	80.8	61.0	35.6
Primary ore		100	100	100	100	94.9	78.6	52.9	25.4
Oxide ore	10	100	100	100	100	100	97.5	88.2	69.8
Transition ore		100	100	100	100	99.7	95.8	81.0	65.6
Primary ore		100	100	100	100	99.0	95.6	78.0	60.3

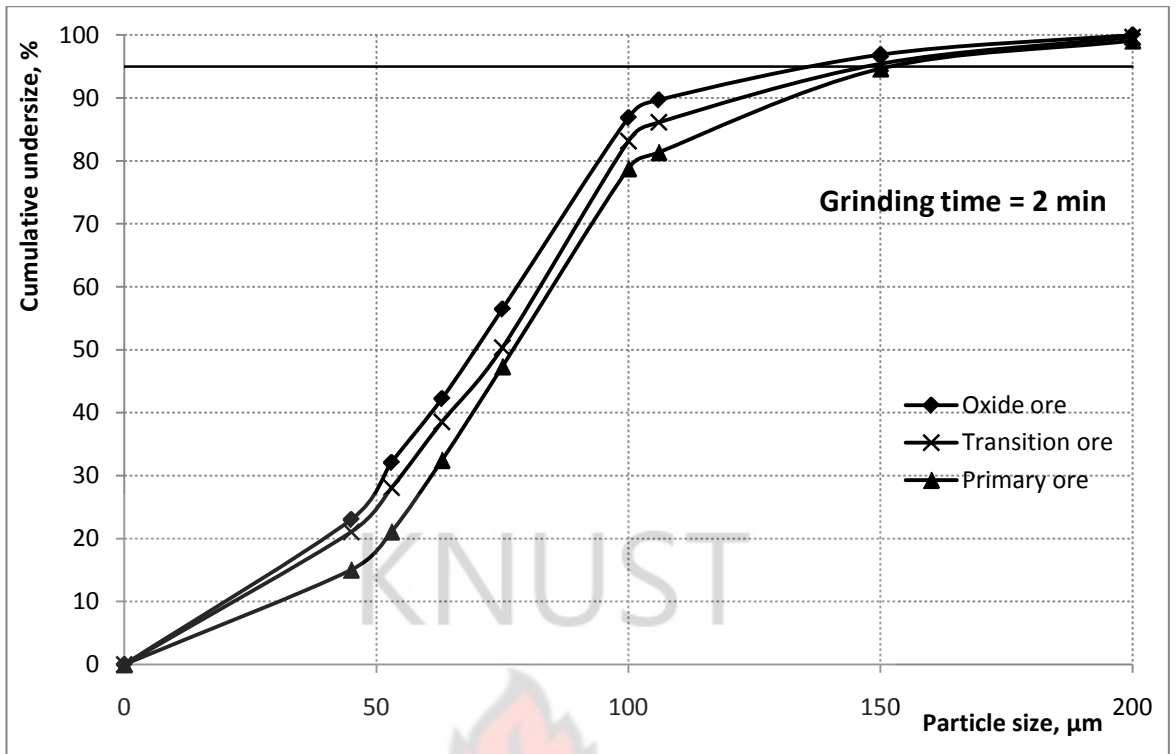


Figure 4.3: Particle size distribution for 2 min grinding time

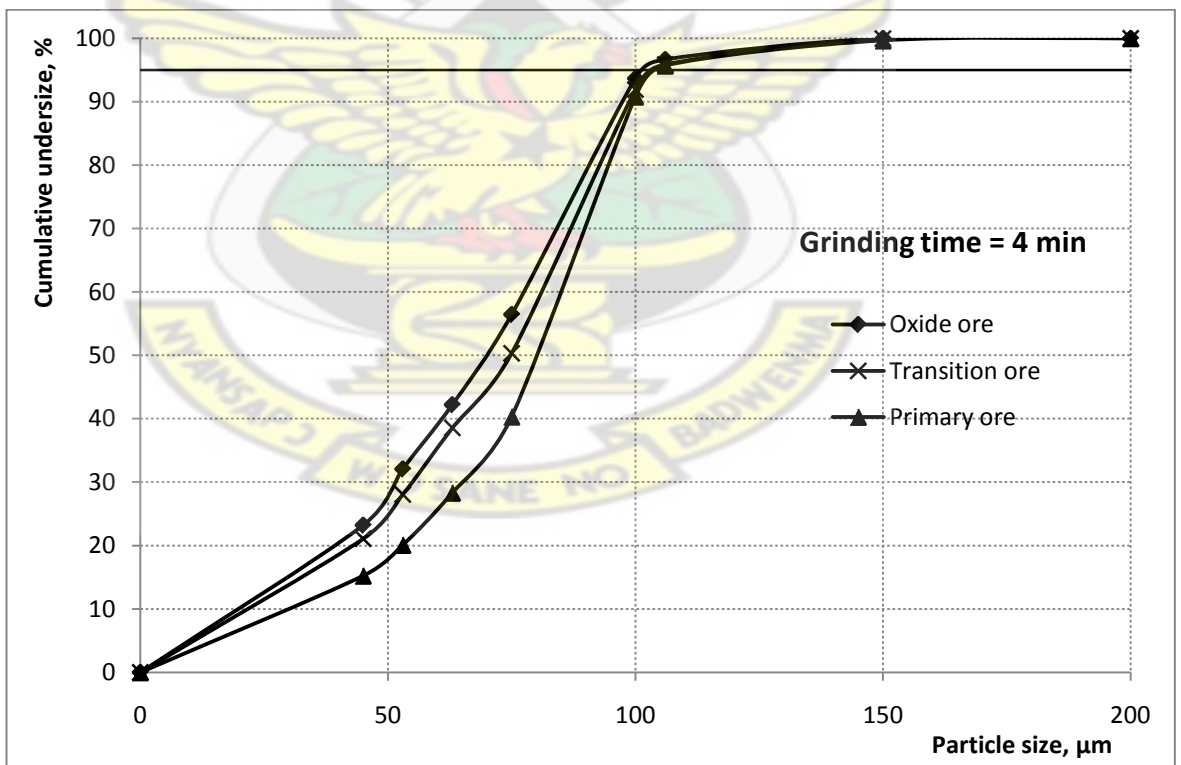


Figure 4.4: Particle size distribution for 4 min grinding time

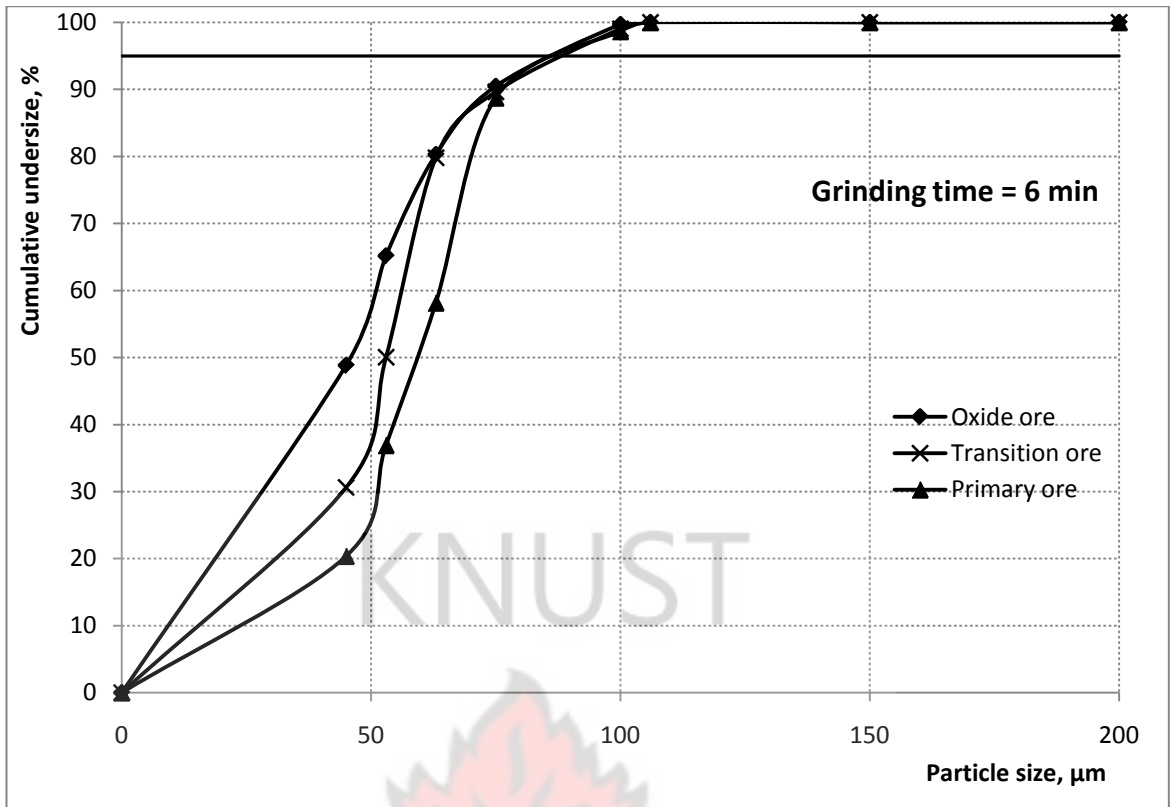


Figure 4.5: Particle size distribution for 6 min grinding time

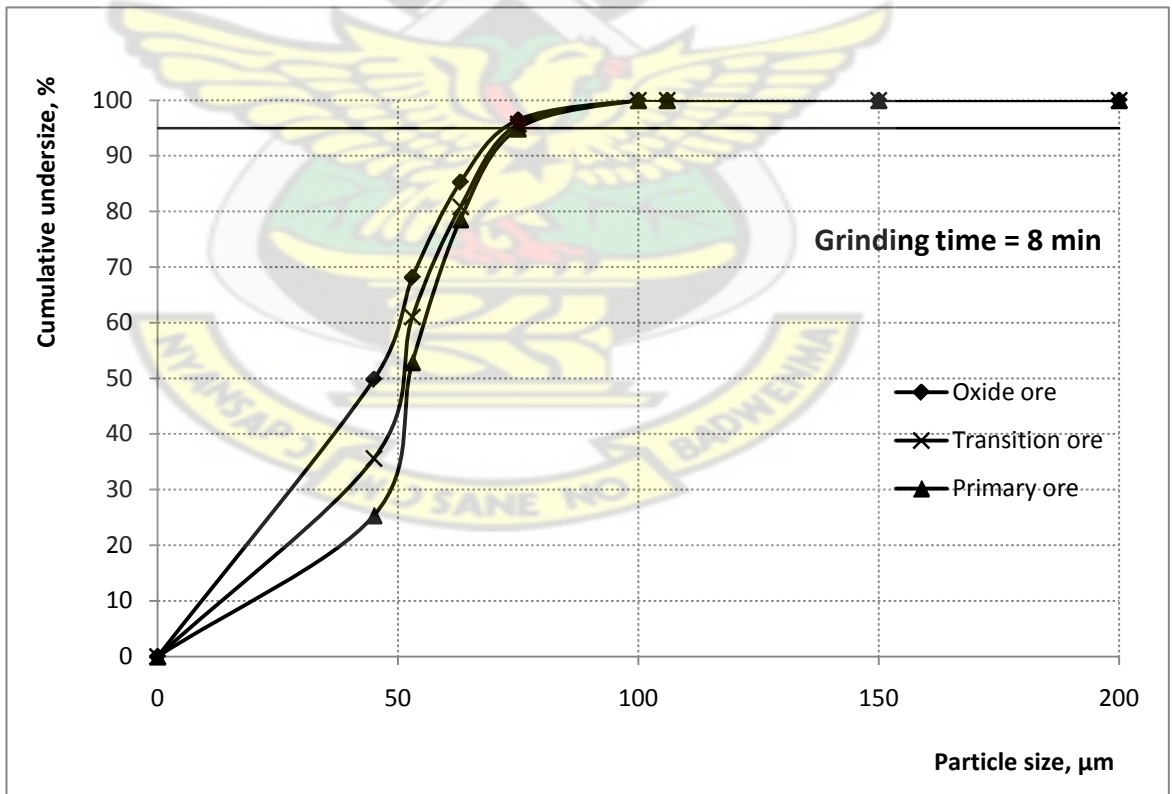


Figure 4.6: Particle size distribution for 8 min grinding time

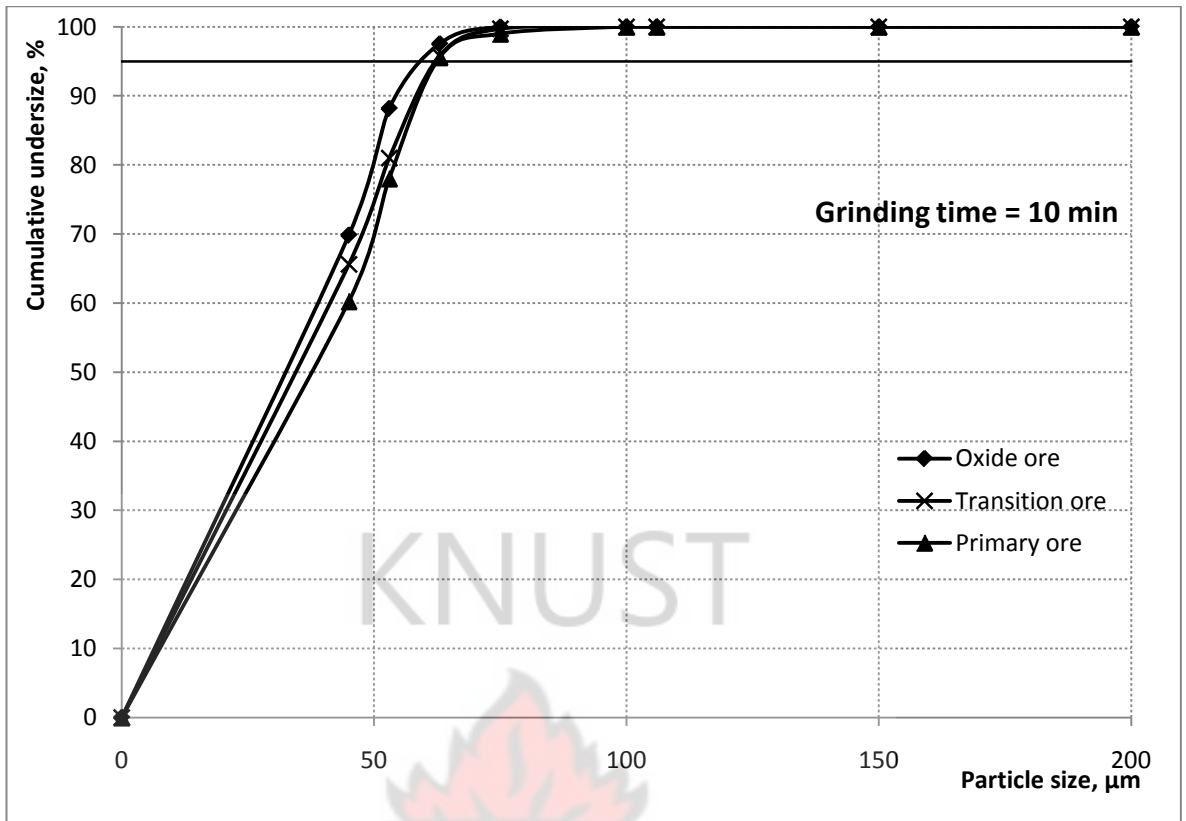


Figure 4.7: Particle size distribution for 10 min grinding time

4.3 Results from Davis tube measurements

The chemical analysis results for the magnetic concentrate and tailings obtained by the Davis tube method for the different fineness of the materials are presented in Tables 4.4-4.8. The calculated mass recovery (MR) and Fe recovery figures are also presented there.

Table 4.4: Davis tube results – 95% of particles under 150 µm

< 150 µm size particles									
Ore zone	Sample	Concentration, %						MR, %	Fe recovery, %
		Davis tube concentrate			Davis tube tailing				
		Fe	SiO₂	Al₂O₃	Fe	SiO₂	Al₂O₃		
Oxide	Ox-T501	68.4	0.8	0.3	53.4	19.1	0.8	17.4	21.3
	Ox-T512	68.5	1.5	1.9	36.0	35.1	6.4	19.4	31.5
	Ox-T520	66.3	0.5	5.0	35.3	20.5	16.6	14.0	23.5
	Ox-T536	68.2	0.9	0.3	47.9	27.5	1.1	23.5	30.4
	Ox-T556	68.7	1.5	0.3	36.5	46.2	1.0	27.7	41.9
	Ox-T594	67.6	1.0	1.8	38.7	28.0	6.1	18.9	29.0
	Ox-T627	67.6	3.4	2.1	38.0	29.0	7.4	20.9	31.9
	Ox-T643	67.0	3.4	0.3	47.4	27.9	0.8	14.4	19.2
	Ox-T662	67.7	2.5	1.0	41.4	32.3	3.2	12.2	18.5
	Ox-T673	67.8	0.9	4.5	45.1	8.0	14.0	6.1	8.9
	Average	67.8	1.6	1.7	42.0	27.4	5.8	17.4	25.6
Transition	Tr-T501	67.4	1.5	0.3	38.1	40.5	1.0	21.0	31.9
	Tr-T512	67.3	1.5	0.2	34.9	49.3	0.7	28.0	42.9
	Tr-T520	68.3	2.2	1.6	27.2	45.5	5.0	7.5	16.8
	Tr-T536	69.9	2.6	0.2	9.2	75.7	0.7	46.3	83.1
	Tr-T556	67.2	2.6	0.1	29.9	53.5	0.4	25.3	43.2
	Tr-T594	67.3	1.5	0.2	37.9	42.5	0.7	20.8	31.8
	Tr-T627	66.9	3.6	0.2	22.8	58.3	0.6	36.5	62.8
	Tr-T643	67.1	3.5	0.5	42.8	30.5	1.5	3.7	5.6
	Tr-T662	67.3	3.6	0.8	22.3	57.8	2.8	24.5	49.5
	Tr-T673	69.2	3.6	0.2	16.9	66.5	0.7	37.0	70.6
	Average	67.8	2.6	0.4	28.2	52.0	1.4	25.1	43.8
Primary	Pr-T501	66.4	2.6	0.1	17.0	74.1	0.4	48.8	78.8
	Pr-T512	65.9	2.6	0.3	16.6	71.7	1.4	43.6	75.4
	Pr-T520	67.0	1.6	0.2	13.9	75.8	1.0	46.6	80.8
	Pr-T536	66.2	2.2	0.2	17.5	71.2	1.1	49.2	81.0
	Pr-T556	67.9	3.6	0.2	10.8	76.8	0.9	48.5	85.6
	Pr-T594	66.0	3.6	0.5	14.2	77.8	2.2	48.0	81.1
	Pr-T627	68.0	3.6	0.1	16.5	64.2	0.2	43.9	76.3
	Pr-T643	68.0	3.6	1.8	18.2	64.0	8.0	41.8	72.9
	Pr-T662	66.3	3.6	0.7	28.4	47.1	2.2	16.9	32.1
	Pr-T673	67.3	3.6	0.3	18.1	63.0	0.9	33.1	64.8
	Average	66.9	3.1	0.4	17.1	68.6	1.8	42.1	72.9

Table 4.5: Davis tube results – 95% of particles under 106 µm

< 106 µm size particles									
Ore zone	Sample	Concentration, %						MR, %	Fe recovery, %
		Davis tube concentrate			Davis tube tailing				
		Fe	SiO₂	Al₂O₃	Fe	SiO₂	Al₂O₃		
Oxide	Ox-T501	66.0	0.8	0.3	53.9	19.1	0.8	17.3	20.4
	Ox-T512	70.0	1.3	2.3	35.7	35.1	6.3	19.2	31.8
	Ox-T520	69.0	1.1	6.2	34.8	20.5	16.4	14.1	24.6
	Ox-T536	66.7	2.8	0.4	48.5	26.8	1.1	23.0	29.1
	Ox-T556	66.1	3.0	0.4	37.5	45.6	1.0	27.6	40.2
	Ox-T594	66.6	1.1	2.3	38.9	28.0	6.0	18.9	28.5
	Ox-T627	66.7	1.2	2.6	38.4	29.5	7.2	20.6	31.0
	Ox-T643	66.8	1.3	0.4	47.4	28.3	0.8	14.3	19.1
	Ox-T662	66.8	2.1	1.3	41.3	32.7	3.2	13.2	19.7
	Ox-T673	66.5	1.4	5.6	45.5	7.9	13.8	4.6	6.5
	Average	67.1	1.6	2.2	42.2	27.3	5.7	17.3	25.1
Transition	Tr-T501	66.9	2.7	0.4	38.2	40.2	1.0	20.9	31.6
	Tr-T512	65.8	2.3	0.3	35.3	49.3	0.7	28.5	42.6
	Tr-T520	69.5	2.4	2.0	26.7	45.9	5.0	8.3	19.1
	Tr-T536	66.2	2.4	0.2	10.2	78.8	0.7	48.3	85.8
	Tr-T556	66.0	2.1	0.2	29.6	54.6	0.4	26.6	44.7
	Tr-T594	65.8	3.0	0.3	38.3	42.1	0.7	20.8	31.1
	Tr-T627	66.9	1.7	0.2	22.9	59.3	0.5	36.5	62.7
	Tr-T643	66.7	1.2	0.6	42.5	30.9	1.5	4.9	7.4
	Tr-T662	66.7	2.8	1.0	22.9	57.5	2.7	23.8	47.6
	Tr-T673	66.8	3.6	0.3	18.6	66.2	0.7	36.7	67.6
	Average	66.7	2.4	0.6	28.5	52.5	1.4	25.5	44.0
Primary	Pr-T501	66.9	2.9	0.1	16.5	73.8	0.3	48.8	79.5
	Pr-T512	66.0	2.3	0.4	16.5	71.9	1.3	43.6	75.5
	Pr-T520	67.0	2.2	0.3	14.1	74.9	0.9	46.4	80.4
	Pr-T536	65.9	2.9	0.3	16.0	73.1	1.0	48.6	79.6
	Pr-T556	66.0	2.3	0.3	12.6	78.0	0.8	48.5	83.1
	Pr-T594	66.0	2.4	0.6	14.2	79.0	2.1	48.1	81.2
	Pr-T627	66.0	2.6	0.1	18.6	64.3	0.2	43.3	73.1
	Pr-T643	66.0	2.8	2.3	20.2	63.8	7.6	41.1	69.5
	Pr-T662	65.2	3.0	0.9	28.4	47.6	2.2	17.5	32.8
	Pr-T673	66.2	3.6	0.3	18.6	63.0	0.9	33.1	63.7
	Average	66.1	2.7	0.6	17.6	69.0	1.7	41.9	71.8

Table 4.6: Davis tube results – 95% of particles under 90 µm

< 90 µm size particles									
Ore zone	Sample	Concentration, %						MR, %	Fe recovery, %
		Davis tube concentrate			Davis tube tailing				
		Fe	SiO₂	Al₂O₃	Fe	SiO₂	Al₂O₃		
Oxide	Ox-T501	66.7	2.8	0.5	53.7	18.7	0.8	17.9	21.3
	Ox-T512	67.9	7.0	4.0	36.2	33.7	5.9	19.4	31.1
	Ox-T520	66.9	3.4	10.9	35.1	20.1	15.6	14.2	24.0
	Ox-T536	66.5	2.6	0.7	48.4	27.1	1.0	23.7	29.9
	Ox-T556	66.9	3.8	0.5	37.2	45.2	0.9	27.5	40.5
	Ox-T594	67.5	2.2	3.8	38.7	27.8	5.7	19.0	29.0
	Ox-T627	67.5	2.4	4.5	38.3	29.0	6.7	20.1	30.7
	Ox-T643	67.7	4.7	0.5	47.2	27.8	0.8	14.8	19.9
	Ox-T662	68.7	4.1	2.1	41.1	32.3	3.1	13.0	20.0
	Ox-T673	67.3	0.1	9.8	46.2	7.7	13.5	1.7	2.4
	Average	67.4	3.3	3.7	42.2	26.9	5.4	17.1	24.9
Transition	Tr-T501	67.0	3.3	0.6	38.2	40.0	0.9	20.9	31.6
	Tr-T512	66.9	2.5	0.4	34.8	49.3	0.6	28.5	43.4
	Tr-T520	68.6	3.6	3.4	26.0	46.6	4.9	10.1	22.9
	Tr-T536	66.3	2.5	0.3	10.0	78.8	0.6	48.5	86.1
	Tr-T556	67.1	4.0	0.2	47.1	28.0	1.1	26.8	45.7
	Tr-T594	67.9	3.8	0.4	37.9	41.7	0.6	20.3	31.4
	Tr-T627	66.9	4.3	0.3	22.9	57.8	0.5	36.4	62.6
	Tr-T643	66.8	3.3	1.0	36.6	37.5	1.6	8.1	12.4
	Tr-T662	69.7	4.3	1.6	22.1	56.9	2.5	23.6	49.3
	Tr-T673	68.9	5.9	0.3	17.6	64.6	0.6	36.4	69.2
	Average	67.6	3.8	0.8	29.3	50.1	1.4	26.0	45.5
Primary	Pr-T501	66.2	2.6	0.1	17.1	74.1	0.3	48.8	78.7
	Pr-T512	67.3	3.4	0.6	15.4	71.3	1.2	43.8	77.3
	Pr-T520	67.5	3.2	0.4	13.3	74.6	0.8	46.8	81.7
	Pr-T536	68.0	2.5	0.5	14.7	72.6	0.9	47.9	81.0
	Pr-T556	67.4	3.3	0.4	11.5	76.7	0.7	48.2	84.5
	Pr-T594	66.6	2.6	1.0	12.7	80.1	1.8	48.9	83.4
	Pr-T627	67.6	3.0	0.1	17.4	63.9	0.2	43.2	74.7
	Pr-T643	68.6	2.4	3.9	17.6	65.0	6.5	42.0	73.8
	Pr-T662	68.3	2.8	1.4	27.8	47.6	2.1	17.4	34.1
	Pr-T673	67.2	2.9	0.5	17.6	64.0	0.8	33.9	66.2
	Average	67.5	2.9	0.9	16.5	69.0	1.5	42.1	73.5

Table 4.7: Davis tube results – 95% of particles under 75 µm

< 75 µm size particles									
Ore zone	Sample	Concentration, %						MR, %	Fe recovery, %
		Davis tube concentrate			Davis tube tailing				
		Fe	SiO₂	Al₂O₃	Fe	SiO₂	Al₂O₃		
Oxide	Ox-T501	66.6	4.1	0.3	54.7	17.4	0.8	17.3	20.5
	Ox-T512	67.2	3.1	1.7	36.2	34.8	6.5	19.8	31.4
	Ox-T520	67.7	2.7	4.5	34.8	20.3	16.7	14.7	25.0
	Ox-T536	67.8	3.8	0.4	47.9	26.7	1.1	23.8	30.6
	Ox-T556	68.9	4.7	0.3	36.5	44.8	1.0	27.4	41.6
	Ox-T594	58.2	2.3	1.7	40.9	27.7	6.2	18.8	24.7
	Ox-T627	68.2	2.5	2.0	38.1	29.1	7.4	20.3	31.4
	Ox-T643	67.5	2.8	0.3	47.3	28.0	0.8	14.5	19.4
	Ox-T662	68.5	2.1	1.0	41.1	32.6	3.3	12.9	19.7
	Ox-T673	69.5	1.5	4.1	46.1	7.7	13.6	1.6	2.4
	Average	67.0	3.0	1.6	42.4	26.9	5.7	17.1	24.7
Transition	Tr-T501	69.5	5.3	0.4	37.6	39.4	1.0	20.8	32.6
	Tr-T512	66.5	4.4	0.3	34.9	48.6	0.7	28.6	43.3
	Tr-T520	66.7	4.4	1.5	27.0	45.7	5.0	8.2	18.1
	Tr-T536	66.6	4.3	0.2	9.9	76.9	0.7	48.3	86.2
	Tr-T556	67.3	5.9	0.2	29.2	53.1	0.3	26.5	45.3
	Tr-T594	67.5	4.8	0.3	38.0	41.5	0.7	20.5	31.4
	Tr-T627	66.3	3.2	0.2	23.0	58.7	0.5	36.7	62.6
	Tr-T643	62.6	3.4	0.5	42.9	30.7	1.5	4.3	6.2
	Tr-T662	66.2	5.1	0.8	23.4	56.4	2.7	23.2	46.1
	Tr-T673	66.8	4.7	0.3	18.6	65.6	0.7	36.8	67.6
	Average	66.6	4.5	0.5	28.4	51.7	1.4	25.4	44.0
Primary	Pr-T501	67.7	2.4	0.2	16.0	73.9	0.3	48.6	80.0
	Pr-T512	66.9	2.2	0.4	15.8	72.1	1.4	43.7	76.6
	Pr-T520	66.7	3.1	0.3	14.7	73.8	0.9	46.1	79.5
	Pr-T536	67.1	3.4	0.3	14.8	72.8	1.1	48.7	81.1
	Pr-T556	66.7	2.1	0.3	11.7	78.5	0.8	48.7	84.4
	Pr-T594	66.5	2.4	0.5	13.4	79.4	2.2	48.4	82.2
	Pr-T627	66.5	2.9	0.1	17.7	64.7	0.2	43.9	74.5
	Pr-T643	66.5	3.3	1.7	18.7	64.9	8.2	42.5	72.5
	Pr-T662	68.1	2.6	0.7	27.8	47.7	2.2	17.5	34.3
	Pr-T673	68.3	2.7	0.3	17.3	63.8	0.9	33.6	66.5
	Average	67.1	2.7	0.5	16.8	69.2	1.8	42.2	73.2

Table 4.8: Davis tube and Satmagan results – 95% of particles under 63 µm

< 63 µm size particles									
Ore zone	Sample	Concentration, %						MR, %	Fe recovery, %
		Davis tube concentrate			Davis tube tailing				
		Fe	SiO₂	Al₂O₃	Fe	SiO₂	Al₂O₃		
Oxide	Ox-T501	69.4	0.9	0.2	53.1	19.2	0.8	18.0	22.3
	Ox-T512	67.9	2.7	1.2	36.1	34.9	6.6	19.5	31.3
	Ox-T520	68.2	0.4	3.2	34.6	20.8	17.0	14.9	25.6
	Ox-T536	68.5	0.6	0.2	47.7	27.7	1.2	23.7	30.8
	Ox-T556	66.7	4.2	0.2	37.3	45.1	1.1	27.5	40.3
	Ox-T594	66.3	1.1	1.1	38.9	28.0	6.3	19.0	28.6
	Ox-T627	66.4	1.3	1.3	38.4	29.5	7.5	20.8	31.2
	Ox-T643	67.9	1.5	0.2	47.2	28.3	0.9	14.7	19.8
	Ox-T662	66.5	2.7	0.6	41.3	32.6	3.3	13.3	19.8
	Ox-T673	66.9	3.2	2.9	46.3	7.6	13.6	0.9	1.3
	Average	67.5	1.8	1.1	42.1	27.4	5.8	17.2	25.1
Transition	Tr-T501	67.3	3.7	0.2	37.9	40.3	1.1	21.6	32.9
	Tr-T512	67.2	4.7	0.1	34.5	48.7	0.7	29.0	44.3
	Tr-T520	69.8	6.5	1.0	27.5	44.8	5.0	6.7	15.4
	Tr-T536	68.6	6.4	0.1	7.5	75.6	0.8	48.8	89.7
	Tr-T556	69.6	6.0	0.1	28.1	53.4	0.4	27.0	47.9
	Tr-T594	67.2	4.2	0.1	37.8	42.0	0.7	21.2	32.4
	Tr-T627	67.4	3.4	0.1	22.2	58.7	0.6	36.9	63.9
	Tr-T643	67.0	2.9	0.3	42.8	30.6	1.5	3.9	6.0
	Tr-T662	69.5	7.1	0.5	22.0	56.2	2.8	23.8	49.6
	Tr-T673	68.0	6.8	0.1	18.2	64.0	0.7	36.3	68.0
	Average	68.2	5.2	0.3	27.8	51.4	1.4	25.5	45.0
Primary	Pr-T501	66.0	2.7	0.1	16.8	74.8	0.4	49.3	79.3
	Pr-T512	67.9	2.3	0.2	14.3	73.0	1.5	44.5	79.2
	Pr-T520	66.9	2.2	0.1	13.6	75.8	1.0	47.0	81.4
	Pr-T536	66.0	3.6	0.2	15.6	72.9	1.2	48.9	80.2
	Pr-T556	67.9	3.2	0.1	10.3	77.8	1.0	49.0	86.4
	Pr-T594	66.9	2.5	0.3	12.5	80.1	2.4	48.9	83.6
	Pr-T627	68.9	3.2	0.0	16.0	64.3	0.2	43.7	77.0
	Pr-T643	67.9	2.5	1.2	18.2	64.8	8.5	41.9	73.0
	Pr-T662	68.7	2.8	0.4	27.7	47.5	2.3	17.3	34.2
	Pr-T673	67.7	2.8	0.2	16.9	64.7	1.0	34.5	67.9
	Average	67.5	2.8	0.3	16.2	69.6	2.0	42.5	74.2

4.3.1 Mass recovery

The Davis tube method shows a higher mass (magnetic material) recovery than the magnetite content of the samples measured by Satmagan. This indicates that there might be other weakly magnetic iron minerals like hematite, ilmenite, pyrite or siderite in the samples apart from magnetite. Additional recovery of closely associated hematite particles with the magnetite and gangue minerals adhering to the surface or locked within a particle of the magnetite may also account for much higher magnetic material recovery than the magnetite content in all the ore zones. The mass recovery of the composite samples with different particles sizes is shown in Figure 4.8. It can be observed that the particle fineness and therefore the grinding time had little effect on magnetic separation by the Davis tube.

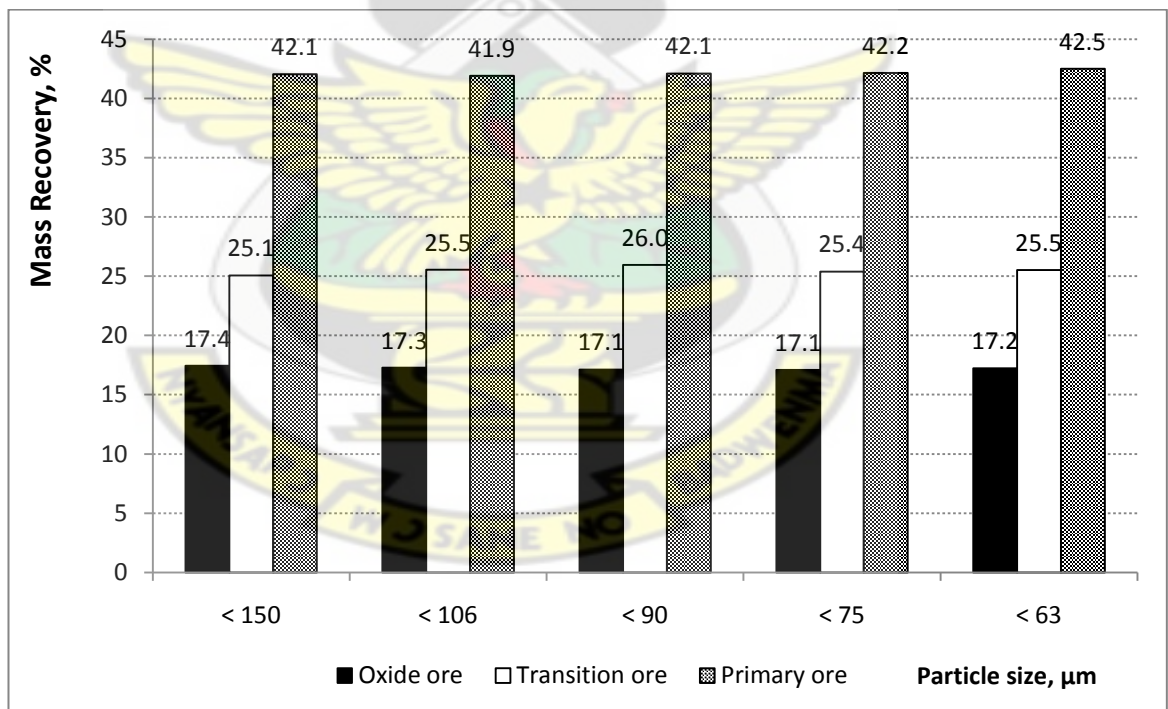


Figure 4.8: Mass recovery

4.3.2 Davis tube concentrate

The average iron content for the magnetic concentrate is summarised in Table 4.9. The iron content indicates the quality of the concentrate.

Table 4.9: Average concentration in the Davis tube magnetic concentrates for the different fineness

Ore zone	Particle size, μm														
	< 150			< 106			< 90			< 75			< 63		
	Average concentration, %														
	Fe	SiO ₂	Al ₂ O ₃	Fe	SiO ₂	Al ₂ O ₃	Fe	SiO ₂	Al ₂ O ₃	Fe	SiO ₂	Al ₂ O ₃	Fe	SiO ₂	Al ₂ O ₃
Oxide	67.8	1.6	1.7	67.1	1.6	2.2	67.4	3.3	3.7	67.0	3.0	1.6	67.5	1.8	1.1
Transition	67.8	2.6	0.4	66.7	2.4	0.6	67.6	3.8	0.8	66.6	4.5	0.5	68.2	5.2	0.3
Primary	66.9	3.1	0.4	66.1	2.7	0.6	67.5	2.9	0.9	67.1	2.7	0.5	67.5	2.8	0.3

The theoretical Fe content of Fe₃O₄ magnetite is 72.4%. The magnetic concentrate produced by the proposed magnetic separation plant should have a minimum 66.5% Fe (see Table 2.7). This specification can be met if the ore is ground before the magnetic separation. For the oxide and transition zone ores it is sufficient to grind them such, that 95% of the particles are below 150 µm size. However, the ore from the primary zone has to be ground finer. The < 90 µm and < 63 µm fineness gave similar Fe content. Based on economic consideration, the < 90 µm fineness is recommended for the primary ore. However, the recovery efficiencies are not the same for the different ore zones and fineness. The average iron concentration of the Davis tube magnetic concentrates is shown in Figure 4.9

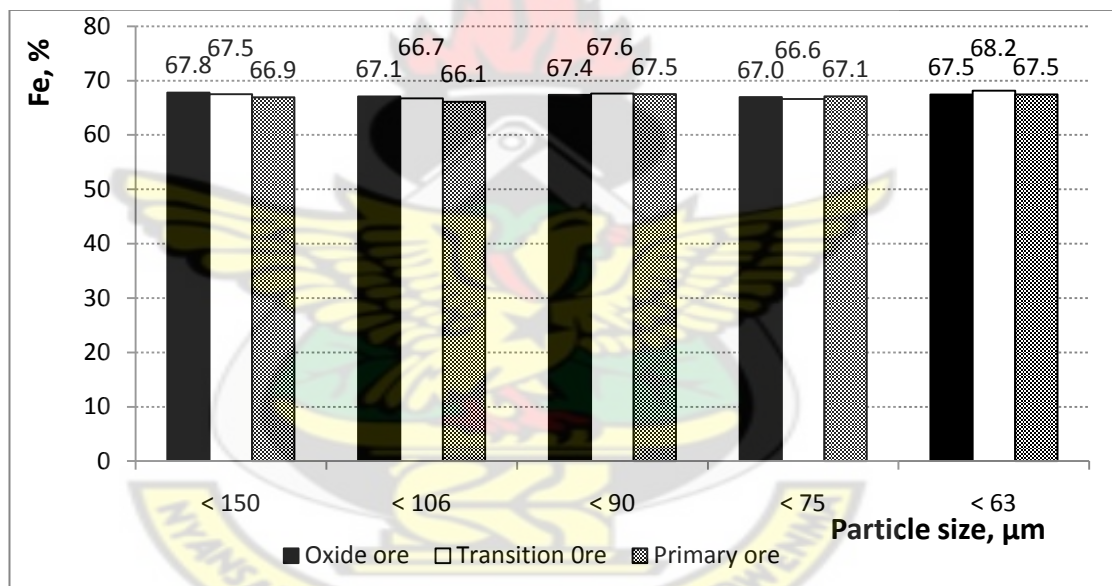


Figure 4.9: Average iron concentration in the Davis tube magnetic concentrates

The average values of silica content are included in Table 4.9. They are presented in Figure 4.10 as well. The required silica content of less than 3% for the proposed beneficiation plant can be achieved by grinding the ores below 150 or 106 µm. However, finer grinding increased the silica content for the transitional ore well above 3%. It is suspected that the ore liberation size may have been exceeded due to overgrinding, resulting in inefficient magnetic separation of iron particles from the fine silica particles.

The average alumina concentrations are also included in Table 4.9 and presented in Figure 4.11. The alumina content has to be below 1.0%, according to the specification of the concentrate to be produced by the new plant. This required concentration is satisfied by the transition and primary ore at all grinding fineness. However, values 2-3 times higher than the specification were measured in case of the oxide ore at all fineness. The reason for this requires further investigation.

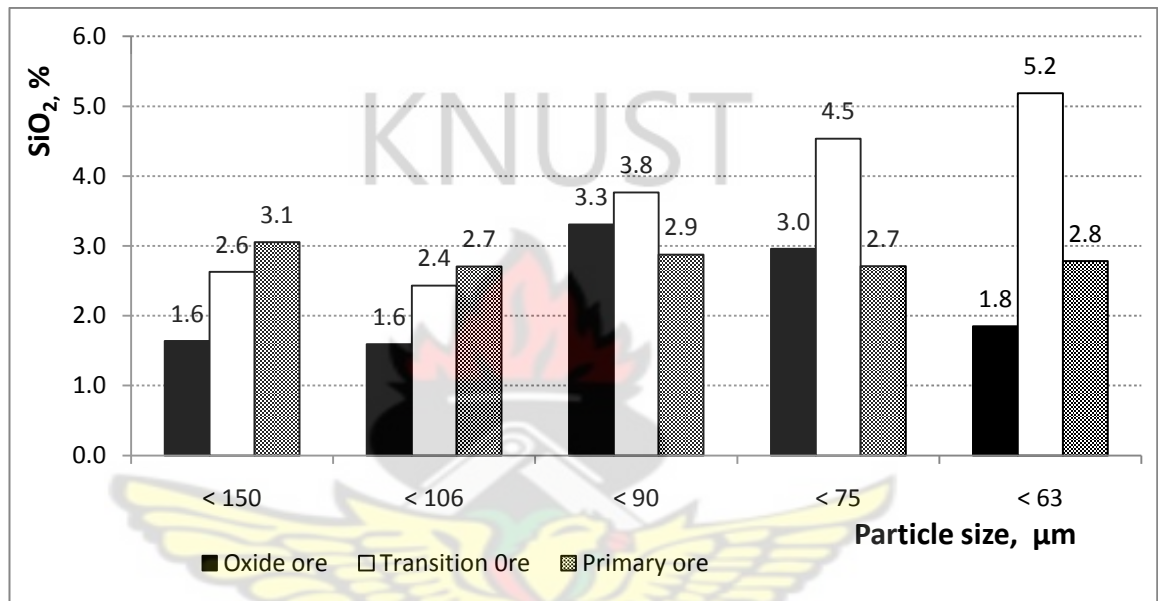


Figure 4.10: Average silica concentration in the Davis tube magnetic concentrate

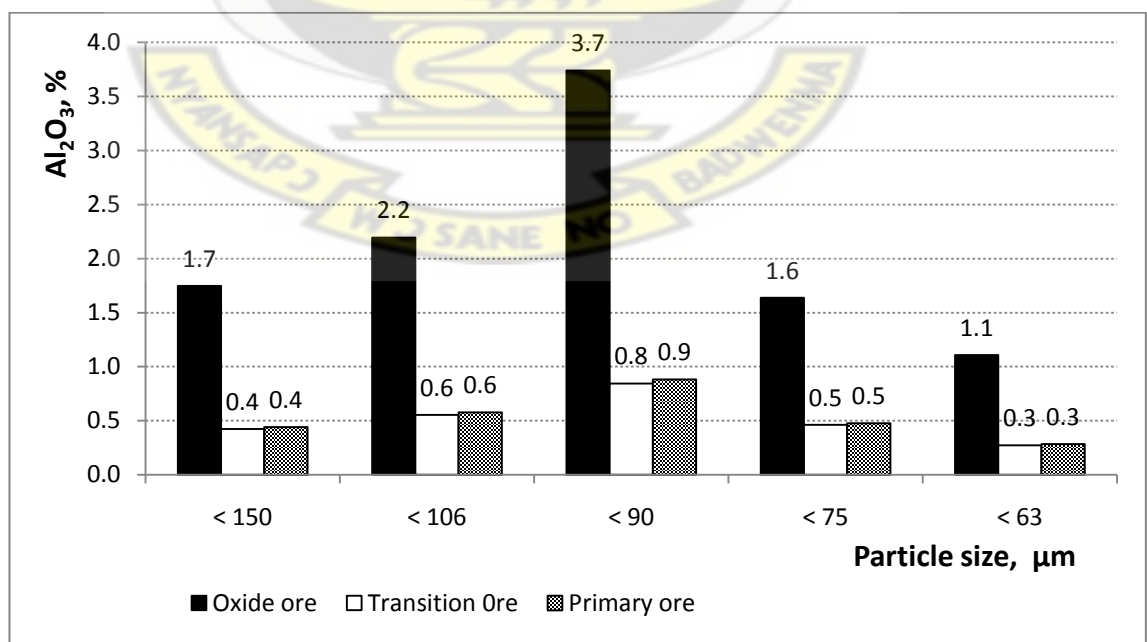


Figure 4.11: Average alumina concentration in the Davis tube magnetic concentrates

4.3.3 Iron recovery

The calculated iron recovery by magnetic separation for each fine is presented in Table 4.10 and graphical illustration shown in Figure 4.12. Hematite is non-magnetic and would not be recovered by magnetic separation, therefore the magnetic concentrate is suspected to contain only magnetite and other magnetic iron minerals present in the sample. The iron recovery data and Figure 4.12 clearly demonstrate that iron cannot be effectively recovered in the oxide zone (only 25%) and transitional zone (only 44-45%) by magnetic separation alone.

Table 4.10: Calculated Fe recovery by Davis tube method

Ore zone	Particle size, μm				
	< 150	< 106	< 90	< 75	< 63
Oxide	25.6	25.1	24.9	24.7	25.1
Transition	43.8	44.0	45.5	44.0	45.0
Primary	72.9	71.8	73.5	73.2	74.2
Total average	47.4	47.0	48.0	47.3	48.1
Average oxide and transition	34.7	34.6	35.2	34.3	35.1

ArcelorMittal Liberia currently only plans to mine the oxide and transitional ore zones. In these zones only 34-35% of iron present can be recovered by magnetic separation. Iron recovery in the primary ore zone is significantly higher (71-74%), which is largely attributed to the presence of magnetite as the main iron bearing mineral.

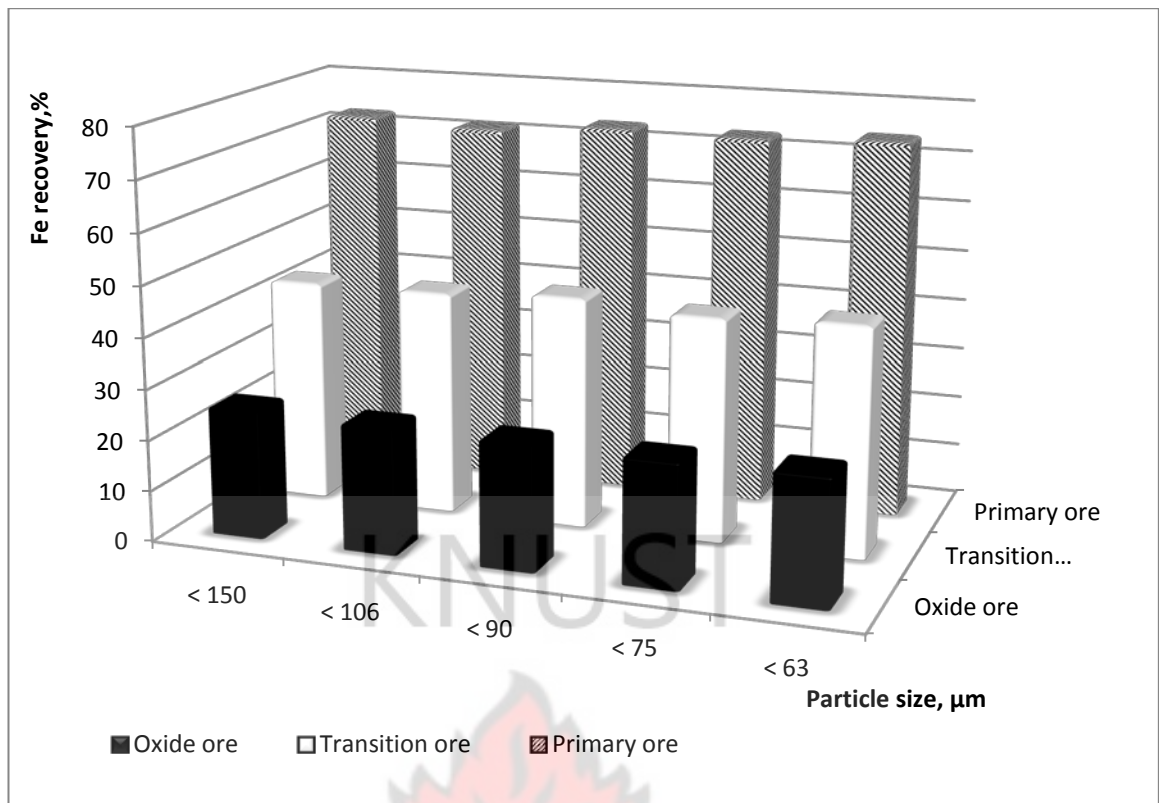


Figure 4.12: Iron recovery

4.3.4 Tailings (Non-magnetic material from the Davis tube separation)

The mean iron, silica and alumina concentration in the non-magnetic tailings is presented in Table 4.11 for each fines. The main iron mineral in the non-magnetic tailings is suspected to be hematite in the oxide zone, hematite and Fe-silicates in the transitional zone, and Fe-silicates in the primary zone. The higher iron content (42-44%) observed for samples from the oxide zone is due to the presence of hematite, which is non-magnetic, and thus cannot be recovered by magnetic separation. The least iron (16-17%) is lost to the tailings for the primary ore. This means, that the iron ore there is mainly in magnetite, which can be effectively recovered by magnetic separation. The particle size of the sample, however, does not significantly affect the quality of the tailings as observed from the results.

Table 4.11: Average concentration in non-magnetic tailings

Ore zone	Particle size, μm														
	< 150			< 106			< 90			< 75			< 63		
	Average concentration, %														
	Fe	SiO ₂	Al ₂ O ₃	Fe	SiO ₂	Al ₂ O ₃	Fe	SiO ₂	Al ₂ O ₃	Fe	SiO ₂	Al ₂ O ₃	Fe	SiO ₂	Al ₂ O ₃
Oxide	42.0	27.4	5.8	42.2	27.3	5.7	42.2	26.9	5.4	44.4	26.9	5.7	42.1	27.4	5.8
Transition	28.2	52.0	1.4	28.5	52.5	1.4	29.3	50.1	1.4	28.4	51.7	1.4	27.8	51.4	1.4
Primary	17.1	68.6	1.8	17.6	69.0	1.7	16.5	69.0	1.5	16.8	69.2	1.8	16.2	69.6	2.0

4.4 Magnetite content of composite samples by Satmagan method

The magnetite content of the ore samples determined by Satmagan method is presented in Table 4.12. The results are also shown in Figure 4.13. The composite sample from the oxide zone has higher iron concentration and lower magnetite content than the ores from transition and primary zones. The higher magnetite content in the primary zones indicates the iron formation there is mainly the mineral magnetite. Magnetite content in the different fines does not show significant variation, thus grinding may have little influence in magnetite measurement by Satmagan.

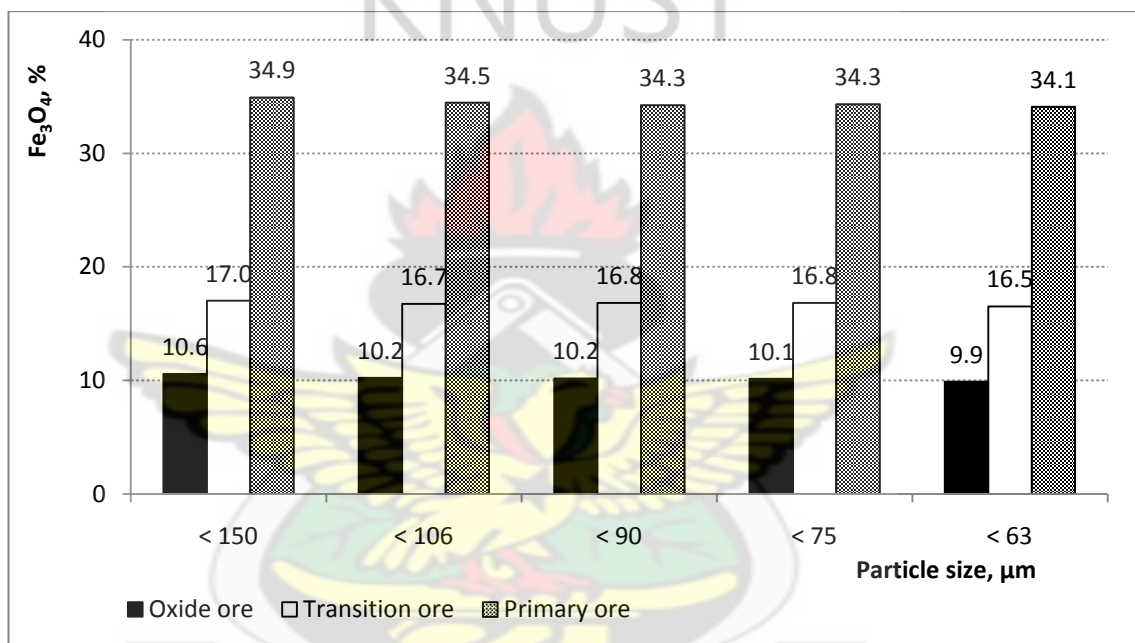


Figure 4.13: Average magnetite concentration

4.5 Magnetite and magnetic material content correlation

The Davis tube method measures the total amount of magnetic material that can be recovered by magnetic separation and the Satmagan method determines the total amount of material that is susceptible to magnetism. Satamagan, therefore, is used to estimate the magnetite content in the iron ores while the Davis tube result is used to predict the feasibility of recovering the magnetic minerals in the ore. The results of Davis tube and Satmagan measurements are summarised in Table 4.12. The average mass recovery and magnetite content for the three ore zones is shown in Figure 4.14.

Table 4.12: Summary Satmagan and Davis tube measurement results

Ore zone	Sample	Particle size, μm									
		< 150	< 106	<90	<75	<63	< 150	< 106	<90	<75	<63
		Satmagan (magnetite content, %)					Davis tube (mass recovery, %)				
Oxide	Ox-T501	11.6	11.0	11.3	11.2	10.8	17.4	17.3	17.9	17.3	18.0
	Ox-T512	13.4	12.9	12.5	12.2	12.1	19.4	19.2	19.4	19.8	19.5
	Ox-T520	6.7	5.9	5.4	5.3	5.2	14.0	14.1	14.2	14.7	14.9
	Ox-T536	15.9	15.6	15.5	15.3	15.2	23.5	23.0	23.7	23.8	23.7
	Ox-T556	19.9	19.1	19.4	19.2	19.1	27.7	27.6	27.5	27.4	27.5
	Ox-T594	11.6	11.0	11.2	11.9	11.0	18.9	18.9	19.0	18.8	19.0
	Ox-T627	13.0	12.6	12.4	12.7	12.1	20.9	20.6	20.1	20.3	20.8
	Ox-T643	6.4	6.8	6.5	6.7	6.3	14.4	14.3	14.8	14.5	14.7
	Ox-T662	5.2	5.7	5.6	5.4	5.5	12.2	13.2	13.0	12.9	13.3
	Ox-T673	1.9	1.7	1.8	1.6	1.5	6.1	4.6	1.7	1.6	0.9
	Average	10.6	10.2	10.2	10.1	9.9	17.4	17.3	17.1	17.1	17.2
Transition	Tr-T501	14.0	13.8	13.6	13.2	13.0	21.0	20.9	20.9	20.8	21.6
	Tr-T512	20.7	20.3	20.5	20.8	20.1	28.0	28.5	28.5	28.6	29.0
	Tr-T520	8.8	8.5	8.3	8.6	8.1	7.5	8.3	10.1	8.2	6.7
	Tr-T536	34.6	34.2	34.9	34.6	34.3	46.3	48.3	48.5	48.3	48.8
	Tr-T556	18.9	18.0	18.2	18.4	18.0	25.3	26.6	26.8	26.5	27.0
	Tr-T594	13.8	13.6	13.3	13.7	13.2	20.8	20.8	20.3	20.5	21.2
	Tr-T627	25.4	25.3	25.7	25.9	25.8	36.5	36.5	36.4	36.7	36.9
	Tr-T643	1.8	1.6	1.5	1.2	1.2	3.7	4.9	8.1	4.3	3.9
	Tr-T662	15.9	15.8	15.5	15.7	15.2	24.5	23.8	23.6	23.2	23.8
	Tr-T673	16.2	16.1	16.9	16.3	16.2	37.0	36.7	36.4	36.8	36.3
	Average	17.0	16.7	16.8	16.8	16.5	25.1	25.5	26.0	25.4	25.5
Primary	Pr-T501	38.9	38.3	38.5	38.6	38.2	48.8	48.8	48.8	48.6	49.3
	Pr-T512	37.4	36.9	36.2	36.7	36.1	43.6	43.6	43.8	43.7	44.5
	Pr-T520	39.0	38.5	38.9	38.5	38.1	46.6	46.4	46.8	46.1	47.0
	Pr-T536	41.9	41.6	41.1	41.6	41.2	49.2	48.6	47.9	48.7	48.9
	Pr-T556	40.9	40.2	39.9	40.0	40.3	48.5	48.5	48.2	48.7	49.0
	Pr-T594	40.8	39.9	39.2	39.2	39.0	48.0	48.1	48.9	48.4	48.9
	Pr-T627	36.9	36.3	36.7	36.5	36.3	43.9	43.3	43.2	43.9	43.7
	Pr-T643	34.7	34.6	34.3	34.2	34.3	41.8	41.1	42.0	42.5	41.9
	Pr-T662	16.7	16.5	16.5	16.7	16.1	16.9	17.5	17.4	17.5	17.3
	Pr-T673	22.1	21.9	21.4	21.1	21.2	33.1	33.1	33.9	33.6	34.5
	Average	34.9	34.5	34.3	34.3	34.1	42.1	41.9	42.1	42.2	42.5

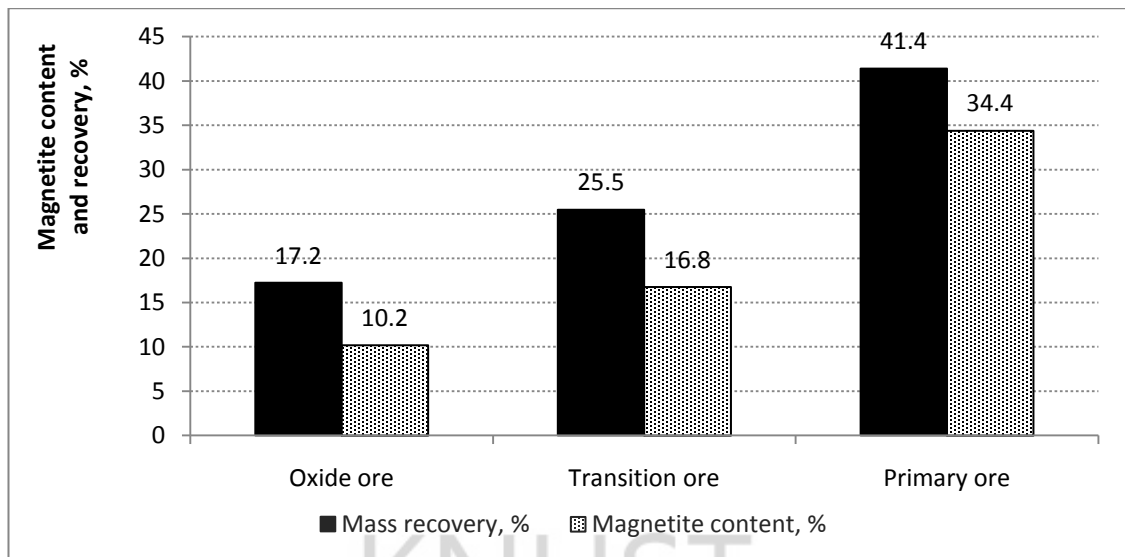


Figure 4.14: Average mass recovery and magnetite content

The results of the magnetite content measurement by Satmagan correlate well with the magnetic material content as determined by Davis tube for all the ore zones as shown in Figures 4.15-4.18. The correlation coefficient between magnetite and magnetic material content in the oxide and primary ore zones is higher (0.91 and 0.92) compared with the transitional ore zone (0.88).

The results clearly show, that samples from all the ore types have linear correlation between the magnetite concentration measured by Satmagan and the magnetic material content determined by Davis tube. It can also be observed that particle size has slight effect on the correlation between the two different methods of determinations.

Samples with low magnetite content also have low magnetic material, which confirms a direct positive relationship between the Satmagan and Davis tube methods of magnetite measurement. The primary ore has the highest magnetite and magnetic material content obtained from both methods, while the oxide ore has the lowest concentration.

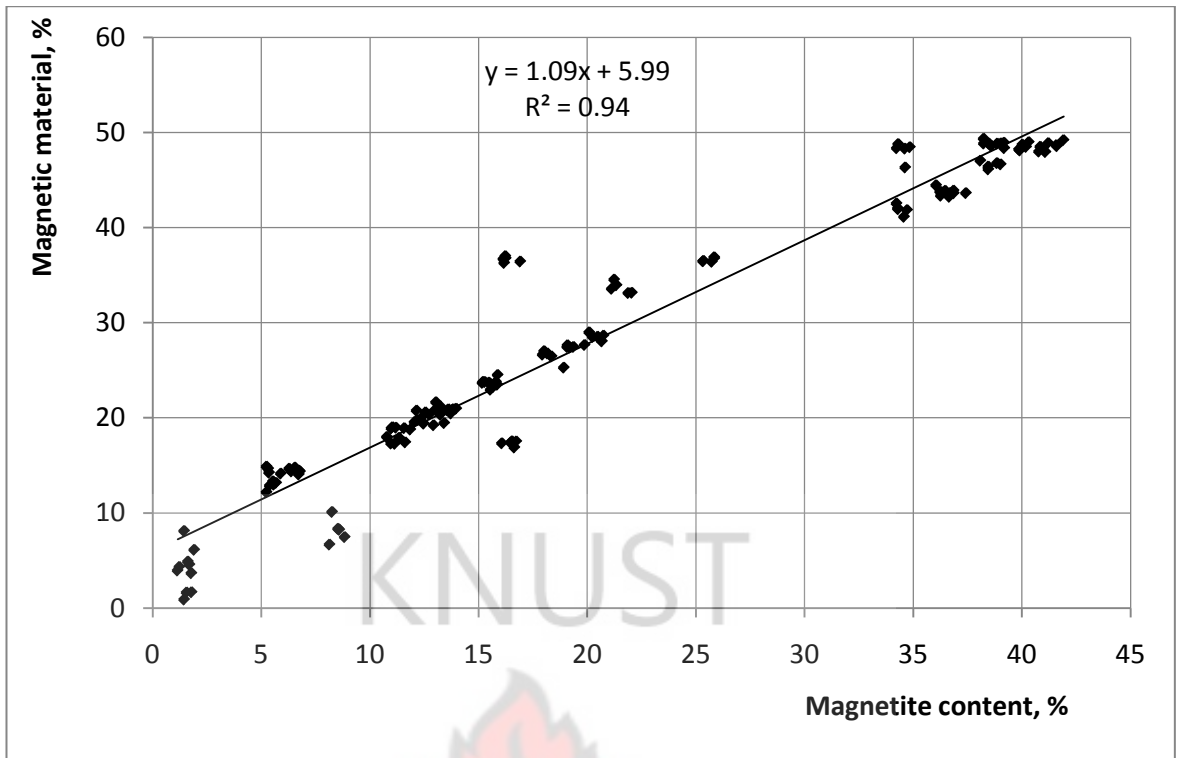


Figure 4.15: Magnetite and magnetic material correlation for all ore zones

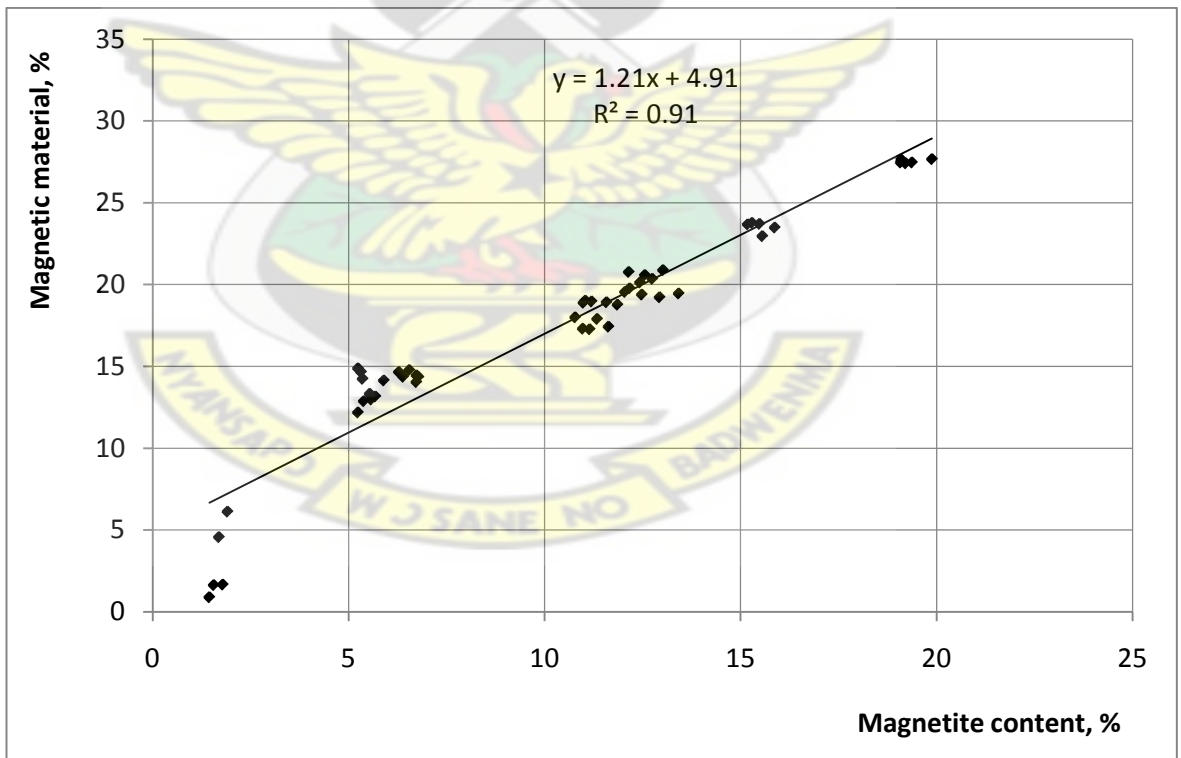


Figure 4.16: Magnetite and magnetic material correlation for the oxide ore

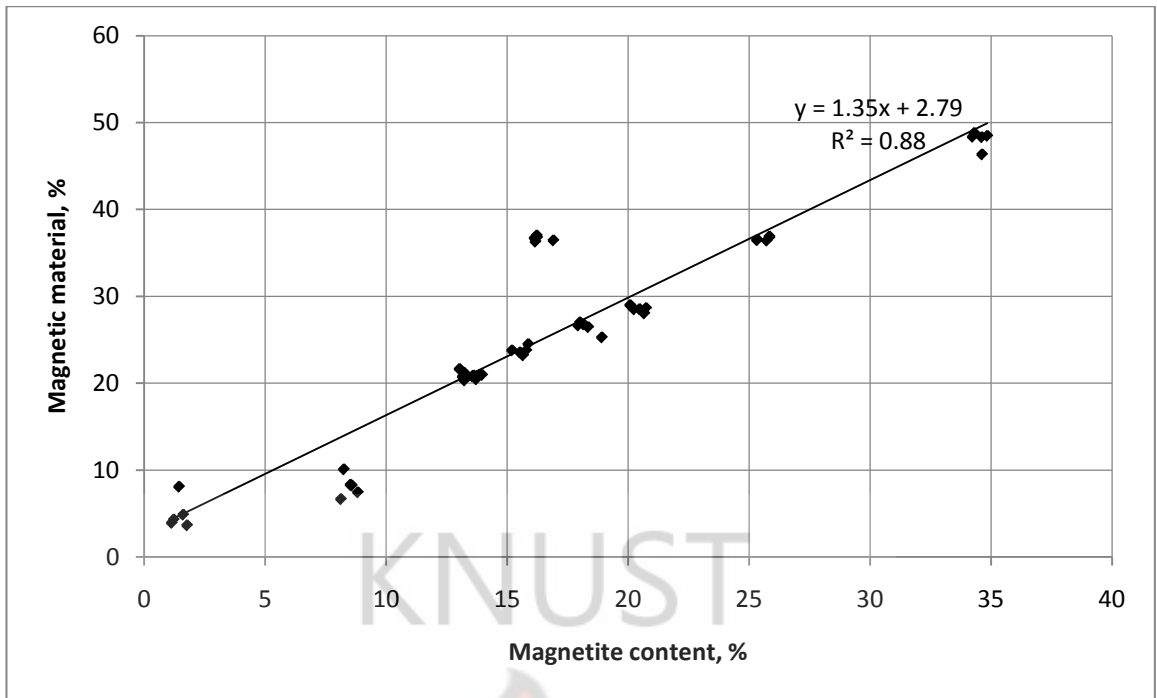


Figure 4.17: Magnetite and magnetic material correlation for the transition ore

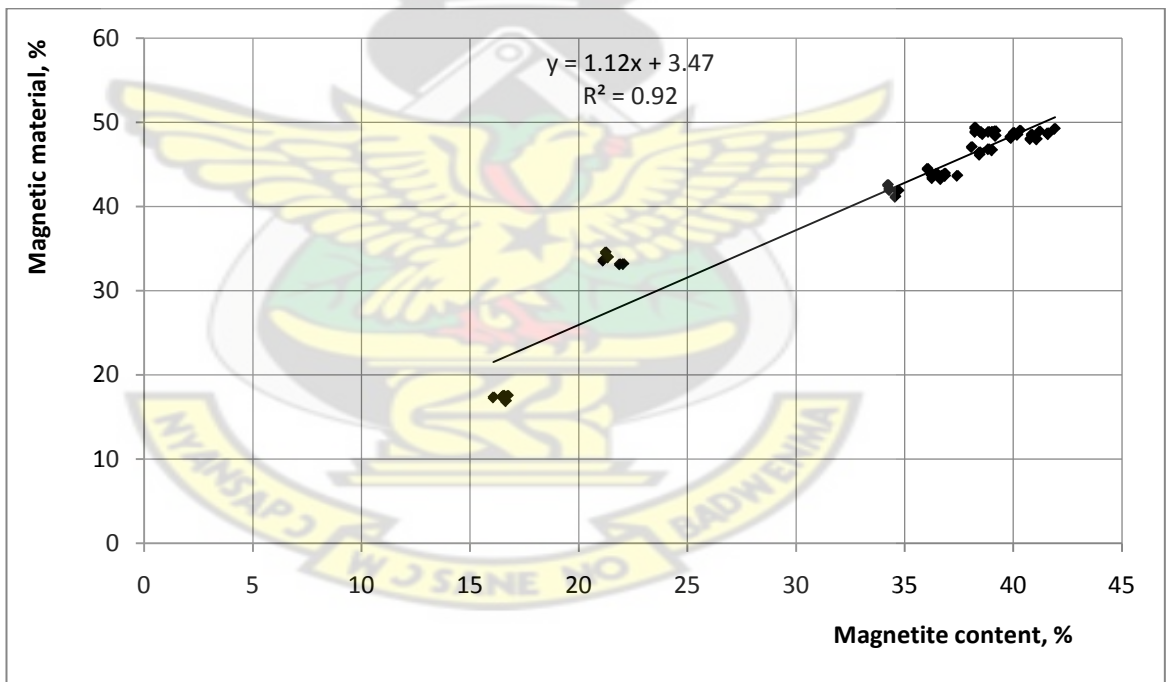


Figure 4.18: Magnetite and magnetic material correlation for the primary ore

CHAPTER FIVE

CONCLUSIONS AND RECOMMENDATIONS

5.1 CONCLUSIONS

The characteristics of the iron ore deposit in Mt. Tokadeh in the Nimba Mountain Range close to the Guinea and Ivory Coast borders in Liberia have been studied. It was further investigated whether magnetic separation, as proposed by ArcelorMittal Liberia, will meet the market requirement of min 66.5% Fe, max 3.0% SiO₂ and max 1.0% Al₂O₃ of the concentrate produced.

The iron ore deposit was sampled by collecting core samples from 10 drill holes between 30 to 275 m deep depending on the thickness of the iron formation.

Based on the various tests carried out in this study, the following conclusions are drawn:

1. The iron ore deposit is made up of 3 layers, the relatively soft oxide ore zone, the medium-hard transition ore zone and the hard primary ore zone.
2. The average iron concentration is 46.6% for the oxide ore, 39.1% for the transition and 38.3% for the primary ore
3. The silica content of the ore increases as the iron content decreases.
4. The average silica content of the oxide ore was found to be 22.4%, 38.2% for the transition ore and 40.4% for the primary ore.
5. In some of the samples from the oxide ore zone (Ox-T512, Ox-T520, Ox-T594, Ox-T627, Ox-T662 and Ox-T673); in two samples from the transition ore (Tr-T520 and Tr-T662) and in one sample (Pr-T643) from the primary ore zone the alumina content was high. This indicates that some of the canga (hard capping with high alumina content) may have affected the alumina content values in the samples from the oxide ore zone. However, the high alumina concentration in the samples from the transition and primary ore zones can be explained by the presence of aluminium

minerals like biotite $[K(Mg,Fe)_3AlSi_3O_{10}(F,OH)_2]$ and garnet schists usually found in the waste zones within the iron formation.

6. The composite samples obtained for the oxide, transition and primary ore zones for each of the 10 drill holes were ground in a disc pulveriser to study the effect of fineness on the magnetic separation. The particle size distribution curves showed that according to expectations, the easiest to grind is the oxide ore and the most difficult to grind is the primary ore.
7. It was further observed that it is sufficient to grind the oxide and transitional ores such, that 95% of the particles are below 150 μm . However, the primary ore should be ground to below 90 μm .
8. The magnetic separation was carried out with the Davis tube tester. The magnetic concentrate is made up of liberated and associated magnetic particles. The results show that the magnetic concentrates have average iron content of 67-67.8% in the soft ore, but only 24.7-25.6% of the iron present in the ore was recovered. The rest was lost to the tailings. The transition ore had 66.6-68.2% iron in the concentrate, and the iron recovery increased to 43.8-45.0%. The primary ore concentrate had 66.1-67.5% iron and 71.8-74.2% of iron present in the ore was found in the concentrate.
9. The very low iron recovery rates indicate that, about 75% of iron present in the oxide ore cannot be recovered by magnetic separation alone. The ore loss to tailings is about 55-56% for the transitional ore and 26-28% for the primary ore.
10. The iron content of the tailings of magnetic separation is high for the oxide ore being an average of 42.0-44.4%, therefore further beneficiation would improve the economics of the mining operation. However, the iron concentration in the tailings for the transitional and primary ore are low, 27.8-29.3% and 16.8-17.6%,

respectively, with very high silica content of 50-70% making it less profitable for beneficiation with the proposed method.

11. The loss of iron to tailings during magnetic separation is the result of the mineral composition of the ore. Since only the magnetite (Fe_3O_4) can be separated by a magnet, iron present as hematite (Fe_2O_3) goethite ($\text{FeO}(\text{OH})$), iron silicates and carbonates are lost to the tailings. Hematite is lost to the tailings in the oxide ore zone while hematite and Fe-silicates are the main minerals suspected to be lost in the transition and primary ore zones.
12. Satmagan analysis was used to measure the magnetic susceptibility of the samples. In this case all the magnetite in the sample gets measured regardless whether it can be separated by a magnet or not. Both the size and the degree of association dictate the behavior of a particle (i.e. whether or not it will be recovered by the magnetic separation method. Therefore, the Davis tube test and the Satmagan measurement will have different results. However, a strong correlation exists between the two measurements.
13. The average magnetite concentrations for the samples were between 10.1-10.6% for the oxide ore, 16.8-17.0% for the transitional ore and 34.1-34.9% in case of the primary ore. These results clearly show that the magnetite content is increasing towards the primary ore zone. This explains why the magnetic separation carried out by the Davis tube was better for the primary ore.
14. The results also show, that as it was expected, particle size does not affect Satmagan measurements.
15. The graphs presented in the results show a clear, strong correlation between the magnetite content measured by Satmagan and the magnetic concentrate amount obtained by the Davis tube operation.

5.2 RECOMMENDATIONS

Based on the results from this research work, the following are the recommendations:

1. The high iron content in the magnetic separation tailings should be recovered by using additional separation methods like flotation.
2. Other processing methods might be required to remove the hematite from the oxide and transitional zones.
3. It is recommended that the first two layers, the oxide and transition ores, should be processed with a different circuit from the primary ore since material from these zones contain a mixture of high hematite and low magnetite compared with the dominant magnetite in the primary zone.
4. X-ray diffraction analysis should be used to verify the ore mineralogy.
5. Further investigation should be done to determine the alumina distribution trend from the oxide ore zone to the primary ore zone and the contribution of canga material to the high alumina content in the oxide ore zone.
6. The relationship between MgO and CaO concentrations and LOI should be further investigated to establish a better understanding of the GOI in the primary ore zone.
7. The proposed plant does not have to grind the ore below 44 μm because finer grinding is observed to have little effect on the magnetic separation results obtained from this research (See Figure 4.8). Moreover, the silica content in the final magnetic concentrate is more than the required value of 3.0%, for the proposed beneficiation plant, with finer grinding below 90 μm for the transitional ore. (See Table 4.9 and Figure 4.10).

REFERENCES

- American Society for Testing and Materials (2008) *Annual book of ASTM Standards*; E877-08: *Standard practice for sampling and sample preparation of Iron ores and related materials for determination of chemical composition*. ASTM, Philadelphia
- ATKINS (2005) *Feasibility Study for the Western Area Deposits, for Mittal Steel*. WS Atkins International Limited, Woodcote Grove, Ashley Road, Epsom Surrey KT18 5BW September 2005, pp. 42-47
- Berge, J.W., Johansson, K., and Jack J. (1977) Geology and origin of the hematite ores of the Nimba Range, Liberia. *Economic Geology*. July 1977, v. 72, pp. 582-607
- Berge, J.W. (1974) Geology, Geochemistry, and Origin of the Nimba Itabirite and Associated Rocks, Nimba County, Liberia. *Economic Geology*; February 1974; v. 69; no. 1; pp. 80-92
- Boudrias-Chapleau, C. (2009) *Project T959 Final report: Physical characterization of a Liberian Mine ore*, Prepared for ArcelorMittal Liberia by COREM Canada. pp. 1-19
- Boudrias-Chapleau, C. and Donald, L. (2009) *COREM Final Report No. T1055*, Laboratory test work of Gangra ore deposit from Liberian mine. Prepared for ArcelorMittal Liberia by COREM Canada. pp. 1-22
- Buro, Y.A. and Alain, D. (2009a) *Wrap-up report*, Technical Assistance in Mining and Metallurgy in Liberia, Prepared for Mittal Steel Liberia Ltd by MetChem Canada Inc. Vol. I of III, May 2009, pp. 1-13
- Buro, Y.A. and Alain, D. (2009b) *Wrap-up report*, Technical Assistance in Mining and Metallurgy in Liberia, Prepared for Mittal Steel Liberia Ltd by MetChem Canada Inc. Vol II of III May 2009, pp. 71-116

- Buro, Y.A. and Alain, D. (2009c) *Wrap-up report*, Technical Assistance in Mining and Metallurgy in Liberia, Prepared for Mittal Steel Liberia Ltd by MetChem Canada Inc. Vol III of III May 2009, pp. 173-180
- Chilson, P. and Horlacher, C. (2009) *2008 iron project review*, Yekepa, Liberia, Faleme River, Senegal. Report prepared for Mittal Steel Liberia Ltd by Pincock Allen & Holt, Report No. 90540 June 5, 2009
- Coakley, J.G. (2004) The Mineral Industry of Liberia, *US Geological Survey Minerals, Yearbook 2004*. [online] Available from:
<<http://www.minerals.usgs.gov/minerals/pubs/country/2004/limyb04.pdf>>
[Accessed 2012 November 5]
- Coats, A.W. and Redfern, J.P. (1963) Thermogravimetric Analysis: Review. *Analyst* Vol. 88 pp. 906-924
- Cripps-Clarke, C.J. and Pepper, M.D. (1981) Technical and economic evaluation of iron ores for blast furnace. *BHP Technical Bulletin* 25 (1), 85-89
- DeVaney, F.D., Dannet, R.L., Hernlund, R.W., Keranen, C.U., Lindroos, E.W., McDermott, W.F., and Van Slyke, W.R. (1985) (eds.) Iron ore, Electrostatic separation: Gravity separation. *SME Mineral Processing Handbook Vol. 2*. pp. 254-289. American Institute of Mining, Metallurgical and Petroleum Engineers. New York
- Edifor, D.R. (2009) ArcelorMittal Liberia Mining, *Yekepa Project Overview*, A presentation prepared for ArcelorMittal Liberia by the Exploration Geology Department, Presentation Slides 12-23, 28 October 2009
- Edwards, R. and Atkinson, K. (1986) *Ore Deposit Geology and its influence on mineral exploration*. p. 779. Chapman and Hall, London

- Ferenczi, P. (2001) Iron ore, manganese and bauxite deposits of the Northern Territory. *Northern Territory Geological Survey*, Report 13, December 2001. pp. 13-41. Government Printer of the Northern Territory, Darwin
- Force, R.E. (1983) Geology of Nimba County, Liberia, U.S. *Geological Survey Bulletin* 1540, pp. 1-23
- Ghosh, A. and Chatterjee, A. (2008) *Ironmaking and Steelmaking: Theory and Practice*. Easton economy edition. pp. 157-172. Prentice-Hall, India
- GIBC, USA (2011) Liberia Export-Import, Trade and Business Directory Vol. 1. *Strategic and practical information*. 2011 edition updated p. 48. International Business Publication, Washington DC
- Goldschmidt, A.B., Simposya, V.M. and Murray, G.P. (2006) *Mineral Resource Estimates for Tokadeh, Gangra and Yuelliton Iron Ore Deposits, Liberia, West Africa*, Report Prepared for Mittal Steel by SRK consulting, Draft Report No 365344/1 October 2006
- Gordon, R.B. (1996) *American Iron 1607-1900*. pp. 7-57. The Johns Hopkins University Press. Baltimore, Maryland
- Gross, G.A. (1993) Industrial and genetic models for iron ore in iron-formations: in Kirkham RV, Sinclair WD, Thorpe RI and Duke JM (eds.) *'Mineral Deposit Modeling.'* Special Paper 40. pp. 151-170. Geological Association of Canada
- Gross, G.A. (1970) Nature and occurrence of iron ore deposits: in United Nations, Department of Economic and Social Affairs (eds) *Survey of world iron ore resources, occurrence and appraisal*. pp. 13-31. United Nations, New York
- Hadden, R.L., (2006) *The Geology of Liberia: a Selected Bibliography of Liberian Geology, Geography and Earth Science*. Originally prepared by the US Geological Survey Library staff as part of a US Department of State project to

restore the Geological Library of Liberia, 1998-1999. Revised and Updated through 2006. 7th May 2006

Harry, K. Harold, L.J. and Donald, G.E. (1973) Iron, in *United States Mineral Resources*, US Geological Survey, Professional Paper 820, pp. 298-299

Heneghan, J. (2010) *Pre-feasibility study, Liberia western range iron ore project, Technical version*. A report prepared for ArcelorMittal Liberia. 3rd revision, 6th January 2010. pp. 32-34

Hitzman, M.W., Oreskes, N. and Einaudi, M. (1992) Geological characteristics and tectonic setting of Proterozoic iron oxide (Cu-U-Au-REE) deposits. *Precambrian Research* 58. pp. 241-287. Elsevier Science B.V. Amsterdam, The Netherlands

Howard, L.H. (ed.) (1987) *Society for Mining, Metallurgy and Exploration, Mining Engineering Handbook*, 2nd ed., vol. 1. p. 212. American Institute of Mining, Metallurgical and Petroleum Engineers. New York

Jorgenson, J.D. (2011) *US Geological Survey, Mineral Commodity Summaries*. [online] Available from: <www.usgs.gov/minerals/pubs/mcs2011/mcs.pdf> [Accessed 2011 September 30]

Jorgenson, J.D. (2012) *US Geological Survey, Mineral Commodity Summaries*. [online] Available from: <www.usgs.gov/minerals/pubs/commodity/iron_ore/mcs-2012-feore.pdf> [Accessed 2012 March 10]

Kamarudin, A. and Ibrahim, S. (2012) *Analysis of iron ore using XRF - on the perspective of ISO 9516-1 and the application of the method in JM*. [online]. Available from: <www.academia.edu/301082/ANALYSIS_OF_IRON_ORE_USING_XRF_-_ON_THE_PERSPECTIVE_OF_ISO_9516-1_AND_THE_APPLICATION_OF_THE_METHOD_IN_JMG> [Accessed 2013 March 17]

- Kelly, E.G. and Spottiswood, D.J. (1989) *Introduction to mineral processing*. pp. 65-167 Mineral Engineering Service Publishers, Denver
- Kennedy, B.A. (1990) *Surface Mining*, Society for Mining, Metallurgy and Exploration Inc. 2nd Edition. pp. 48-60. Port City Press. Baltimore, Maryland
- Kimberley, M.M. (1989) Nomenclature for iron formations. *Ore Geology Reviews* 5. pp. 1-12
- Klemic, H., James, H.L. and Eberlein, D.G. (1973) Iron: in Brobst D.A. and Pratt W.P. (eds) '*United States Mineral Resources*.' US Geological Survey Professional Paper 820, 291-306
- Kogel, E.J., Trivedi, C.N., Barker, M.J., and Krukowski, S.T. (eds.) (2006) *Industrial Minerals and Rocks: Commodities, Markets, and Uses*. p. 1392. Society for Mining, Metallurgy and Exploration Inc. (SME). Littleton, Colorado
- Madsen, I. and Scarlett, N. (2010) *Using x-ray diffraction to solve minerals processing problems, the science behind x-ray diffraction (XRD)*. [online] Available from: <<http://www.csiro.au/en/Organisation-Structure/Divisions/Process-Science-and-Engineering/XRD-analysis.aspx>> [Accessed 2012 November 30. Last modified 2011 October 14]
- Malley, B. (2002) *Operator's and Maintenance Manual: Saturation Magnetization Analyzer, Corrigan Satmagan Model 135, Version 1.3*. June 2002
- Mineral Information Institute (2006) "Iron ore - Hematite, Magnetite & Taconite". [online] Mineral Information Institute (MII). Available from: <<http://www.mii.org/Minerals/photoiron.html>>. [Accessed 7 April 2010].
- Mishra, B.K., Reddy, P.S.R. Das, B. Biswal, S.K. Prakash, S. and Das, S.K., (2007) *Issues relating to characterisation and beneficiation of low grade iron ore fines*, November 2007, pp. 34-36. Institute of Minerals and Material Technology Bhubaneswar. Orissa, India

- Mular, A.L., Halbe, D.U., and Barratt, D.J. (2002) (eds.) *Mineral processing plant design, practice and control*. Proceedings Vol. 1 pp. 176-182. Society for Mining, Metallurgy and Exploration Inc. (SME). Littleton, Colorado
- Norman N.G. and Alan E. (eds.) (1997) *Chemistry of the Elements* 2nd ed. pp. 10-386 Butterworth–Heinemann. Oxford
- Olubambi, P. and Potgieter, J. (2005) Effectiveness of Gravity Concentration for the Beneficiation of Itakpe (Nigeria) Iron Ore Achieved through Jigging Operation. *Journal of Minerals and Materials Characterization and Engineering*, 4, 21-30.
- Petruk, W. (2000) *Applied Mineralogy in the Mining Industry*, 1st ed., p. 151. Elsevier Science B.V. Amsterdam, The Netherlands
- Pietsch, W. (2008) *What is agglomeration* [online] Available from: <<http://www.powderbulksolid.com/article/what-agglomeration>> [Accessed 2012 October 17]
- Pollard, P.J. (ed.) (2000) Evidence of a magmatic fluid and metal source for Fe-oxide Cu-Au mineralisation: in Porter T.M. *Hydrothermal iron-oxide copper-gold and related ore deposits: a global prospective*. Australian Mineral Foundation, Adelaide, pp. 27-41
- Porter, T.M. (ed.) (2000) Hydrothermal iron-oxide copper-gold and related ore deposits: in Porter, T.M. *Hydrothermal iron-oxide copper-gold and related ore deposits: a global prospective*. Australian Mineral Foundation, Adelaide, pp. 3-5
- Pratt, R. (1993) *Australia's iron ore resources*. Resource report. Bureau of Resource Sciences, Canberra. pp. 1-56
- Prinsloo, L., (2010) *Iron ore production* [online] Available from: <<http://www.miningweekly.com/article/ironoreproductionfalls62in2009>> unctad report-2010-07-30 [Accessed 2011 December 22]
- Rao, D.S., Vijaya Kumar, T.V., Subba Rao, S. Prabhakar, S. and Bhaskar Raju, G. (2009) Mineralogy and Geochemistry of a low grade iron ore sample from

- Bellary-Hospet sector, India and their implications on beneficiation. *Journal of Minerals & Materials Characterization & Engineering*, Vol. 8, No.2. pp. 116-117.
- Rao, G.V. and Misra, V.N. (2004) *Mineral Processing Technology* (MPT-2004). p. 122. Feb 19-21, 2004. Allied Publishers PVT. Ltd. Oxford.
- Reading, H.G. (1996) *Sedimentary Environments and facies*. p. 198. Blackwell Scientific Publication, Oxford
- Robb, L. (2004) *Introduction to ore-forming processes*. pp. 247-266. Black Well Scientific Publication, Oxford
- Rosenqvist, T. (1983) *Principles of Extractive Metallurgy*, p. 311. McGraw-Hill Book Company, New York
- Rostoker, W. and Bronson, B. (1990), *Pre-Industrial Iron: Its Technology and Ethnology*, Archeomaterials Monograph No. 1. p. 22. Privately published Philadelphia, Pennsylvania
- Rostoker, W., Bronson, B. and Dvorak, J. (1984) "The Cast-Iron Bells of China", *Technology and Culture* (The Society for the History of Technology) 25 (4):750. 767, [Online] Available from:
<<http://jstor.org/stable/3104621>>, <<http://dx.doi.org/10.2307/3104621>>
[Accessed 2011, April 15]
- Roy, S. and Das, A. (2008) Characterization and processing of low-grade iron ore slimes from the Jilling area of India. *Mineral Processing and Extractive Metallurgy Review*, 29(3), pp. 213-231
- Sarangi, A. and Sarangi, A. (2011) *Sponge Iron Production in Rotary Kiln* (2011), PH1 Larming Private Limited, New Delhi pp. 262–266

- Strassburger, J.H. Brown, D.C. Dancy, T.E. and Stephenson, R.L. (eds.) (1969) *Blast Furnace – Theory and Practice*, vol. 2, pp. 578-579. Gordon and Breach Science Publishers, New York
- Taylor, D., Dalstra, H.J., Harding A.E., Broadbent G.C. and Barley M.E. (2001) Genesis of high-grade hematite ore bodies of the Hamersley province, Western Australia. *Economic Geology* 96 (4). pp. 837-873
- Taylor, H.F.W. (ed.) (1997) *Cement Chemistry*. pp. 263-264. Thomas Telford publications, London
- Tomlinson, S. (2004) *Liberia projects* [online] Available from:
<http://www.westpeakiron.com.au/liberia_projects> [Accessed 2011 October 10]
- US Environmental Protection Agency, EPA 530-R-94-030 *Technical Resource Document, Extraction and Beneficiation of Ores and Minerals Volume 3*, August 1994 Office of Solid Waste, Special Waste Branch 401 M Street, SW Washington, DC 20460
- Van Der Kraaij F.P.M., (2001) *Iron ore* [online] Available from:
<<http://www.liberiapastandpresent.org/ODP/IronOre/IronOreC.htm#return01>>
[Accessed 2010 June 2]
- Van Houten, F.B. and Hou, H.F. (eds.) (1990) Stratigraphic and palaeogeographic distribution of Palaeozoic oolitic ironstones: in McKerrow WS and Scotese CR 'Palaeozoic Palaeogeography and Biogeography.' *Geological Society Memoir* 12, pp. 87-93.
- Venugopal, R., Sharma, T., Saxena, V.K. and Mandre, N.R. (eds.) (2005) *Mineral Processing Technology*. International Seminar on Mineral Processing Technology (MPT-2005). pp. 63-98. Tata McGraw-Hill Pub. Co. New Delhi

Verhoeven, J.D. (2007) Steel metallurgy for the non-metallurgist. pp. 56–57. ASM

International. Materials Park, Ohio

World Steel Association, (2012) World steel in figures 2012. [online] Available from:

<[http://www.worldsteel.org/dms/internetDocumentList/bookshop/WSIF_2012/d](http://www.worldsteel.org/dms/internetDocumentList/bookshop/WSIF_2012/document/World%20Steel%20in%20Figures%202012.pdf)

ocument/World%20Steel%20in%20Figures%202012.pdf> [Accessed 2013

March 18]

KNUST



APPENDIX

Table A1: Drill hole T501 and T512 physical data

Drill hole	Core length, m			Lithology	Weathering	Colour	Grain size	Mineralogy								Texture	Structure	Strength/ Cohesion (Hardness)
	From	To	Interval					hem	qtz	lim	mag	goe						
T501	0	4	4	IFL	4	LR,RB	3	hem	qtz	lim	mag	goe			Diss,Gr	Fra	2	
T501	4	40	36	IFOhm	4	RB,YB	3	hem	mag	lim	qtz				Diss,Gr	Bd,Fra	3	
T501	40	46	6	IFShigh	3	DRB,YB	3	mag	amp	hem	qtz	lim			Rc,Gr	QV, Lam,Fol	3	
T501	46	68	22	IFSlow	1	YB,GG	3	mag	amp	hem	qtz	bio			Rc,Gr	Fol	3	
T501	68	70	3	GNf	4	W	3	plg	qtz	bio	Kao				Gr	Fol	3	
T501	70	72	2	IFShigh	3	G,DO	3	mag	amp	hem	qtz				Rc,Gr	Fra	2	
T501	72	100	28	GNk	1	W,PO	3	Kfeld	qtz	bio	plg				Gr	Fra	4	
T512	0	1	1	SOIL	4	YB	2								cly		1	
T512	1	2	1	CANG	4	RB	3	lim	hem	mag					Diss		2	
T512	2	6	3	SCHb	4	YO	1	lim	kao						Grit		1	
T512	6	22	16	IFOhm	3	LG-DB	3	hem	mag	qtz					Gr	lam	3	
T512	22	28	6	IFSlow	2	LG	3	mag	amp	chlo	qtz				Gr	Fra-Scho	3	
T512	28	62	34	IFShigh	1	LG-MG	3	mag	amp	chlo	qtz	plg			Gr	lam	3	
T512	62	78	16	GNf	1	PO-LG	4	Kfeld	plg	qtz	amp	chlo			Gr,Spd	lam	4	
T512	78	101	23	IFShigh	1	MG-LG	3	mag	amp	chlo	qtz	plg			Gr, Diss	lam	3	
T512	101	107	6	PEG	1	PO	4	Kfeld	qtz	mic	px				Spd		4	
T512	107	135	28	IFShigh	1	MG-LG	3	mag	amp	chlo	qtz	plg	gar		Gr	lam	3	
T512	135	142	7	SCHb	1	MB	3	bio	qtz	chlo	amp	plg			Spd	Fr	3	
T512	142	143	1	IFSlow	1	MG-LG	3	mag	amp	chlo	gar	sd			Gr	lam	3	
T512	143	147	4	GNf	1	LG-MG	3	qtz	bio	plg	amp				Gr		3	
T512	147	231	84	IFShigh	1	MG-LG	3	mag	amp	chlo	qtz	plg	gar	sd	Gr	lam, Fra	3	
T512	231	249	18	GNk	1	PO-LG	4	Kfeld	qtz	amp	gar	plg	bio		Gr-Spt	lam	4	

Table A2: Drill hole T520 physical data

Drill hole	Core length, m			Lithology	Weathering	Colour	Grain size	Mineralogy								Texture	Structure	Strength/ Cohesion (Hardness)
	From	To	Interval															
T520	0	4	4	IFL	4	LR	3	mag	hem	qtz	lim	cly			Gr		2	
T520	4	47	43	SCH	4	DR	3	kao	lim	bio	qtz				Gr	Scho	2	
T520	47	49	2	GNf	4	LO-PO	3	kao	qtz	bio	lim				Gr		3	
T520	49	50	1	SCH	4	DR	3	kao	lim	bio	qtz				Gr	Scho	1	
T520	50	53	3	SCHbg	4	DR	3	bio	kao	gar	mag	lim	qtz		Gr	Scho	3	
T520	53	62	10	SCHbg	3	DG	3	bio	kao	gar	chlo	qtz			Gr	BX	3	
T520	62	65	3	QTE	3	MO-DRB	3	bio	gar	qtz	chlo	plg	mag		Gr	BX	3	
T520	65	67	2	SCH	3	DO-MO	3	mag	qtz	chlo	act	gar			Gr	FLT	2	
T520	67	78	11	IFShigh	3	DO-MO	3	mag	qtz	act	chlo	gar			Gr	FLT	3	
T520	78	81	3	GNm	3	MG	3	qtz	bio	gar	Kfeld	plg			Gr	FLT	3	
T520	81	95	14	GNf	2	MG	3	plg	qtz	Kfeld	bio				Gr		3	
T520	95	109	14	GNf	2	MG-PO	3	plg	qtz	Kfeld	bio				Gr		3	
T520	109	120	11	SCHbg	2	PO-DR	3	bio	gar	qtz	plg				Gr	Scho	3	
T520	120	130	10	IFShigh	1	MO	2	mag	qtz	chlo	py	py	act		Gr	Lam	3	
T520	130	132	2	IFShigh	1	MG	3	mag	qtz	chlo	py	act			Gr	Lam	3	
T520	132	134	2	IFShigh	1	MG	3	mag	qtz	chlo	py				Gr	Lam	3	
T520	134	228	94	IFShigh	1	MG	3	mag	qtz	chlo	py	py			Gr	Lam	3	
T520	228	246	18	IFShigh	1	M	3	mag	qtz	chlo	gar				Gr	Lam	3	
T520	246	247	1	SCHb	1	LG	2	bio	plg	qtz	chlo	py			Grit	Scho	3	
T520	247	265	18	IFShigh	2	MG	2	mag	qtz	plg	chlo	epi			Gr	mass	3	
T520	265	267	1	IFShigh	1	DG	3	amp	qtz	gar	epi	chlo	cal		Grit	RX	3	
T520	267	268	1	IFShigh	2	MG	2	mag	qtz	plg	chlo	epi			Grit	Lam	3	
T520	268	275	7	GNf	2	LG	3	Kfeld	qtz	plg	amp				Grit	Bd	3	

Table A3: Drill T536 T556 physical data

Drill hole	Core length, m			Lithology	Weathering	Colour	Grain size	Mineralogy							Texture	Structure	Strength/ Cohesion (Hardness)
	From	To	Interval					lim	qtz	goe	kao	hem	mag				
T536	0	9	9	IFL	4	DB	2	lim	qtz	goe	kao	hem	mag		Gr	lam	1
T536	9	30	21	IFL	4	RB	2	lim	qtz	goe	hem	mag			Gr	mass	1
T536	30	34	4	IFLc	3	DY-RB	3	lim	qtz	goe	hem	mag			Gr	mass	2
T536	34	53	19	IFOhm	4	DY-LG	2	lim	qtz	goe	hem	mag			Grit	lam	1
T536	53	56	3	IFSlow	2	MG-LB	2	hem	qtz	chlo	mag				Gr	lam	2
T536	56	59	2	IFLc	3	YB	2	hem	qtz	mag	lim				Grit	lam	1
T536	59	68	10	IFOhm	2	MG-DB	3	mag	qtz	chlo	hem				Grit	lam	2
T536	68	73	5	IFOhm	3	LB	2	mag	chlo	qtz	plg				Grit	lam	1
T536	73	86	13	IFShigh	1	LG	2	mag	qtz	plg	chlo				Grit	lam	1
T536	86	89	3	IFSlow	1	MG	3	mag	chlo	qtz	plg				Grit	lam	1
T536	89	96	7	IFShigh	1	LG	2	mag	qtz	chlo	-1				Gr	lam	1
T536	96	98	2	IFShigh	1	MG	3	mag	gar	chlo	qtz				Gr	lam	3
T536	98	105	6	IFSlow	1	DG	2	mag	chlo	qtz	chlo				Gr	lam	3
T536	105	108	4	IFShigh	1	DG	3	mag	qtz	chlo	chlo				Gr	lam	3
T536	108	113	5	GNk	1	LG-PO	3	chlo	amp	plg	kfeld	qtz			Grit	Bd	4
T556	0	6	6	IFOhm	4	DB-RB	3	qtz	hem	mag	goe	lim			Gr	mass	1
T556	6	13	7	IFOhm	4	MB-RB	3	qtz	hem	mag	goe	lim			Gr	mass	2
T556	13	19	6	IFOhm	4	DB-MB	3	qtz	hem	mag	goe	lim			Gr	mass	1
T556	19	42	23	IFOhm	4	DB-MB	2	qtz	hem	mag	goe	lim			Gr	mass	2
T556	42	46	4	IFOhm	3	DB-LG	2	qtz	mag	hem	goe	lim			Gr	mass	3
T556	46	58	11	IFShigh	2	DG	2	qtz	mag	hem	goe	lim			Gr	lam	3
T556	58	59	1	IFShigh	1	DG-LG	2	qtz	mag	chlo	goe	lim			Gr	lam	4
T556	59	60	1	PEG	1	W-PO	4	Kfeld	qtz	plg	tou				Gr	RX	4
T556	60	63	3	IFShigh	1	DG-MG	2	mag	qtz	chlo	amp	bio			Gr	lam	4
T556	63	73	10	IFShigh	1	DG	2	mag	qtz	chlo	amp				Gr	Bd	4
T556	73	74	1	IFSlow	1	LG-MD	2	mag	qtz	chlo	amp				Gr	lam	4
T556	74	75	1	IFShigh	1	LG-MG	2	qtz	mag	chlo	amp				Gr	lam	4
T556	75	77	1	IFSlow	1	MG-LG	2	qtz	mag	chlo	amp				Gr	lam	4
T556	77	81	5	IFShigh	1	LG	2	qtz	mag	chlo	amp				Gr	lam	4
T556	81	88	7	GNk	1	LG-PO	3	qtz	plg	kfeld	bio				Grit	Bd	4

Table A4: Drill hole T594, T627 and T643 physical data

Drill hole	Core length, m			Lithology	Weathering	Colour	Grain size	Mineralogy							Texture	Structure	Strength/ Cohesion (Hardness)
	From	To	Interval					lim	hem	qtz	kao	mag	sd	chlo			
T594	0	4	4	IFL	4	RB	4	lim	hem	qtz	kao				Gr		2
T594	4	6	2	IFOhm	4	YB	3	lim	hem	qtz	kao	mag			Gr		2
T594	6	11	5	IFOhm	3	LB	3	hem	mag	qtz					Gr		3
T594	11	15	4	GNf	4	YO	2	kao	qtz						Grit		1
T594	15	16	2	SCHb	4	YO	2	bio	ser	kao	qtz	sd			Grit		1
T594	16	30	14	SCHb	1	LG	5	bio	gar	qtz	chlo	amp			mass	scho	4
T627	0	5	5	IFLc	2	RB	4	hem	mag	qtz	plg				Gr		2
T627	5	8	4	SCH	4	PO_PaO	1	hem	qtz	plg					Cly		1
T627	8	30	21	IFOhm	3	DB_LB	2	hem	mag	qtz	plg	lim			Gr		3
T627	30	49	19	IFShigh	2	MG	2	mag	qtz	plg	hem				Gr	lam,FLT,Fra	2
T627	49	54	5	IFShigh	1	MG_LO	2	mag	qtz	plg					Gr	FLT,lam	1
T643	0	4	4	CANG	3	RB	3	hem	mag	goe	spec				Gr	mass	3
T643	4	29	25	IFOhm	4	MB	2	mag	goe	hem	lim	qtz	plg		Gr	mass	1
T643	29	34	5	IFOhm	3	MB	2	mag	goe	hem	lim	qtz	plg		Gr	mass	2
T643	34	39	5	IFOhm	2	MB	2	mag	goe	hem	lim	qtz	plg		Gr	mass	3
T643	39	46	7	SCH	4	PO	2	plg	qtz	kfeld					Gr	mass	1
T643	46	60	13	GNf	2	PO	3	plg	kfeld	qtz	gar				Gr	lam	3
T643	60	66	7	GNf	1	PO	3	plg	kfeld	qtz					Gr	lam	4

Table A5: Drill hole T662 and T673 physical data

Drill hole	Core length, m			Lithology	Weathering	Colour	Grain size	Mineralogy							Texture	Structure	Strength/ Cohesion (Hardness)
	From	To	Interval					Kfeld	qtz	plg	mus						
T662	1	7	7	SCH	4	PO	2	Kfeld	qtz	plg	mus				Mass		1
T662	7	11	4	IFOhm	4	MB	2	mag	hem	qtz	goe	spec			Mass		1
T662	11	21	10	SCH	4	PO	1	Kfeld	plg	qtz					Grit		1
T662	21	22	1	IFOhm	4	MB	2	mag	goe	hem	qtz	spec			Mass		2
T662	22	28	6	SCH	4	PO	1	Kfeld	plg	qtz					Grit		1
T662	28	34	7	GNkf	4	PO	3	qtz	plg	Kfeld	amp				Mass		2
T662	34	40	6	IFShigh	2	DO	2	mag	amp	plg	qtz	chlo	epi		Lam	FLTZ	1
T662	40	42	2	IFSlow	2	MG	2	mag	qtz	amp	plg				Gr		3
T662	42	44	2	IFSlow	1	MG	2	mag	qtz	amp	plg				Lam		4
T673	0	5	5	IFL	4	MB_RB	4	hem	mag	goe	spec	lim	kao		Gr		1
T673	5	12	7	SCH	4	LO_PO	1	mus	bio	plg	kfeld	qtz			Gr	Scho	1
T673	12	26	15	SCH	3	LO_PO	1	mus	bio	plg	kfeld	qtz			Gr	Scho	1
T673	26	30	3	IFOhm	3	MB_DB	2	mag	hem	qtz	plg	lim			Gr	lam	3
T673	30	56	26	IFShigh	3	DO_DG	3	chlo	mag	amp	px	plg	sd	mus	Gr	lam	2
T673	56	59	3	IFSlow	3	MB_B	3	mag	plg	hem	qtz	lim	chlo	px	Gr	lam	3
T673	59	70	11	IFShigh	2	MG_DG	3	mag	chlo	amp	plg	qtz	sd	px	Gr	lam	3-4
T673	70	74	4	IFShigh	1	MG_DG	3	mag	chlo	amp	plg	qtz	sd	px	Gr	lam	4

Table A6: ArcelorMittal Liberia Lithology codes

	Regolith	Codes	Rock type	Description
Waste		SOIL	Soil	Soil, organic material
		LATc	Clayey Laterite	Clayey Laterite (unknown rock)
Ore	Oxide	CANG	Canga or Cuirasse	Canga (breccia with IF fragments) or cuirasse (indurated crust of massive hematite)
		IFL	Laterite - IF	Lateritic Iron Formation
		IFLc	Clayey Laterite - IF	Clayey lateritic iron Formation
	Transition	IFC	Transition Iron Formation	Clayey Iron Formation
		IFOhm		Iron Formation: hematite/specularite+magnetite
		IFOh		Iron Formation: hematite/specularite
	Fresh	IFPh	Primary Iron Formation	Qtz + hematite/specularite
		IFPm		Qtz + magnetite
		IFPhm		Qtz hematite/specularite + magnetite
		IFSlow	Primary Silicate Iron Formation	IF < 30% silicate
		IFShigh		IF > 30% silicate
	Waste		SCH	Schist
SCHb			Biotite schist	
SCHbg			Biotite and Garnet schist	
SCHc			Chlorite schist	
GNm			Gneiss, mafic	Banded; feldspar, biotite, amphibole predominant
GNf			Gneiss, felsic	Banded; quartz, feldspar predominant
GNk			Gneiss, potassic + Bsmt Gneiss	
AMT			Amphibolite	
PEG			Pegmatite	
DIA			Mafic dyke	
ATE			Quartzite	
QV			Quartz vein	
FLTZ			Fault zone	

Table A7: ArcelorMittal Liberia Minerals code

Mineral	Code	Mineral	Code
Hematite (Martite)	hem	Chlorite	chlo
Magnetite	mag	Sericite	ser
Goethite	goe	Muscovite	mus
Limonite	lim	Plagioclase	plg
Specularite	spec	K-Feldspar	Kfeld
Actinolite	act	Kaolinite	kao
Tremolite	tre	Clay	cly
Diopside	dio	Pyrite	py
Grunerite	gru	Chalcopyrite	cpy
Pyroxene	px	Pyrrhotite	po
Amphibolite	amp	Sulphide	sd
Tourmaline	tou	Carbonate	cb
Garnet	gar	Calcite	cal
Biotite	bio	Ankerite	ank
Mica	mic	Siderite	sid
Epidote	epi		

Table A8: ArcelorMittal Liber Grain size codes

Grain size	Code
<0.06 mm	1
0.06-0.2 mm	2
0.2-1 mm	3
1-2 mm	4
>2 mm	5

Table A9: ArcelorMittal Liberia Structure code

Structure	Code
Mylonitic	Myl
Breccia	BX
Breccia zone	BXZ
Brecciated	BXD
Fracture	fra
Fault	FLT
Fault zone	FLTZ
Fault Gouge	FLTG
Faulted contact zone	FCZ
Recrystallised	RX
Fold	Fol
Micr-folds	Folmc
S-fold	FolS
Z-fold	FolZ
M-fold	FolM

Table A10: ArcelorMittal Liberia Texture codes

TEXTURE	CODE
Laminated	Lam
Banded	Bd
Massive	Mass
Schistose, foliated	Scho
Recemented	Rc
Granular	Gr
Silty (gritty)	Grit
Clayey	Cly
Disseminated	Diss
Spotted	spd

Table A11: ArcelorMittal Liberia Weathering codes

WEATHERING	CODE
Intensely oxidized or weathered	4
Moderately oxidized or weathered	3
Mildly oxidized or weathered (joints only)	2
Fresh and unweathered	1

Table A12: ArcelorMittal Liberia Colour codes

Colour	Code (*)	Colour	Code (*)
White	W	Dark red brown	DRB
Light yellow	LY	Yellow brown	YB
Medium Yellow	MY	Red brown	RB
Dark Yellow	DY	Dark grey	DG
Yellow Orange	YO	Medium grey	MG
Pink Orange	PO	Light grey	LG
Light Orange	LO	Olive grey	OG
Pale Orange	PaO	Green grey	GG
Light Red	LR	Blue grey	BG
Dark Red	DR	Dark olive	DO
Light Brown	LB	Medium olive	MO
Medium Brown	MB	Light olive	LO
Dark Brown	DB	Black	BG

(*) Based on CORSTOR's colour chart

Table A13: ArcelorMittal Liberia Strength/Cohesion codes

Strength/Cohesion	Code
Soft (disintegrates when handled)	1
Weak (thin slabs broken by hand)	2
Strong (breaks with geological hammer blow)	3
Very strong (rings with hammer blow)	4



Figure A1: Atlas Copco ROC L8 drill rig

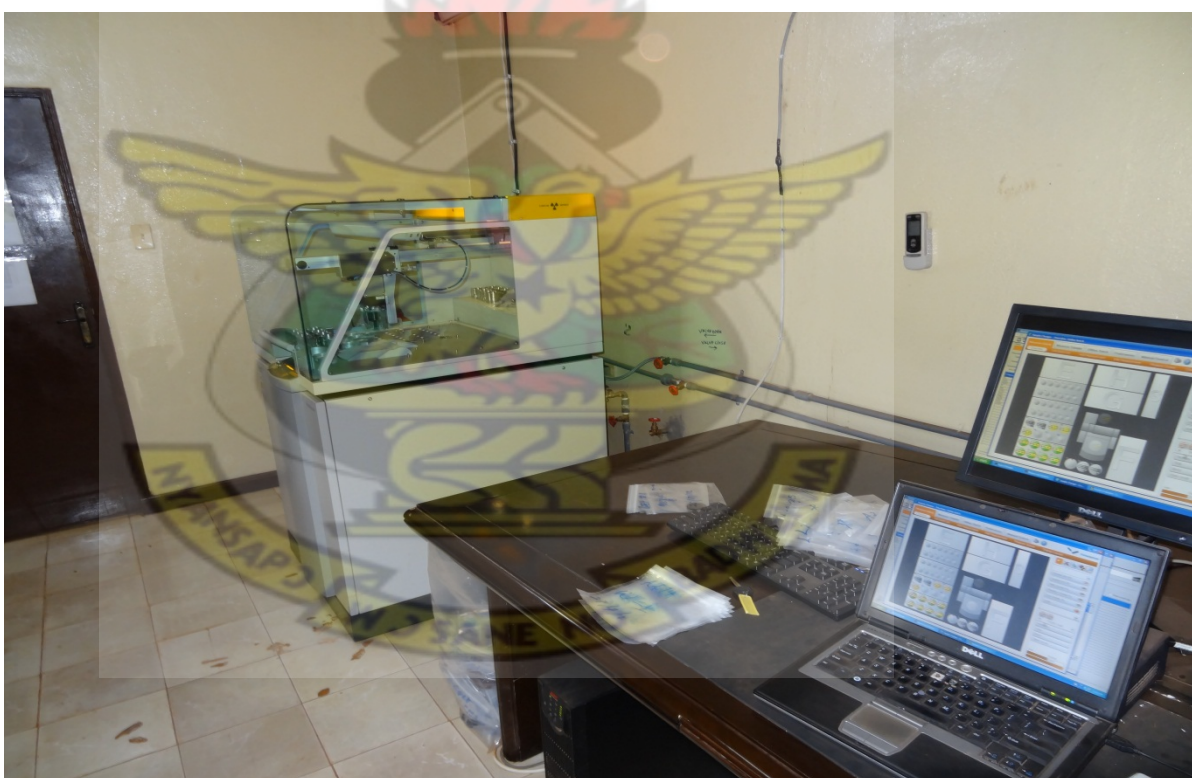


Figure A2: Panalytical Axios^{mAX} X-ray fluorescence spectrometer